# SEMI-ANALYTICAL METHODS FOR VIBRATION AND STABILITY ANALYSIS OF PRESSURIZED AND ROTATING TOROIDAL SHELLS BASED ON THE ENERGY APPROACH

Ivo Senjanović, Neven Alujević, Ivan Ćatipović,
Damjan Čakmak, Nikola Vladimir

# CONTENTS

**Summary**

In this self-contained paper, free vibrations of a pressurised toroidal shell, rotating around its axis of symmetry, are considered. Extensional and bending strain-displacement relationships are derived from general expressions for a thin shell of revolution. The strain and kinetic energies are determined in the co-rotating reference frame. The strain energy is first specified for large deformations, and then split into a linear and a non-linear part. The non-linear part, which is subsequently linearized, is necessary in order to take into account the effects of centrifugal and pressure pre-tensions. The Green-Lagrange non-linear strains are considered. The kinetic energy is formulated taking into account the centrifugal and the Coriolis terms. The variation of displacements $u$, $v$ and $w$ in the circumferential direction is described exactly. The dependence of the displacements on the meridional coordinate is described through the Fourier series. The Rayleigh-Ritz method is applied to determine the Fourier coefficients. As a result thereof, an ordinary stiffness matrix, a geometric stiffness matrix due to pressurisation and centrifugal forces, and three inertia matrices incorporating squares of natural frequencies, products of rotational speed and natural frequencies and squares of the rotational speed, are derived. The application of the developed procedure is illustrated in cases of a closed and open toroidal shell and a thin-walled toroidal ring. The obtained results are compared with FEM results, and a very good agreement is observed. The advantage of the proposed semi-analytical method is high accuracy and low CPU time-consumption.

Additionally, a finite strip for vibration analysis of rotating toroidal shells subjected to internal pressure is developed. The expressions for strain and kinetic energies are taken from the previous Rayleigh-Ritz method. The variation of displacements $u$, $v$ and $w$ with the meridional coordinate is modelled through a discretization with a number of finite strips. The finite strip properties, i.e. the stiffness matrix, the geometric stiffness matrix and the mass matrices are defined by employing bar and beam shape functions, and by minimizing the strain and kinetic energies. In order to improve the convergence of the results, the strip of a higher order is developed too. The application of the finite strip method is illustrated in case of closed toroidal shell. The obtained results are compared with those determined by the Rayleigh-Ritz method and the finite element method.

The rigorous formulae for natural frequencies of in-plane and out-of-plane free vibrations of a rotating ring are derived. An in-plane vibration mode of the ring is characterised by coupled flexural and extensional deformations, whereas an out-of-plane mode is distinguished by coupled flexural and torsional deformations. For the in-pane vibrations, the ring is considered to be a short top segment of a toroidal shell. The expressions for the ring strain and kinetic energies are deduced from the corresponding expressions for the torus. It is shown that the ring rotation causes the bifurcation of natural frequencies for the in-plane vibrations only. The bifurcation of natural frequencies of the out-of-plane vibrations does not occur. The derived analytical results are validated by a comparison with FEM and FSM (Finite Strip Method) results, as well as with experimental results available in the literature.

**Keywords:** toroidal shell, ring; vibration; buckling; pressure; rotation; the Rayleigh-Ritz method; finite strip method.

# 1. INTRODUCTION

The statics and dynamics of thin shells have been a subject of investigation for over a century. In the beginning of the 20th century, statics problems were mainly considered, and the achievements are summarised in some capital books [1]-[4]. Later on, following the rapid development in all branches of the engineering science, dynamics problems became more and more relevant, [5]. In the recent decades, vibrations of rotating shells of revolution, especially cylindrical shells, are being extensively investigated [6]-[8], considering their significance in modelling rotating structures, such as automotive tires, Fig. 1, [9],[10].
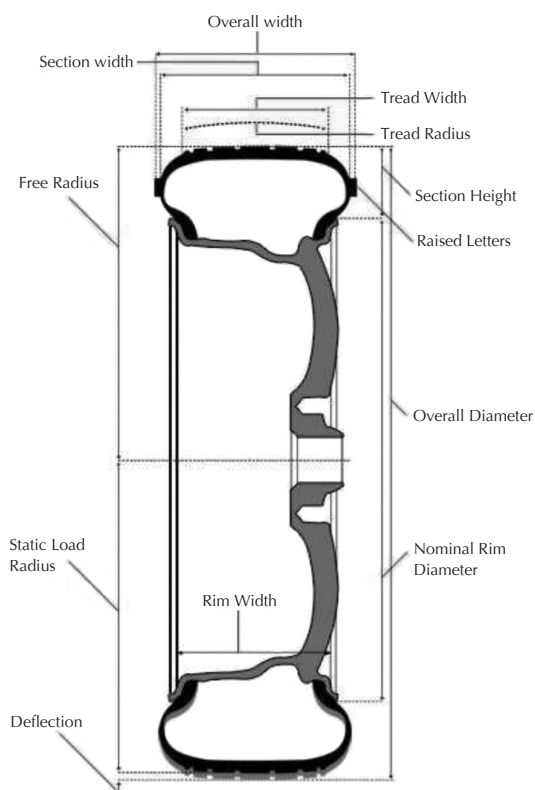
Fig. 1. Automotive wheel with tyre
*Sl. 1.* Automobilski kotač s gumom

Toroidal shells are usually used in axisymmetric shell structures as a transition structural element from cylindrical body to a spherical head, in order to smoothen the stress concentration. Such a design solution can be found in heads of cargo tanks on liquefied gas carriers, off-shore structures, submarine pressure hulls, pressure vessels, etc., Figs. 2, 3 and 4, [11] [14].

The toroidal shell theory is rather complicated due to the double curvature associated with the toroidal geometry, [4]. Partial differential equations of motion can be derived directly by considering the equilibrium of sectional forces, inertia forces and external loads on an infinitesimal shell element. They can also be obtained indirectly from the strain and kinetic energies of the complete shell by applying Hamilton's principle. Differential equations of motion are normally expressed in terms of tensional and flexural displacements. In case of a closed toroidal shell, the variation of displacements in the circumferential direction can be described by the Fourier series. In this way, partial differential equations are reduced to a set of ordinary differential equations. However, due to variable coefficients, it is not possible to obtain a closed-form analytical solution. Therefore, numerical methods are ordinarily used.
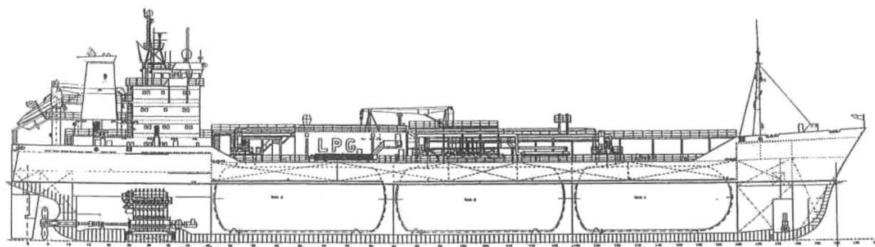


**Fig. 2.** Liquefied Gas Carrier (LPG), capacity 8350 m3
*Sl. 2.* Brod za prijevoz ukapljenog plina (LPG), kapacitet 8350 m3
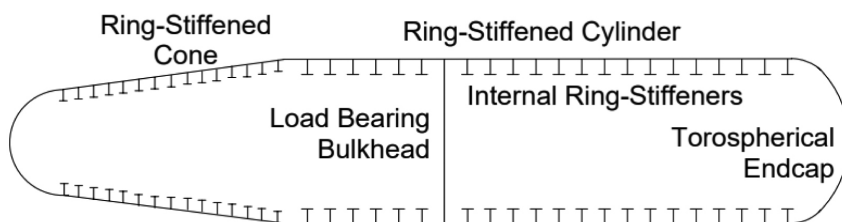


**Fig. 3.** Submarine pressure hull
*Sl. 3.* Čvrsti trup podmornice

Nowadays, vibration analysis of pre-stressed and rotating shells of revolution is becoming more and more relevant. A shell, either opened or closed in the circumferential direction, can be modelled by shell finite elements, [15], [16]. A general formulation of double-curved shell finite elements is presented in [17]. For the vibration analysis of shells closed in the circumferential direction, special waveguide finite elements have been developed, [18]-[21]. In this case a 3D problem is reduced to a 2D problem, which results in significant savings of the computational time. A comparison of these two types of finite elements is given in [22].
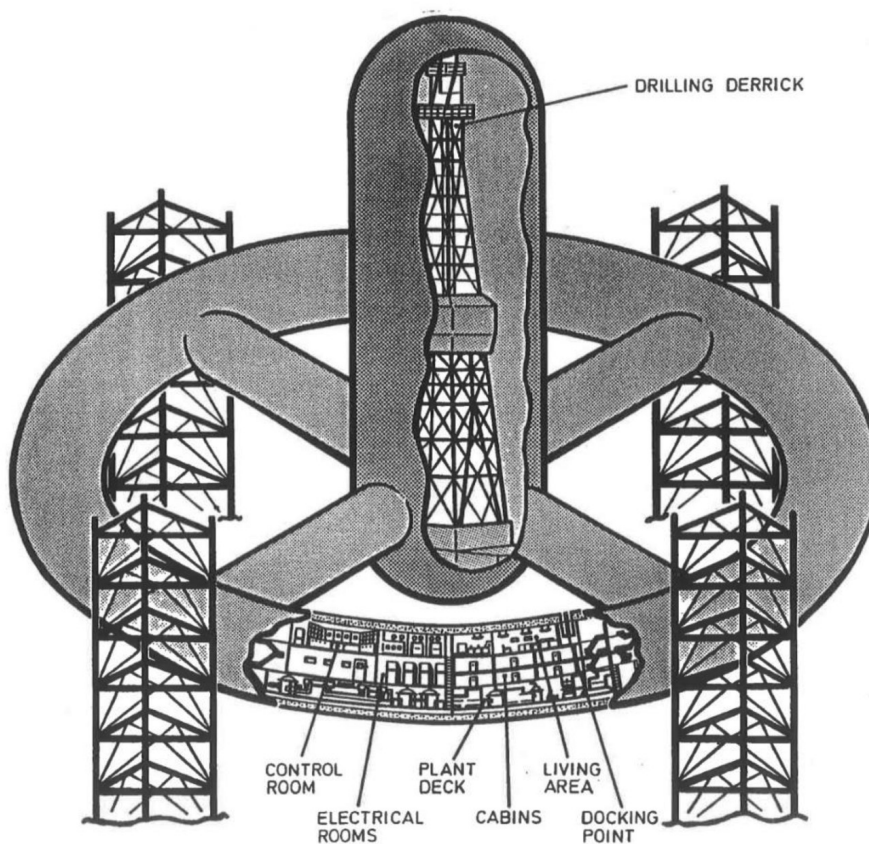


**Fig. 4.** Underwater drilling rig
*Sl. 4.* Podvodni bušaći toranj

The present state-of-the-art motivates to find a rigorous solution for the free vibrations problem of rotating and pressurised toroidal shells. The paper is dedicated to this problem with a particular aim of better understanding the dynamic behaviour of rotating tires. For this purpose, the Rayleigh-Ritz method is used [23]. Ordinary strain energy, strain energy due to pre-stressing, and the kinetic energy are formulated taking into account the variation of shell displacements in the circumferential direction exactly, by using simple trigonometric functions [24]. Mode profiles of the shell cross-section (the variation in the meridional direction) are described by the Fourier series. Minimizing the total energy by its differentiation per the Fourier coefficients, a matrix equation of motion is obtained. The application of the presented numerical procedure is illustrated in the case of a closed toroidal shell and a thin-walled toroidal ring. The buckling problem of closed toroidal shell is also analysed by the same approach, [25].

In order to analyse vibrations of toroidal shells with open cross-section and arbitrary boundary conditions in a relatively simple way, a dedicated finite strip is derived in this paper [26]. Ordinary strain energy, strain energy due to pre-stressing, and the kinetic energy are formulated by describing variations of the shell displacements in the circumferential direction using simple trigonometric functions (sine and cosine). Bar and beam shape functions are employed in order to describe the displacement variations in the meridional direction within a finite strip. The equation of motion of the finite strip is obtained by minimizing the total energy. The ordinary stiffness matrix, geometric stiffness matrix and three mass matrices related to: 1) natural frequencies (inertia), 2) rotation speed (centrifugal load), and 3) the Coriolis effect, consist of sets of submatrices with variable coefficients. In order to improve the convergence of the results, a finite strip of higher order is also presented. The application of the developed finite strip is illustrated in cases of toroidal shells with both closed and open cross-sections. The advantages of the finite strip method with respect to the ordinary finite element method and the waveguide finite element method include: explicit equations, physical insight, and a considerable reduction of the number of degrees of freedom in the former case, which results in significant savings of the CPU time.

As a third subject in this paper, a mathematical model for the in-plane and out-of-plane free vibrations of a rotating ring is formulated, [27]. In the former case, the flexural vibrations are coupled with the tensional vibrations, whilst in the latter, they are coupled with torsional vibrations. The governing equations of motion are deduced from the toroidal shell theory. In this way, the universality of the toroidal shell theory is demonstrated. The characteristic equations of motion are solved in a rigorous and approximate analytical way.

The paper is structured in 8 sections. The state-of-the-art in the considered field is described in the Introduction, Section 1. In Section 2, general toroidal shell theory for the forthcoming special cases is presented as a starting point. General expressions for the linear strain energy due to pre-stressing, as well as kinetic energies due to rotation and vibration are derived. In Section 3, application of the Rayleigh-Ritz method for the vibration analysis of rotating closed and open toroidal shell is presented. Section 4 deals with the finite strip method. Ordinary stiffness matrix, geometric stiffness matrix, and mass matrices related to the centrifugal force, the Coriolis force and vibration, are derived. In Section 5, the pre-stressing tension forces due to pressure and rotation are formulated. In Section 6, the ring vibration theory is presented based on the toroidal shell theory. In Section 7, the application of the presented theories is illustrated by numerical examples and validated by comparing the obtained results with the FEM results. In Section 8, several useful concluding remarks of the performed analysis are drawn.

## 2. AN OUTLINE OF TOROIDAL SHELL THEORY

### 2.1 Strain-displacement relationship

The thin shell theory is presented in [5] in general form using Lamé parameters, $A_1$, $A_2$, the main radii of curvature, $R_1$, $R_2$, the in-plane displacements, $u_1$, $u_2$, and normal displacement (deflection), $u_3$.

A toroidal shell with the main dimensions and displacements is shown in Fig. 5. The shell parameters are the following:

$$A_1 = a, \quad A_2 = r, \quad \alpha_1 = \vartheta, \quad \alpha_2 = \varphi,$$

$$r = R + a\sin\vartheta, \quad R_1 = a, \quad R_2 = \frac{r}{\sin\vartheta}, \tag{1}$$

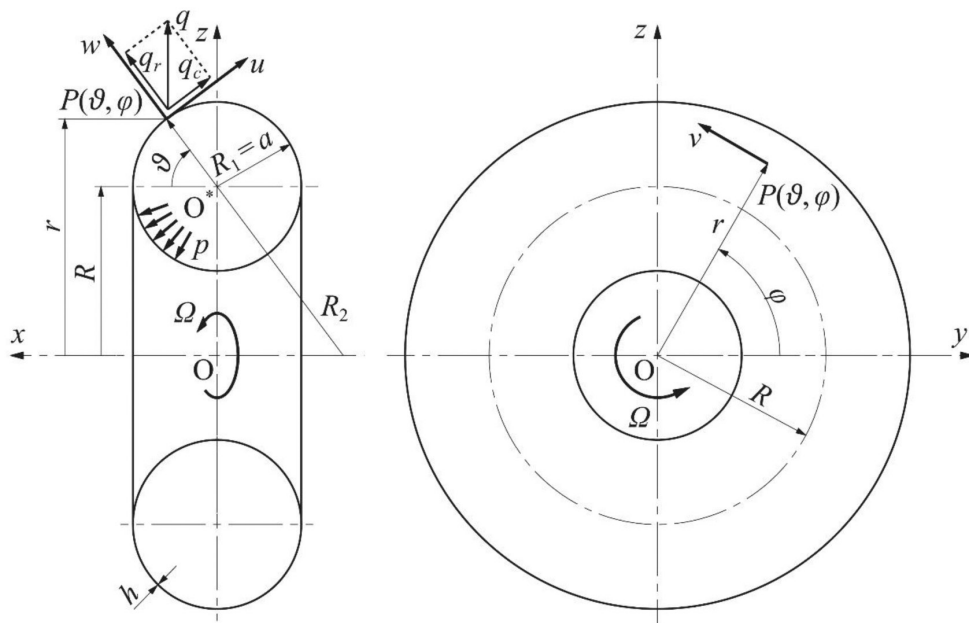$$u_1 = u, \quad u_2 = v, \quad u_3 = w.$$



**Fig. 5.** Closed toroidal shell, main dimensions and displacements
*Sl. 5.* Zatvorena toroidna ljuska, glavne izmjere i pomaci

Referring to [24] and employing (1), the expressions for toroidal shell deformations take the following form:
in-plane strains

$$\varepsilon_\vartheta = \frac{1}{a}\left(\frac{\partial u}{\partial \vartheta} + w\right)$$

$$\varepsilon_\varphi = \frac{1}{r}\left(\frac{\partial v}{\partial \varphi} + u\cos\vartheta + w\sin\vartheta\right) \tag{2}$$

$$\varepsilon_{\vartheta\varphi} = \frac{1}{r}\frac{\partial u}{\partial \varphi} + \frac{1}{a}\frac{\partial v}{\partial \vartheta} - \frac{\cos\vartheta}{r}v,$$

curvature changes

$$\kappa_\vartheta = \frac{1}{a^2}\left(\frac{\partial u}{\partial \vartheta} - \frac{\partial^2 w}{\partial \vartheta^2}\right)$$

$$\kappa_\varphi = \frac{\cos\vartheta}{ar}\left(u - \frac{\partial w}{\partial \vartheta}\right) + \frac{1}{r^2}\left(\frac{\partial v}{\partial \varphi}\sin\vartheta - \frac{\partial^2 w}{\partial \varphi^2}\right) \tag{3}$$

$$\kappa_{\vartheta\varphi} = \frac{1}{ar}\left[\frac{\partial u}{\partial \varphi} + \frac{\partial v}{\partial \vartheta}\sin\vartheta + \cos\vartheta\left(1 - 2\frac{a}{r}\sin\vartheta\right)v - 2\frac{\partial^2 w}{\partial \vartheta\partial \varphi} + 2\frac{a}{r}\cos\vartheta\frac{\partial w}{\partial \varphi}\right],$$

rotation angles

$$\beta_1 = \frac{1}{a}\left(u - \frac{\partial w}{\partial \vartheta}\right)$$

$$\beta_2 = \frac{1}{r}\left(v\sin\vartheta - \frac{\partial w}{\partial \varphi}\right). \tag{4}$$

## 2.2 Strain and kinetic energy

The ordinary strain energy due to extension and bending, according to [24], reads

$$E_s = \frac{1}{2} \int_0^{2\pi} \int_{\vartheta} \left\{ K \left[ \varepsilon_\vartheta^2 + \varepsilon_\varphi^2 + 2\nu \varepsilon_\vartheta \varepsilon_\varphi + \frac{1}{2}(1-\nu) \varepsilon_{\vartheta\varphi}^2 \right] \right. \\ \left. + D \left[ \kappa_\vartheta^2 + \kappa_\varphi^2 + 2\nu \kappa_\vartheta \kappa_\varphi + \frac{1}{2}(1-\nu) \kappa_{\vartheta\varphi}^2 \right] \right\} ar \mathrm{d}\varphi \mathrm{d}\vartheta, \tag{5}$$

where

$$K = \frac{Eh}{1-\nu^2}, \qquad D = \frac{Eh^3}{12(1-\nu^2)} \tag{6}$$

are the membrane and bending stiffness, respectively, $E$ is Young's modulus, $\nu$ is Poisson's ratio, and $h$ is the shell thickness.

Referring to [24], the strain energy due to pre-stressing by tension forces $N_\vartheta$ and $N_\varphi$, is presented in the form

$$E_G = \int_0^{2\pi} \int_{\vartheta} \left( \varepsilon_\vartheta^* N_\vartheta + \varepsilon_\varphi^* N_\varphi \right) ar \mathrm{d}\vartheta \mathrm{d}\varphi, \tag{7}$$

where $\varepsilon_\vartheta^*$ and $\varepsilon_\varphi^*$ are the second order strains based on the Green-Lagrange tensor [28]

$$\varepsilon_\vartheta^* = \frac{1}{2a^2} \left[ \left( \frac{\partial u}{\partial \vartheta} \right)^2 + \left( \frac{\partial v}{\partial \vartheta} - \frac{v}{r} \frac{\partial r}{\partial \vartheta} \right)^2 + \left( \frac{\partial w}{\partial \vartheta} \right)^2 \right]$$

$$\varepsilon_\varphi^* = \frac{1}{2r^2} \left[ \left( \frac{\partial v}{\partial \varphi} \right)^2 + \left( \frac{\partial u}{\partial \varphi} \right)^2 + \left( \frac{\partial w}{\partial \varphi} \right)^2 \right]. \tag{8}$$

According to [24], the kinetic energy of the rotating toroidal shell reads

$$
E_k = \frac{1}{2} \rho h \int\limits_0^{2\pi} \int\limits_\vartheta \left[ \left( \frac{\partial u}{\partial t} - v\Omega \cos\vartheta \right)^2 + \left( \frac{\partial v}{\partial t} + u\Omega \cos\vartheta + w\Omega \sin\vartheta \right)^2 \right.
$$
$$
\left. + \left( \frac{\partial w}{\partial t} - v\Omega \sin\vartheta \right)^2 \right] ar\,\mathrm{d}\vartheta\,\mathrm{d}\varphi,
$$

(9)

where $\rho$ is the mass density and $\Omega$ is the rotational speed.

## 2.3 The condensation of strain and kinetic energy to shell cross-section

For a toroidal shell closed in the circumferential direction, with either an open or a closed cross-section, having arbitrary cross-sectional boundary conditions, the displacement components can be assumed in the form

$$
u(\vartheta, \varphi, t) = U(\vartheta) \cos(n\varphi + \omega t)
$$
$$
v(\vartheta, \varphi, t) = V(\vartheta) \sin(n\varphi + \omega t)
$$
$$
w(\vartheta, \varphi, t) = W(\vartheta) \cos(n\varphi + \omega t),
$$

(10)

where $U(\vartheta)$, $V(\vartheta)$ and $W(\vartheta)$ are functions of the cross-sectional mode profiles, and $\omega$ is natural frequency. The argument $n\varphi + \omega t$ is used in order to enable describing the travelling modes that normally appear due to shell rotation, and $n$ is the circumferential mode number.

Substituting (10) into Eqs. (2) and (3), and then into the strain energies (5) and (7), one obtains products of two displacement amplitudes or their derivatives, with squares of sine and cosine functions (10). Their integrals over the circumferential angle $\varphi$ within the domain 0-2$\pi$ equals $\pi$. Thus, the temporal variation vanishes, and the strain and kinetic energies become time-invariant. This is due to the fact that the natural modes rotate while keeping a fixed cross-sectional profile. As a result thereof, Eqs. (5) and (7) are reduced to the following form:

$$
\begin{aligned}
E_s = \int_{\vartheta} \Bigg[ & \frac{1}{2} p_1 (U')^2 + \frac{1}{2} p_2 U^2 + p_3 U'U + \frac{1}{2} p_4 (V')^2 + \frac{1}{2} p_5 V^2 + p_6 V'V \\
& + p_7 U'V + p_8 UV' + p_9 UV \\
& + \frac{1}{2} q_1 (W'')^2 + \frac{1}{2} q_2 (W')^2 + \frac{1}{2} q_3 W^2 + q_4 W''W' + q_5 W''W + q_6 W'W \\
& + q_7 W''U' + q_8 (W''U + W'U') + q_9 W'U + q_{10} WU' + q_{11} WU \\
& + q_{12} W''V + q_{13} W'V' + q_{14} W'V + q_{15} WV' + q_{16} WV \Bigg] d\vartheta,
\end{aligned}
\tag{11}
$$

$$
\begin{aligned}
E_G = \int_{\vartheta} \Bigg[ & \frac{1}{2} c_1 (U')^2 + \frac{1}{2} c_2 U^2 + \frac{1}{2} c_3 (V')^2 + \frac{1}{2} c_4 V^2 + c_5 V'V \\
& + \frac{1}{2} c_6 (W')^2 + \frac{1}{2} c_7 W^2 + c_8 UV + c_9 (U'W - UW') + c_{10} UW + c_{11} VW \Bigg] d\vartheta,
\end{aligned}
\tag{12}
$$

where the integrals over the meridional coordinate $\vartheta$ are for the moment left open. Parameters $p_i(\vartheta)$, i=1,2…9, $q_i(\vartheta)$, i=1,2…16, and $c_i(\vartheta)$, i=1,2…11, in Eqs. (11) and (12) are variable coefficients specified in Appendices A and B, respectively.

In a similar way substituting expressions (10) into (9), one obtains for the condensed kinetic energy

$$
\begin{aligned}
E_k = \frac{1}{2} \pi \rho h a \int_{\vartheta} r \Big[ & \left( \omega^2 + \Omega^2 \cos^2 \vartheta \right) U^2 + \left( \omega^2 + \Omega^2 \right) V^2 + \int_{\vartheta} r \Big[ \left( \omega^2 + \Omega^2 \sin^2 \vartheta \right) W^2 \\
& + \omega \Omega \left( \cos \vartheta UV + \sin \vartheta VW \right) + 2\Omega^2 \sin \vartheta \cos \vartheta UV \Big] d\vartheta.
\end{aligned}
\tag{13}
$$

## 3. THE APPLICATION OF THE RAYLEIGH-RITZ METHOD

### 3.1 Displacement field

In case of a closed toroidal shell, Fig. 5, there are no boundary conditions, and shell displacements can be assumed in the form of the complete Fourier series. Hence, by applying matrix notation, one can write

$$U\left(\vartheta\right)=\left\langle\left\langle f_{m}\right\rangle\left\langle g_{m}\right\rangle\right\rangle\left\{\begin{matrix}\left\{A_{m}\right\}\\\left\{B_{m}\right\}\end{matrix}\right\}$$

$$V\left(\vartheta\right)=\left\langle\left\langle f_{m}\right\rangle\left\langle g_{m}\right\rangle\right\rangle\left\{\begin{matrix}\left\{C_{m}\right\}\\\left\{D_{m}\right\}\end{matrix}\right\} \qquad (14)$$

$$W\left(\vartheta\right)=\left\langle\left\langle f_{m}\right\rangle\left\langle g_{m}\right\rangle\right\rangle\left\{\begin{matrix}\left\{E_{m}\right\}\\\left\{F_{m}\right\}\end{matrix}\right\},$$

where $A_{m}$, $B_{m}$, $C_{m}$, $D_{m}$, $E_{m}$ and $F_{m}$ are the unknown Fourier coefficients, and

$$f_{m}=\cos m\vartheta, \qquad g_{m}=\sin m\vartheta, \qquad m=0,1,2,...,N \qquad (15)$$

are the coordinate functions.

## 3.2 Stiffness matrix

Substituting expressions for displacement field (14) into (11) and differentiating the strain energy by the Fourier coefficients, a system of three matrix equations is obtained

$$
\begin{Bmatrix} \dfrac{\partial E_S}{\{\partial A_k\}} \\[2mm] \dfrac{\partial E_S}{\{\partial B_k\}} \end{Bmatrix} = \int_0^{2\pi} \left( p_1 [k]_1 + p_2 [k]_2 + p_3 [k]_3 \right) \mathrm{d}\vartheta \begin{Bmatrix} \{A_m\} \\ \{B_m\} \end{Bmatrix}
$$

$$
+ \int_0^{2\pi} \left( p_7 [k]_4^0 + p_8 [k]_4^* + p_9 [k]_2 \right) \mathrm{d}\vartheta \begin{Bmatrix} \{C_m\} \\ \{D_m\} \end{Bmatrix}
$$

$$
+ \int_0^{2\pi} \left( q_7 [k]_5^0 + q_8 \left( [k]_1 + [k]_6^0 \right) + q_9 [k]_4^* + q_{10} [k]_4^0 + q_{11} [k]_2 \right) \mathrm{d}\vartheta \begin{Bmatrix} \{E_m\} \\ \{F_m\} \end{Bmatrix}
$$

$$
\begin{Bmatrix} \dfrac{\partial E_S}{\{\partial C_k\}} \\[2mm] \dfrac{\partial E_S}{\{\partial D_k\}} \end{Bmatrix} = \int_0^{2\pi} \left( p_7 [k]_4^* + p_8 [k]_4^0 + p_9 [k]_2 \right) \mathrm{d}\vartheta \begin{Bmatrix} \{A_m\} \\ \{B_m\} \end{Bmatrix}
$$

$$
+ \int_0^{2\pi} \left( p_4 [k]_1 + p_5 [k]_2 + p_6 [k]_3 \right) \mathrm{d}\vartheta \begin{Bmatrix} \{C_m\} \\ \{D_m\} \end{Bmatrix}
$$

$$
+ \int_0^{2\pi} \left( q_{12} [k]_6^0 + q_{13} [k]_1 + q_{14} [k]_4^* + q_{15} [k]_4^0 + q_{16} [k]_2 \right) \mathrm{d}\vartheta \begin{Bmatrix} \{E_m\} \\ \{F_m\} \end{Bmatrix}
$$

$$
\begin{Bmatrix} \dfrac{\partial E_S}{\{\partial E_k\}} \\[2mm] \dfrac{\partial E_S}{\{\partial F_k\}} \end{Bmatrix} = \int_0^{2\pi} \left( q_7 [k]_5^* + q_8 \left( [k]_1 + [k]_6^* \right) + q_9 [k]_4^0 + q_{10} [k]_4^* + q_{11} [k]_2 \right) \mathrm{d}\vartheta \begin{Bmatrix} \{A_m\} \\ \{B_m\} \end{Bmatrix}
$$

$$
+ \int_0^{2\pi} \left( q_{12} [k]_6^* + q_{13} [k]_1 + q_{14} [k]_4^0 + q_{15} [k]_4^* + q_{16} [k]_2 \right) \mathrm{d}\vartheta \begin{Bmatrix} \{C_m\} \\ \{D_m\} \end{Bmatrix}
$$

$$
+ \int_0^{2\pi} \left( q_1 [k]_7 + q_2 [k]_1 + q_3 [k]_2 + q_4 [k]_8 + q_5 [k]_9 + q_6 [k]_3 \right) \mathrm{d}\vartheta \begin{Bmatrix} \{E_m\} \\ \{F_m\} \end{Bmatrix},
$$

$$(16)$$

where $p_i(\vartheta), i = 1, 2...9$ and $q_i(\vartheta), i = 1, 2...16$ are variable coefficients, depending on the meridional coordinate $\vartheta$, specified in Appendix A. Submatrices $[k]_i$, whose elements are products of sine and cosine functions or their derivatives per $\vartheta$, are listed in Appendix C.

The system of three matrix equations (16) can be presented in a condensed form

$$\frac{\partial E_S}{\partial \{\delta\}} = [K]\{\delta\},\tag{17}$$

where

$$\{\delta\}^T = \langle\delta\rangle = \left\langle \langle A_m \rangle \langle B_m \rangle \langle C_m \rangle \langle D_m \rangle \langle E_m \rangle \langle F_m \rangle \right\rangle\tag{18}$$

is the vector of the Fourier coefficients, and

$$[K] = \begin{bmatrix} [K]_{11} & [K]_{12} & [K]_{13} \\ [K]_{21} & [K]_{22} & [K]_{23} \\ [K]_{31} & [K]_{32} & [K]_{33} \end{bmatrix}\tag{19}$$

is the stiffness matrix. Submatrices $[K]_{ij}, i, j = 1, 2, 3$ encompass the integrals in Eqs. (16).

### 3.3 Geometric stiffness matrix

Geometric stiffness matrix is derived from the strain energy component, which is due to pre-stressing, Eq. (12). Substituting expressions (14) for displacements into (12) and differentiating it per the Fourier coefficients, the following three matrix equations are obtained

$$
\begin{Bmatrix} \dfrac{\partial E_G}{\{\partial A_k\}} \\[2ex] \dfrac{\partial E_G}{\{\partial B_k\}} \end{Bmatrix} = \int\limits_0^{2\pi} \left( c_1 [k]_1 + c_2 [k]_2 \right) \mathrm{d}\vartheta \begin{Bmatrix} \{A_m\} \\ \{B_m\} \end{Bmatrix} + \int\limits_0^{2\pi} c_8 [k]_2 \, \mathrm{d}\vartheta \begin{Bmatrix} \{C_m\} \\ \{D_m\} \end{Bmatrix}
$$

$$
+ \int\limits_0^{2\pi} \left( c_9 \left( [k]_4^0 - [k]_4^* \right) + c_{10} [k]_2 \right) \mathrm{d}\vartheta \begin{Bmatrix} \{E_m\} \\ \{F_m\} \end{Bmatrix}
$$

$$
\begin{Bmatrix} \dfrac{\partial E_G}{\{\partial C_k\}} \\[2ex] \dfrac{\partial E_G}{\{\partial D_k\}} \end{Bmatrix} = \int\limits_0^{2\pi} c_8 [k]_2 \, \mathrm{d}\vartheta \begin{Bmatrix} \{A_m\} \\ \{B_m\} \end{Bmatrix} + \int\limits_0^{2\pi} \left( c_3 [k]_1 + c_4 [k]_2 + c_5 \left( [k]_4^0 + [k]_4^* \right) \right) \mathrm{d}\vartheta \begin{Bmatrix} \{C_m\} \\ \{D_m\} \end{Bmatrix}
$$

$$
+ \int\limits_0^{2\pi} c_{11} [k]_2 \, \mathrm{d}\vartheta \begin{Bmatrix} \{E_m\} \\ \{F_m\} \end{Bmatrix}
$$

$$
\begin{Bmatrix} \dfrac{\partial E_G}{\{\partial E_k\}} \\[2ex] \dfrac{\partial E_G}{\{\partial F_k\}} \end{Bmatrix} = \int\limits_0^{2\pi} \left( c_9 \left( [k]_4^* - [k]_4^0 \right) + c_{10} [k]_2 \right) \mathrm{d}\vartheta \begin{Bmatrix} \{A_m\} \\ \{B_m\} \end{Bmatrix} + \int\limits_0^{2\pi} c_{11} [k]_2 \, \mathrm{d}\vartheta \begin{Bmatrix} \{C_m\} \\ \{D_m\} \end{Bmatrix}
$$

$$
+ \int\limits_0^{2\pi} \left( c_6 [k]_1 + c_7 [k]_2 \right) \mathrm{d}\vartheta \begin{Bmatrix} \{E_m\} \\ \{F_m\} \end{Bmatrix}, \tag{20}
$$

where variable coefficients $c_i(\vartheta)$, $i = 1, 2 \ldots 11$ are specified in Appendix B, and submatrices $[k]_i$ are given in Appendix C.

The system of three matrix equations (20) can be presented in a condensed form by following the layout of Eq. (17)

$$\frac{\partial E_G}{\partial \{\delta\}} = [G]\{\delta\}, \tag{21}$$

where

$$[G] = \begin{bmatrix} [G]_{11} & [G]_{12} & [G]_{13} \\ [G]_{21} & [G]_{22} & [G]_{23} \\ [G]_{31} & [G]_{32} & [G]_{33} \end{bmatrix} \tag{22}$$

is the geometric stiffness matrix. Submatrices $[G]_{ij}$, $i, j = 1, 2, 3$ now represent the integrals in Eqs. (20).

According to the composition of the membrane forces $N_\vartheta$ and $N_\varphi$, Section 5.1, and the formulation of coefficients $c_i(\vartheta)$, Eqs. (B1), the geometric stiffness matrix can be split into two matrices, *i.e.* one due to the internal pressure, and the other related to the centrifugal forces, *i.e.*

$$[G] = p[G]_p + \Omega^2 [G]_\Omega. \tag{23}$$

## 3.4 Mass matrices

Mass matrices are derived from the kinetic energy, Eq. (13). By substituting expressions (14) into (13), and differentiating the kinetic energy per the Fourier coefficients, one obtains the following system of algebraic equations

$$
\begin{Bmatrix} \dfrac{\partial E_k}{\{\partial A_k\}} \\[2ex] \dfrac{\partial E_k}{\{\partial B_k\}} \end{Bmatrix} = \alpha \int_0^{2\pi} r\left(\omega^2 + \Omega^2 \cos^2 \vartheta\right)[k]_2 \, \mathrm{d}\vartheta \begin{Bmatrix} \{A_m\} \\ \{B_m\} \end{Bmatrix}
$$

$$
+ 2\alpha\omega\Omega \int_0^{2\pi} r\cos\vartheta [k]_2 \, \mathrm{d}\vartheta \begin{Bmatrix} \{C_m\} \\ \{D_m\} \end{Bmatrix}
$$

$$
+ \alpha\Omega^2 \int_0^{2\pi} r\sin\vartheta\cos\vartheta [k]_2 \, \mathrm{d}\vartheta \begin{Bmatrix} \{E_m\} \\ \{F_m\} \end{Bmatrix}
$$

$$
\begin{Bmatrix} \dfrac{\partial E_k}{\{\partial C_k\}} \\[2ex] \dfrac{\partial E_k}{\{\partial D_k\}} \end{Bmatrix} = 2\alpha\omega\Omega \int_0^{2\pi} r\cos\vartheta [k]_2 \, \mathrm{d}\vartheta \begin{Bmatrix} \{A_m\} \\ \{B_m\} \end{Bmatrix}
$$

$$
+ \alpha(\omega^2 + \Omega^2) \int_0^{2\pi} r[k]_2 \, \mathrm{d}\vartheta \begin{Bmatrix} \{C_m\} \\ \{D_m\} \end{Bmatrix}
$$

$$
+ 2\alpha\omega\Omega \int_0^{2\pi} r\sin\vartheta [k]_2 \, \mathrm{d}\vartheta \begin{Bmatrix} \{E_m\} \\ \{F_m\} \end{Bmatrix}
$$

$$
\begin{Bmatrix} \dfrac{\partial E_k}{\{\partial E_k\}} \\[2ex] \dfrac{\partial E_k}{\{\partial F_k\}} \end{Bmatrix} = \alpha\Omega^2 \int_0^{2\pi} r\sin\vartheta\cos\vartheta [k]_2 \, \mathrm{d}\vartheta \begin{Bmatrix} \{A_m\} \\ \{B_m\} \end{Bmatrix} \tag{24}
$$

$$
+ 2\alpha\omega\Omega \int_0^{2\pi} r\sin\vartheta [k]_2 \, \mathrm{d}\vartheta \begin{Bmatrix} \{C_m\} \\ \{D_m\} \end{Bmatrix}
$$

$$
+ \alpha \int_0^{2\pi} r\left(\omega^2 + \Omega^2 \sin^2 \vartheta\right)[k]_2 \, \mathrm{d}\vartheta \begin{Bmatrix} \{E_m\} \\ \{F_m\} \end{Bmatrix},
$$

where $\alpha = \pi \rho h a$. The three matrix equations (16) can be presented in the form

$$\frac{\partial E_k}{\partial \{\delta\}} = \left( \Omega^2 [B] + \omega \Omega [C] + \omega^2 [M] \right) \{\delta\},$$

(25)

where

$$[B] = \begin{bmatrix} [B]_{11} & [0] & [B]_{13} \\ [0] & [B]_{22} & [0] \\ [B]_{31} & [0] & [B]_{33} \end{bmatrix}$$

$$[C] = \begin{bmatrix} [0] & [C]_{12} & [0] \\ [C]_{21} & [0] & [C]_{23} \\ [0] & [C]_{32} & [0] \end{bmatrix}$$

(26)

$$[M] = \begin{bmatrix} [M]_{11} & [0] & [0] \\ [0] & [M]_{22} & [0] \\ [0] & [0] & [M]_{33} \end{bmatrix}$$

are mass matrices related to the centrifugal force $(\Omega^2)$, the Coriolis force $(\omega \Omega)$, and the ordinary inertia force $(\omega^2)$. Submatrices $[B]_{ij}, [C]_{ij}$ and $[M]_{ij}, i, j = 1, 2, 3$ are specified in Appendix D. All of them depend on the symmetric matrix $[k]_2$, Appendix C. Therefore, all mass matrices (19), including the Coriolis matrix, are symmetric.

### 3.5 Matrix equation of motion and buckling

If a linear conservative dynamic system vibrates at its natural frequency, then it interchanges vibration energy from a purely potential state with the maximum strain energy, $E_{s\max}$, to a purely kinetic state where the kinetic energy is maximum $E_{k\max}$, [23]. Hence, the difference of the maximum energies, $\Pi = E_{s\max} - E_{k\max}$, equals zero. If these energies are determined for approximated mode shapes, then the difference $\Pi$ is not zero. However, for a successful approximation of the true mode shape, it should be as close to zero as possible.

In the considered case of a rotating toroidal shell, the balance of energies reads

$$\Pi = E_S + E_G - E_k \, . \tag{27}$$

Here, the situation is somewhat different, since all the terms on the right-hand side are time-invariant. This time-invariance is only due to the fact that fixed mode profiles rotate around the axis of symmetry of the torus. Natural frequency is in fact the speed of this rotation. Then the integration over the circumferential coordinate eliminates temporal variations since it is irrelevant how the mode profile is positioned with reference to $\varphi = 0$. Nevertheless, each particle on the shell still undergoes motions where minima and maxima of the displacement and velocity are interchanged. If the modes are determined approximately with truncated series, the governing equation of motion can still be obtained from the minimum total energy principle [23]

$$\frac{\partial \Pi}{\partial \{\delta\}} = \frac{\partial E_S}{\partial \{\delta\}} + \frac{\partial E_G}{\partial \{\delta\}} - \frac{\partial E_k}{\partial \{\delta\}} = \{0\} \, . \tag{28}$$

Taking into account relations (17), (21) with (23), and (25) respectively, one obtains the following matrix equation for natural vibrations

$$\left([K] + p[G]_p + \Omega^2 \left([G]_\Omega - [B]\right) - \omega\Omega[C] - \omega^2[M]\right)\{\delta\} = \{0\} \, . \tag{29}$$

The matrix [C] multiplying the mixed $\omega\Omega$ term, which results from the Coriolis term in the kinetic energy expression(13), is the only one causing a bifurcation of natural frequencies. The geometric stiffness matrix $[G]_\Omega$ and the mass matrix $[B]$ are related to the centrifugal force with stiffening and softening effect respectively.

If a toroidal shell is exposed to influence of the external pressure, it can lose stability. The corresponding matrix equation of buckling for determining critical pressure is deduced from (29), i.e., [25]

$$\left([K] - p[G]_p\right)\{\delta\} = \{0\} \, . \tag{30}$$

### 3.6 Open toroidal shell

The previous consideration is related to a closed toroidal shell, Fig. 5. In case of an open toroidal shell shown in Fig. 6, the convention of meridional coordinate is changed. Now the $\vartheta$ angle is measured from the shell top due to reason of simplicity. The central angle reads $2\vartheta_0$, Fig. 6.
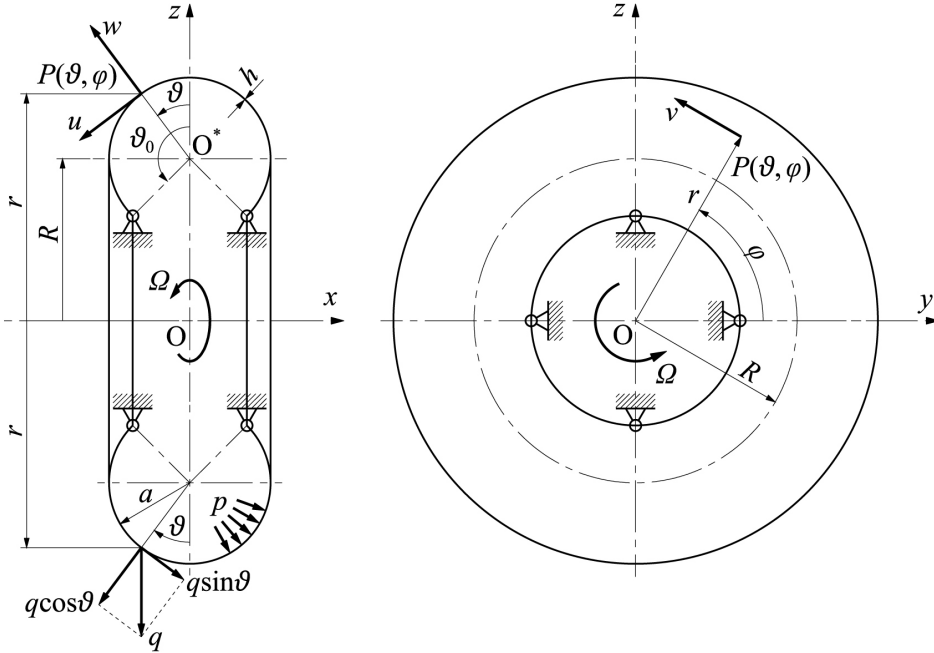


**Fig. 6.** Simply supported open toroidal shell, main dimensions and displacements
***Sl. 6.*** *Slobodno oslonjena otvorena toroidna ljuska, glavne izmjere i pomaci*

A simply supported toroidal shell is analysed, and the meridional displacement functions can also be assumed in the form of the trigonometric series (14). The coordinate functions have to satisfy boundary conditions $U(\vartheta) = V(\vartheta) = W(\vartheta) = 0$ at $\vartheta = \pm\vartheta_0$. This is the achieved setting:

$$f_m = \cos \xi_m \vartheta, \quad g_m = \sin \eta_m \vartheta,$$

$$\xi_m = m\frac{\pi}{2\vartheta_0}, \quad \eta_m = (m+1)\frac{\pi}{2\vartheta_0}, \quad m = 1,3,5...N. \tag{31}$$

The formulation of the stiffness and mass matrices is the same as in the case of closed toroidal shell. Variable stiffness coefficients $p_i(\vartheta)$, $q_i(\vartheta)$ and $c_i(\vartheta)$, Appendices A and B, as well as the mass matrices, Eqs (24) have to be adopted due to the change of $\vartheta$ angle convention. Accordingly, $\sin\vartheta$ is replaced with $\cos\vartheta$, and $\cos\vartheta$ with $-\sin\vartheta$. The integration domain of the meridional coordinate is now changed from $0 \le \vartheta \le 2\pi$ to $-\vartheta_0 \le \vartheta \le \vartheta_0$.

## 4. FINITE STRIP METHOD

### 4.1 Shape functions

The two-node finite strip of a toroidal shell is shown in Fig. 7. It is used to discretise the shell in the meridional direction, and it has 8 degrees of freedom (d.o.f.). The strip follows the shell meridional curvature with radius $a$, and is defined by the central angle $\gamma = \vartheta_2 - \vartheta_1$. The strip properties are derived using the energy approach.
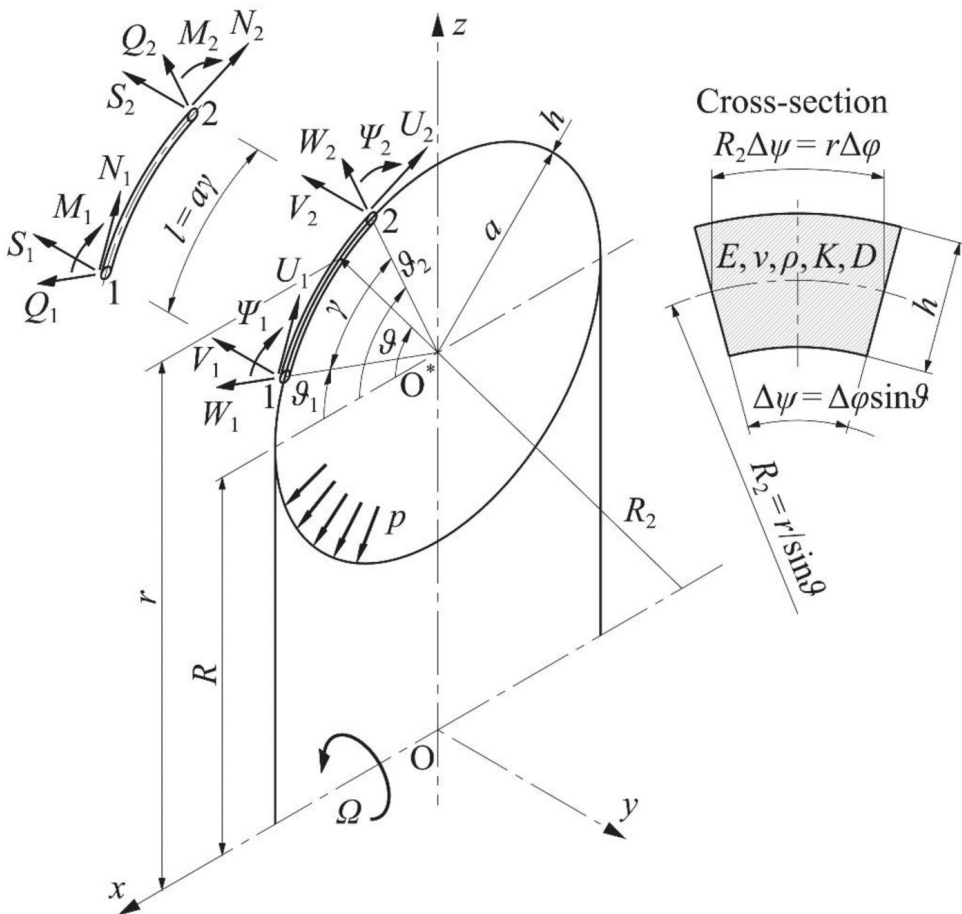


**Fig. 7.** The finite strip nodal displacements and forces
***Sl. 7.*** Pomaci i sile vrpčastog elementa torusne ljuske

The strip displacements are approximated by the following interpolation functions:

$$U(\vartheta) = \sum_{j=1}^{2} U_j g_j(\vartheta), \quad V(\vartheta) = \sum_{j=1}^{2} V_j g_j(\vartheta), \quad W(\vartheta) = \sum_{j=1}^{4} \Delta_j f_j(\vartheta), \quad (32)$$

where nodal displacements, Fig. 7, can be presented through the following three vectors:

$$\{U\} = \begin{Bmatrix} U_1 \\ U_2 \end{Bmatrix}, \quad \{V\} = \begin{Bmatrix} V_1 \\ V_2 \end{Bmatrix}, \quad \{\Delta\} = \begin{Bmatrix} W_1 \\ \Psi_1 \\ W_2 \\ \Psi_2 \end{Bmatrix}. \quad (33)$$

The cross-sectional rotation due to bending is designated by $\psi = -dW / (a\,d\vartheta)$, Fig. 7. The in-surface displacements are interpolated by polynomial bar shape functions, whereas the bending deflections are interpolated by the beam shape functions (Hermitian polynomials):

$$\begin{aligned}
g_1 &= 1 - \xi, \quad g_2 = \xi \\
f_1 &= 1 - \xi^2(3 - 2\xi), \quad f_2 = -a\gamma\xi(1 - \xi)^2, \\
f_3 &= \xi^2(3 - 2\xi), \quad f_4 = a\gamma\xi^2(1 - \xi),
\end{aligned} \quad (34)$$

where

$$\xi = \frac{\vartheta - \vartheta_1}{\gamma} \quad (35)$$

is the normalised strip angle, and $\gamma = \vartheta_2 - \vartheta_1$ is the strip central angle, so that $\xi$ is the strip arch dimensionless coordinate within a domain $0 \le \xi \le 1$.

## 4.2 Stiffness matrix

Substituting expressions (32) into the strain energy equation (11) and differentiating by nodal displacements, the following system of eight algebraic equations is obtained:

$$
\left\{\frac{\partial E_s}{\partial U_i}\right\}_{i=1,2} = \int_{\vartheta_1}^{\vartheta_2}\left(p_1[k]_1 + p_2[k]_2 + p_3[k]_3\right)\mathrm{d}\vartheta\{\mathrm{U}\}
$$

$$
+ \int_{\vartheta_1}^{\vartheta_2}\left(p_7[k]_{13} + p_8[k]_{14} + p_9[k]_{15}\right)\mathrm{d}\vartheta\{\mathrm{V}\}
$$

$$
+ \int_{\vartheta_1}^{\vartheta_2}\left(q_7[k]_{16} + q_8[k]_{17} + q_9[k]_{18} + q_{10}[k]_{19} + q_{11}[k]_{20}\right)\mathrm{d}\vartheta\{\Delta\}
$$

$$
\left\{\frac{\partial E_s}{\partial V_i}\right\}_{i=1,2} = \int_{\vartheta_1}^{\vartheta_2}\left(p_4[k]_4 + p_5[k]_5 + p_6[k]_6\right)\mathrm{d}\vartheta\{\mathrm{V}\}
$$

$$
+ \int_{\vartheta_1}^{\vartheta_2}\left(p_7[k]_{13}^T + p_8[k]_{14}^T + p_9[k]_{15}^T\right)\mathrm{d}\vartheta\{\mathrm{U}\} \tag{36}
$$

$$
+ \int_{\vartheta_1}^{\vartheta_2}\left(q_{12}[k]_{21} + q_{13}[k]_{22} + q_{14}[k]_{23} + q_{15}[k]_{24} + q_{16}[k]_{25}\right)\mathrm{d}\vartheta\{\Delta\}
$$

$$
\left\{\frac{\partial E_s}{\partial \Delta_i}\right\}_{i=1,2,3,4} = \int_{\vartheta_1}^{\vartheta_2}\left(q_1[k]_7 + q_2[k]_8 + q_3[k]_9 + q_4[k]_{10} + q_5[k]_{11} + q_6[k]_{12}\right)\mathrm{d}\vartheta\{\Delta\}
$$

$$
+ \int_{\vartheta_1}^{\vartheta_2}\left(q_7[k]_{16}^T + q_8[k]_{17}^T + q_9[k]_{18}^T + q_{10}[k]_{19}^T + q_{11}[k]_{20}^T\right)\mathrm{d}\vartheta\{\mathrm{U}\}
$$

$$
+ \int_{\vartheta_1}^{\vartheta_2}\left(q_{12}[k]_{21}^T + q_{13}[k]_{22}^T + q_{14}[k]_{23}^T + q_{15}[k]_{24}^T + q_{16}[k]_{25}^T\right)\mathrm{d}\vartheta\{\mathrm{V}\}.
$$

Variable coefficients $p_i(\vartheta), i = 1, 2...9$ and $q_i(\vartheta), i = 1, 2...16$, are specified in Appendix A. Elements of the submatrices $[k]_i, i = 1, 2...25$ are products of the shape functions (34) and their spatial derivatives. Equations (36) can be presented in the matrix notation as

$$\frac{\partial E_S}{\partial \{\delta\}} = [K]\{\delta\}, \tag{37}$$

where

$$\{\delta\}^T = \langle \delta \rangle = \langle U_1 \quad U_2 \quad V_1 \quad V_2 \quad W_1 \quad \Psi_1 \quad W_2 \quad \Psi_2 \rangle \tag{38}$$

is the vector of nodal displacements, Fig. 7, and

$$[K] = \begin{bmatrix} [K]_{11}^* & [K]_{12}^* & [K]_{13}^* \\ [K]_{21}^* & [K]_{22}^* & [K]_{23}^* \\ [K]_{31}^* & [K]_{32}^* & [K]_{33}^* \end{bmatrix} \tag{39}$$

is the stiffness matrix, where

$$[K]_{11}^* = \sum_{i=1}^{3} [K]_i$$

$$[K]_{22}^* = \sum_{i=4}^{6} [K]_i$$

$$[K]_{33}^* = \sum_{i=7}^{12} [K]_i$$

$$[K]_{12}^* = \sum_{i=13}^{15} [K]_i \tag{40}$$

$$[K]_{13}^* = \sum_{i=16}^{20} [K]_i$$

$$[K]_{23}^* = \sum_{i=21}^{25} [K]_i$$

$$[K]_{21}^* = \left([K]_{12}^*\right)^T, \quad [K]_{31}^* = \left([K]_{13}^*\right)^T, \quad [K]_{32}^* = \left([K]_{23}^*\right)^T.$$

Submatrices $[K]_i$, $i = 1, 2 \ldots 25$ are given in Appendix E.

## 4.3 Geometric stiffness matrix

The geometric stiffness matrix is derived from the strain energy due to pre-stressing. Substituting expressions (32) for displacements into (12) and differentiating by nodal displacements, a system of eight algebraic equations is obtained

$$
\left\{ \frac{\partial E_G}{\partial U_i} \right\}_{i=1,2} = \int_{\vartheta_1}^{\vartheta_2} \left( c_1 [g]_1 + c_2 [g]_2 \right) \mathrm{d}\vartheta \{U\} + \int_{\vartheta_1}^{\vartheta_2} c_8 [g]_8 \, \mathrm{d}\vartheta \{V\}
$$

$$
+ \int_{\vartheta_1}^{\vartheta_2} \left( c_9 [g]_9 + c_{10} [g]_{10} \right) \mathrm{d}\vartheta \{\Delta\}
$$

$$
\left\{ \frac{\partial E_G}{\partial V_i} \right\}_{i=1,2} = \int_{\vartheta_1}^{\vartheta_2} \left( c_3 [g]_3 + c_4 [g]_4 + c_5 [g]_5 \right) \mathrm{d}\vartheta \{V\}
$$

$$
+ \int_{\vartheta_1}^{\vartheta_2} c_8 [g]_8^T \, \mathrm{d}\vartheta \{U\} + \int_{\vartheta_1} c_{11} [g]_{11} \, \mathrm{d}\vartheta \{\Delta\}
$$

$$
\left\{ \frac{\partial E_G}{\partial \Delta_i} \right\}_{i=1,2,3,4} = \int_{\vartheta_1}^{\vartheta_2} \left( c_6 [g]_6 + c_7 [g]_7 \right) \mathrm{d}\vartheta \{\Delta\}
$$

$$
+ \int_{\vartheta_1}^{\vartheta_2} \left( c_9 [g]_9^T + c_{10} [g]_{10}^T \right) \mathrm{d}\vartheta \{U\} + \int_{\vartheta_1} c_{11} [g]_{11}^T \, \mathrm{d}\vartheta \{V\}.
$$

(41)

Variable coefficients $c_i(\vartheta)$, $i = 1, 2 \ldots 11$ are specified in Appendix B. Elements of the submatrices $[g]_i$, $i = 1, 2 \ldots 11$ are again products of the shape functions (34) and their spatial derivatives.

The system of algebraic equations (41) can be presented in a matrix notation

$$
\frac{\partial E_G}{\partial \{\delta\}} = [G]\{\delta\},
$$

(42)

where $\{\delta\}$ is the vector of nodal displacements, Eq. (38). The geometric stiffness matrix reads

$$[G] = \begin{bmatrix} [G]_1 + [G]_2 & [G]_8 & [G]_9 + [G]_{10} \\ [G]_8^T & [G]_3 + [G]_4 + [G]_5 & [G]_{11} \\ [G]_9^T + [G]_{10}^T & [G]_{11}^T & [G]_6 + [G]_7 \end{bmatrix}, \tag{43}$$

where submatrices $[G]_i$, $i = 1, 2 \dots 11$ are specified in Appendix F.

## 4.4 Mass matrices

Mass matrices are derived from the expression for the kinetic energy, Eq. (13). Substituting expressions (32) into (13), and differentiating the kinetic energy by nodal displacements, one obtains the following system of eight algebraic equations:

$$\left\{ \frac{\partial E_k}{\partial U_i} \right\}_{i=1,2} = \omega^2 \int_{\vartheta_1}^{\vartheta_2} d_1 [m]_1 \, d\vartheta \{U\} + \Omega^2 \int_{\vartheta_1}^{\vartheta_2} d_2 [m]_3 \, d\vartheta \{U\}$$

$$+ 2\omega\Omega \int_{\vartheta_1}^{\vartheta_2} d_4 [m]_6 \, d\vartheta \{V\} + \Omega^2 \int_{\vartheta_1}^{\vartheta_2} d_6 [m]_5 \, d\vartheta \{\Delta\}$$

$$\left\{ \frac{\partial E_k}{\partial V_i} \right\}_{i=1,2} = (\omega^2 + \Omega^2) \int_{\vartheta_1}^{\vartheta_2} d_1 [m]_1 \, d\vartheta \{V\} + 2\omega\Omega \int_{\vartheta_1}^{\vartheta_2} d_4 [m]_6 \, d\vartheta \{U\}$$

$$+ 2\omega\Omega \int_{\vartheta_1}^{\vartheta_2} d_5 [m]_7 \, d\vartheta \{\Delta\} \tag{44}$$

$$\left\{ \frac{\partial E_k}{\partial \Delta_i} \right\}_{i=1,2,3,4} = \omega^2 \int_{\vartheta_1}^{\vartheta_2} d_1 [m]_2 \, d\vartheta \{\Delta\} + \Omega^2 \int_{\vartheta_1}^{\vartheta_2} d_3 [m]_4 \, d\vartheta \{\Delta\}$$

$$+ 2\omega\Omega \int_{\vartheta_1}^{\vartheta_2} d_5 [m]_7^T \, d\vartheta \{V\} + \Omega^2 \int_{\vartheta_1}^{\vartheta_2} d_6 [m]_5^T \, d\vartheta \{U\}.$$

The variable coefficients in (44) are the following:

$$d_1 = \pi \rho h a r$$
$$d_2 = \pi \rho h a r \cos^2 \vartheta$$
$$d_3 = \pi \rho h a r \sin^2 \vartheta$$
$$d_4 = \pi \rho h a r \cos \vartheta \tag{45}$$
$$d_5 = \pi \rho h a r \sin \vartheta$$
$$d_6 = \pi \rho h a r \sin \vartheta \cos \vartheta.$$

The elements of the submatrices $[m]_i$, $i = 1, 2 ... 7$ are products of the shape functions (34) and their spatial derivatives.

The system of algebraic equations (44) can be split into three matrices, which are multiplied by the squared rotational speed, by a squared natural frequency, or by a product of the rotational speed and a natural frequency as follows:

$$\frac{\partial E_k}{\partial \{\delta\}} = \left( \Omega^2 [B] + \omega \Omega [C] + \omega^2 [M] \right) \{\delta\}, \tag{46}$$

where

$$[B] = \begin{bmatrix} [M]_3 & [0] & [M]_5 \\ [0] & [M]_1 & [0] \\ [M]_5^T & [0] & [M]_4 \end{bmatrix} \tag{47}$$

$$[C] = \begin{bmatrix} [0] & [M]_6 & [0] \\ [M]_6 & [0] & [M]_7 \\ [0] & [M]_7^T & [0] \end{bmatrix} \tag{48}$$

$$[M] = \begin{bmatrix} [M]_1 & [0] & [0] \\ [0] & [M]_1 & [0] \\ [0] & [0] & [M]_2 \end{bmatrix} \tag{49}$$

are the mass matrices due to the centrifugal force, due to the Coriolis force, and due to the inertial force, respectively. Submatrices $[M]_i, i = 1, 2...7$ are specified in Appendix G.

### 4.5 Finite strip equation

In the natural vibration, the total strain energy equals the total kinetic energy. However, these energies are not balanced at the finite strip level. Their difference is compensated with the work of nodal forces

$$W_F = -\langle \delta \rangle \{F\},$$  (50)

where $\langle \delta \rangle$ is the vector of nodal displacements, Eq. (38), and

$$\{F\}^T = \langle F \rangle = \langle N_1 \quad N_2 \quad S_1 \quad S_2 \quad Q_1 \quad M_1 \quad Q_2 \quad M_2 \rangle$$  (51)

is the vector of the corresponding nodal forces, in which $N_i$ and $S_i$, $i = 1, 2$ are the tension and in-plane shear forces, while $Q_i$ and $M_i$, $i = 1, 2$ are the transverse shear forces and bending moments, respectively, Fig. 7. Hence, one can write the energy balance

$$\Pi = E_S + E_G - E_k + W_F,$$  (52)

where $\Pi = 0$ for exact values of the energies. Since the displacement field within a finite strip is described approximately by the shape functions, $\Pi$ has to be minimum, referring to the minimum total energy principle, [23], i.e. $\partial \Pi / \partial \{\delta\} = \{0\}$. Satisfying this condition yields

$$\{F\} = \frac{\partial E_S}{\partial \{\delta\}} + \frac{\partial E_G}{\partial \{\delta\}} - \frac{\partial E_k}{\partial \{\delta\}}.$$  (53)

Substituting Eqs. (37), (42) and (46) into (53), the finite strip equation is obtained in the following form:

$$\{F\} = \left([K] + p[G]_p + \Omega^2\left([G]_\Omega - [B]\right) - \omega\Omega[C] - \omega^2[M]\right)\{\delta\}. \tag{54}$$

Hardening centrifugal geometric stiffness matrix $[G]_\Omega$ is dominant with respect to the softening centrifugal mass matrix $[B]$. Therefore, the increase in the shell rotation speed generally increases the values of natural frequencies. Furthermore, the Coriolis term with $\omega\Omega$ causes bifurcations of natural frequencies.

### 4.6 The assembly of finite strips

In order to increase the accuracy of the vibration analysis, the shell should be modelled by a large number of finite strips. Before assembling, the finite strip equation (54) has to be rearranged in such a way that the nodal displacements and the nodal forces, Eqs. (38) and (51), are first set up for node 1, and then for node 2, i.e.

$$
\begin{aligned}
\left\langle \tilde{\delta} \right\rangle &= \left\langle U_1 \quad V_1 \quad W_1 \quad \Psi_1 \quad U_2 \quad V_2 \quad W_2 \quad \Psi_2 \right\rangle \\
\left\langle \tilde{F} \right\rangle &= \left\langle N_1 \quad S_1 \quad Q_1 \quad M_1 \quad N_2 \quad S_2 \quad Q_2 \quad M_2 \right\rangle.
\end{aligned}
\tag{55}
$$

This implies the rearrangement of the rows and columns of all matrices in Eq. (54) accordingly.

Since the finite strip is curved and defined in the polar coordinate system, the strip equations can be assembled directly like links of a chain. This is also valid for shell structures consisting of different shell segments in case they have the same slope angle at the joints. Otherwise, the finite strip equation has to be transformed from the local (polar) coordinate system into the global (orthogonal) coordinate system of the shell structure.

If vibrations of a closed toroidal shell are analysed, the assembling of the finite strip equations is obtained in a circular form looking like a necklace, Fig. 8a. In order to formulate the eigenvalue problem in the ordinary form, the "necklace" has to be unclasped at a joint and stretched, and the compatibility conditions of displacements at the joint have to be satisfied. This is achieved by superimposing the last rows and columns of the matrix related to the last node, to the first rows and columns related to the first node, Figs. 8b and c.
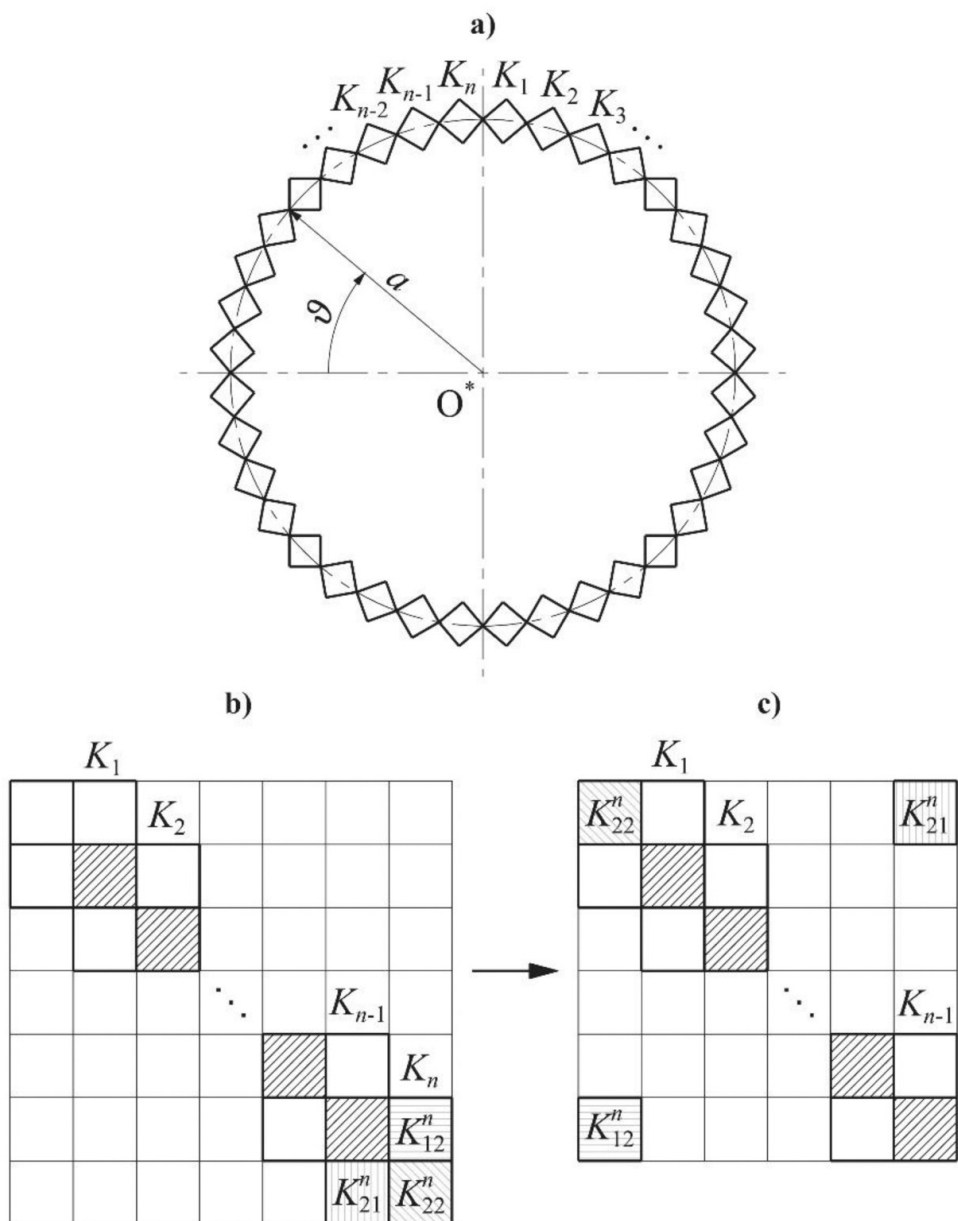
**Fig. 8.** Assembling of finite strip dynamic stiffness matrices of closed toroidal shell
*Sl. 8.* Sprezanje matrica dinamičke krutosti zatvorene torusne ljuske

### 4.7 Finite strip of higher order

Numerical examples show that the convergence of natural frequencies determined in the above way, by employing simple two-node finite strips, is rather slow. To improve the convergence of the results, finite strips of higher order with three nodes are used.

The shape functions of a bar with three nodes reads, [29]

$$
\begin{aligned}
g_1 &= 1 - 3\xi + 2\xi^2 \\
g_2 &= 4\xi(1-\xi) \\
g_3 &= \xi(2\xi - 1).
\end{aligned}
\tag{56}
$$

For a three-node beam, one finds the following shape functions:

$$
\begin{aligned}
f_1 &= 1 - 23\xi^2 + 66\xi^3 - 68\xi^4 + 24\xi^5 \\
f_2 &= -a\gamma\xi\left(1 - 6\xi + 13\xi^2 - 12\xi^3 + 4\xi^4\right) \\
f_3 &= 16\xi^2\left(1 - \xi\right)^2 \\
f_4 &= 8a\gamma\xi^2\left(1 - 4\xi + 5\xi^2 - 2\xi^3\right) \\
f_5 &= \xi^2\left(7 - 34\xi + 52\xi^2 - 24\xi^3\right) \\
f_6 &= a\gamma\xi^2\left(1 - 5\xi + 8\xi^2 - 4\xi^3\right),
\end{aligned}
\tag{57}
$$

where $\gamma = \vartheta_2 - \vartheta_1$, Fig. 3.

The condensation of stiffness matrix of the three-node finite strip to the end nodes is illustrated as follows. The full stiffness matrix reads

$$
\begin{bmatrix}
[K]_{11} & [K]_{12} & [K]_{13} \\
[K]_{21} & [K]_{22} & [K]_{23} \\
[K]_{31} & [K]_{32} & [K]_{33}
\end{bmatrix}
\begin{Bmatrix}
\{\delta\}_1 \\
\{\delta\}_2 \\
\{\delta\}_3
\end{Bmatrix}
= \{0\},
\tag{58}
$$

where $\{\delta\}_i, i = 1, 2, 3$ are the nodal displacement vectors, Eqs. (55). Eq. (58) can be written as a system of three matrix equations. Extracting $\{\delta\}_2$ from the second equation and substituting it into the first and the last one yields the condensed finite strip equation

$$\{F\} = \begin{bmatrix} [K]_{11} - [K]_{11}^* & [K]_{13} - [K]_{12}^* \\ [K]_{31} - [K]_{21}^* & [K]_{33} - [K]_{22}^* \end{bmatrix} \begin{Bmatrix} \{\delta\}_1 \\ \{\delta\}_3 \end{Bmatrix}, \tag{59}$$

where

$$
\begin{aligned}
[K]_{11}^* &= [K]_{12} [K]_{22}^{-1} [K]_{21} \\
[K]_{12}^* &= [K]_{12} [K]_{22}^{-1} [K]_{23} \\
[K]_{21}^* &= [K]_{32} [K]_{22}^{-1} [K]_{21} \\
[K]_{22}^* &= [K]_{32} [K]_{22}^{-1} [K]_{23}.
\end{aligned}
\tag{60}
$$

The stiffness matrix, as well as the geometric stiffness matrix, depend on strains, i.e. on the derivatives of displacements $u$, $v$ and $w$, and are very sensitive to the used interpolation (shape) functions. Therefore, the application of the higher order finite strips is very effective. On the other hand, however, mass matrices depend on the displacements and can be determined by simple two-node finite strips.

## 5. PRE-STRESSING TENSION FORCES

### 5.1 Analytical membrane solution

A toroidal shell can be pre-stressed by uniform internal pressure, *p*, and/or centrifugal load due to rotation, $q = \rho h \Omega^2 r$, Fig. 5. In case of a closed toroidal shell, the generated tension forces can be determined analytically, based on the membrane shell theory, [30]

$$N_{\vartheta p} = \frac{1}{2} pa \frac{2R + a \sin \vartheta}{R + a \sin \vartheta}, \qquad N_{\varphi p} = \frac{1}{2} pa, \tag{61}$$

$$N_{\vartheta \Omega} = 0, \qquad N_{\varphi \Omega} = \rho h \Omega^2 \left( R + a \sin \vartheta \right)^2. \tag{62}$$

Expressions (61) are reliable, since the closed shell bending due to internal pressure is quite small. Eqs. (61) can also be used for a rough approximation of tension forces in an open toroidal shell. On the contrary, the shell bending due to centrifugal load is pronounced, and the corresponding tension forces have to be determined by employing the shell theory, [24] and [26].

### 5.2 Application of the Rayleigh-Ritz method

Closed toroidal shell is exposed to centrifugal load components, Fig. 5

$$q_c = \rho h \Omega^2 r \cos \vartheta, \qquad q_r = \rho h \Omega^2 r \sin \vartheta . \tag{63}$$

An axisymmetric shell deformation is assumed: *u=U, v=V, w=W*. The total energy consists of the strain energy $E_s(U, W)$, Eq. (11) and work of centrifugal load

$$W_q = \int_0^{2\pi} \int_0^{2\pi} \left( q_c U + q_r W \right) ra \, \mathrm{d}\vartheta \mathrm{d}\varphi = 2\pi a \int_0^{2\pi} \left( q_c U + q_r W \right) r \, \mathrm{d}\vartheta . \tag{64}$$

Due to energy balance, the difference of these energies has to be zero in the case of exact solution, and has to take minimum value in the approximate solution. Hence, one can write

$$\Pi = E_s - W_q \ . \tag{65}$$

Substituting Eqs. (63) for load and Eqs. (14) for displacements into (64), the derivatives of the load per the Fourier coefficients read

$$\frac{\partial W_q}{\partial \{\delta\}} = \{F\}, \tag{66}$$

where

$$\langle \delta \rangle = \langle \langle A_m \rangle \langle B_m \rangle \langle E_m \rangle \langle F_m \rangle \rangle \tag{67}$$

$$\langle F \rangle = 2\pi \rho h a \Omega^2 \langle I_{k1}, I_{k2}, I_{k3}, I_{k4} \rangle \tag{68}$$

$$
\begin{aligned}
I_{k1} &= \int_0^{2\pi} r^2 \cos k\vartheta \cos \vartheta \, \mathrm{d}\vartheta \\
I_{k2} &= \int_0^{2\pi} r^2 \sin k\vartheta \cos \vartheta \, \mathrm{d}\vartheta \\
I_{k3} &= \int_0^{2\pi} r^2 \cos k\vartheta \sin \vartheta \, \mathrm{d}\vartheta \\
I_{k4} &= \int_0^{2\pi} r^2 \sin k\vartheta \sin \vartheta \, \mathrm{d}\vartheta .
\end{aligned}
\tag{69}
$$

Using the principle of minimum total energy, [23], (*i.e.* minimum error)

$$\frac{\partial \Pi}{\partial \{\delta\}} = \frac{\partial E_S}{\partial \{\delta\}} - \frac{\partial W_q}{\partial \{\delta\}} = \{0\} \tag{70}$$

and relation (17), a system of non-homogenous algebraic equations is obtained

$$2[K]\{\delta\} = \{F\}. \tag{71}$$

Stiffness matrix, Eq. (19), is reduced to

$$[K] = \begin{bmatrix} [K]_{11} & [K]_{13} \\ [K]_{31} & [K]_{33} \end{bmatrix}. \tag{72}$$

It is multiplied by 2 in Eq. (71), since in derivation of stiffness matrix, Eq. (19), integration for mode wave number $n>0$ is performed resulting in $I = \int_0^{2\pi} \cos^2(n\varphi)\mathrm{d}\varphi = \pi$. However, in the considered case of axisymmetric deformation $n=0$, and $I=2\pi$.

Since the Fourier coefficients $B_0 = F_0 = 0$, the corresponding equations are excluded from the matrix equation (71). For coefficients in the Fourier series characterised by $k=1$, two identical equations are obtained in (71) for $B_1$ and $F_1$, as can be seen in the load terms, Eq. (69). Therefore, one of these equations is omitted in order to avoid the singularity of the stiffness matrix.

By calculating displacements $U$ and $W$, Eqs. (14), it is possible to determine the tension strains, Eqs. (2), and finally the tension forces by employing Hooke's law

$$N_{\vartheta} = \frac{Eh}{1-v^2}\left[\frac{1}{a}\frac{\mathrm{d}U}{\mathrm{d}\vartheta} + \frac{v}{r}U\cos\vartheta + \left(\frac{1}{a} + \frac{v}{r}\sin\vartheta\right)W\right]$$

$$N_{\varphi} = \frac{Eh}{1-v^2}\left[\frac{1}{r}U\cos\vartheta + \frac{v}{a}\frac{\mathrm{d}U}{\mathrm{d}\vartheta} + \left(\frac{1}{r}\sin\vartheta + \frac{v}{a}\right)W\right]. \tag{73}$$

### 5.3 Application of the finite strip method

In general case of an open toroidal shell, the tension forces can be determined numerically by the finite strip method. Work of pressure, $p$, and centrifugal load, Eq. (63), on the corresponding displacement reads

$$W_q = \int\limits_0^{2\pi}\int\limits_{\vartheta_1}^{\vartheta_2} \left[q_c u + (p + q_r)w\right] ar\, \mathrm{d}\vartheta\, \mathrm{d}\varphi \ . \tag{74}$$

The considered statics problem is axisymmetric and $n=0$, $u=U$, $v=V=0$, $w=W$. According to Eqs. (32), the displacements are approximated by the shape functions, $U = \langle U\rangle\{g\}$ and $W = \langle\Delta\rangle\{f\}$. If one substitutes these relations and Eqs. (63) into (74), then integrates (74) per $\varphi$, and finally differentiates it per nodal displacements, the nodal load forces are obtained as

$$\{F\}_q = -\left\{\begin{matrix}\dfrac{\partial W_q}{\partial\{U\}}\\[2mm]\dfrac{\partial W_q}{\partial\{\Delta\}}\end{matrix}\right\} = -2\pi\, pa\int\limits_{\vartheta_1}^{\vartheta_2}\left\{\begin{matrix}0\\0\\rf_1\\rf_2\\rf_3\\rf_4\end{matrix}\right\}\mathrm{d}\vartheta - 2\pi\,\rho h\Omega^2 a\int\limits_{\vartheta_1}^{\vartheta_2}\left\{\begin{matrix}rg_1\cos\vartheta\\rg_2\cos\vartheta\\rf_1\sin\vartheta\\rf_2\sin\vartheta\\rf_3\sin\vartheta\\rf_4\sin\vartheta\end{matrix}\right\}\mathrm{d}\vartheta. \tag{75}$$

The finite strip equation reads

$$\{F\} = 2[K]\{\delta\} + \{F\}_q , \tag{76}$$

where, according to Eqs. (51) and (38), respectively

$$\begin{aligned}\langle F\rangle &= \langle\, N_1 \quad N_2 \quad Q_1 \quad M_1 \quad Q_2 \quad M_2\,\rangle\\ \langle\delta\rangle &= \langle\, U_1 \quad U_2 \quad W_1 \quad \Psi_1 \quad W_2 \quad \Psi_2\,\rangle.\end{aligned} \tag{77}$$

The stiffness matrix according to Eq. (39) is reduced to

$$[K] = \begin{bmatrix} [K]^*_{11} & [K]^*_{13} \\ [K]^*_{31} & [K]^*_{33} \end{bmatrix}. \tag{78}$$

The stiffness matrix $[K]$ in Eq. (76) is multiplied by 2 due to the same reason as in the previous section.

After assembling the finite strips of the complete toroidal shell, the resulting non-homogenous equation

$$[\widetilde{K}]\{\widetilde{\delta}\} = -\{\widetilde{F}\}_q \tag{79}$$

is solved, and the nodal displacements $\{\delta\}$, Eqs. (77), for each finite strip are determined. The tension forces are calculated by Eqs. (73).

## 6. RING VIBRATION THEORY

### 6.1 In-plane vibration

Ring vibration analysis in this paper is based on the toroidal shell theory. For this purpose, a toroidal shell segment in the vicinity of angle $\vartheta = \pi/2$ is considered a ring, as shown in Fig. 9. For the in-plane vibrations, the relevant displacements are the circumferential and the radial ones, $V$ and $W$, [27]. The expressions for the strain energy, the geometric strain energy and the kinetic energy, Eqs. (11), (12) and (13), respectively, are after integration no longer functions of the angle $\vartheta$. Therefore, they are reduced to the following form for a unit length of the arch ($b=1$):

$$E_S = \frac{1}{2} p_5 V^2 + \frac{1}{2} q_3 W^2 + q_{16} VW$$

$$E_G = \frac{1}{2} c_4 V^2 + \frac{1}{2} c_7 W^2 + c_{11} VW \tag{80}$$

$$E_K = \frac{1}{2} \alpha \left[ \left( \omega^2 + \Omega^2 \right) V^2 + \left( \omega^2 + \Omega^2 \right) W^2 + 4\omega\Omega VW \right],$$

where $\alpha = \pi\rho\, har$. The terms in $E_K$ with $\Omega^2$ and $\Omega$ represent the kinetic energy due to the centrifugal and the Coriolis forces, respectively. Coefficients $p_i$, $q_i$ and $c_i$ in (80) are specified according to Appendices A and C, taking into account that $\vartheta = \pi/2$ and $v = 0$ for the ring as a one-dimensional structural element

$$\frac{p_5}{\alpha} = \frac{K}{\rho h r^2} n^2 \left( 1 + \frac{D}{K r^2} \right)$$

$$\frac{q_3}{\alpha} = \frac{K}{\rho h r^2} \left( 1 + n^4 \frac{D}{K r^2} \right)$$

$$\frac{q_{16}}{\alpha} = \frac{K}{\rho h r^2} n \left( 1 + n^2 \frac{D}{K r^2} \right) \tag{81}$$

$$\frac{c_4}{\alpha} = \frac{c_7}{\alpha} = \left( n^2 + 1 \right) \Omega^2$$

$$\frac{c_{11}}{\alpha} = 2n\Omega^2 \,,$$

where

$$K = Eh, \quad D = \frac{Eh^3}{12}.$$

(82)

The coefficients $c_4$, $c_7$ and $c_{11}$ take into account the pre-stressing membrane force $N_\varphi = \rho h r^2 \Omega^2$ due to the centrifugal load.
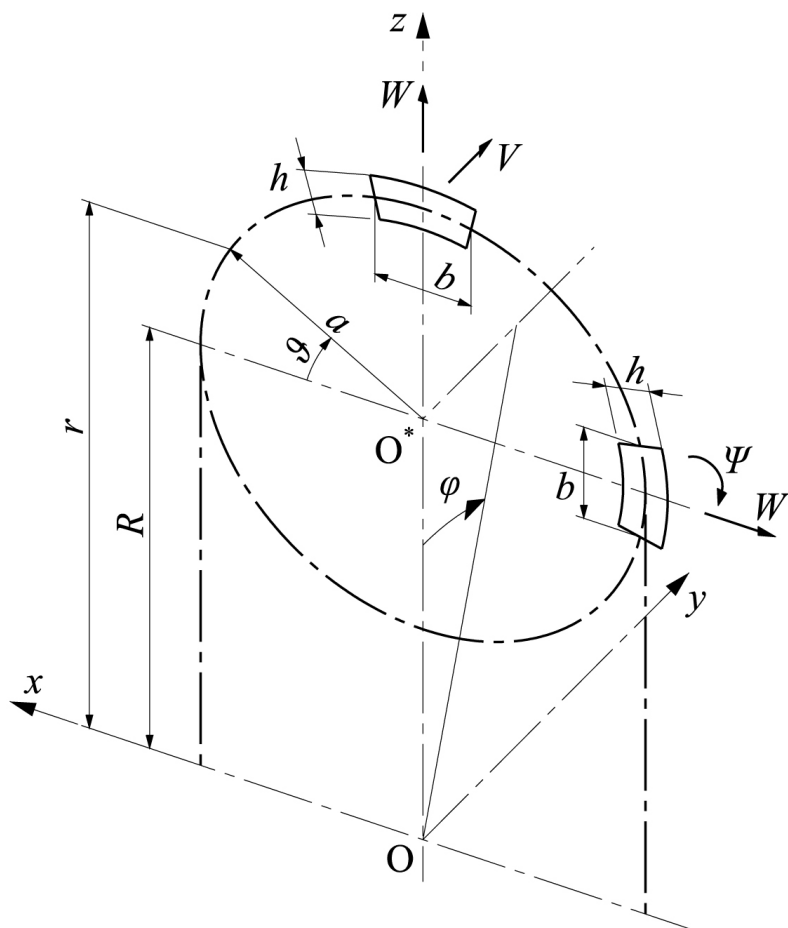


**Fig. 9.** Rings as segments of toroidal shell
***Sl. 9.*** Prstenovi kao isječci torusne ljuske

Minimizing the total energy $E = E_S + E_G - E_K$ by setting its derivatives per $V$ and $W$ equal to zero yields a symmetric matrix equation

$$\begin{bmatrix} a_{11} - \omega^2 & a_{12} - 2\Omega\omega \\ a_{21} - 2\Omega\omega & a_{22} - \omega^2 \end{bmatrix} \begin{Bmatrix} V \\ W \end{Bmatrix} = \{0\}, \tag{83}$$

where

$$a_{11} = \frac{p_5}{\alpha} + \frac{c_4}{\alpha} - \Omega^2$$

$$a_{22} = \frac{q_3}{\alpha} + \frac{c_7}{\alpha} - \Omega^2 \tag{84}$$

$$a_{33} = a_{21} = \frac{q_{16}}{\alpha} + \frac{c_{11}}{\alpha}.$$

The non-trivial solution of Eq. (83) is obtained from the condition that the determinant of its matrix vanishes. Applying this condition results in the following characteristic equation in the form of a fourth order (quartic) polynomial:

$$\omega^4 - a_2\omega^2 + a_1\omega + a_0 = 0,$$

where

$$a_2 = a_{11} + a_{22} + 4\Omega^2$$

$$a_1 = 4a_{12}\Omega \tag{85}$$

$$a_0 = a_{11}a_{22} - a_{12}^2.$$

Substituting Eqs. (84) into (86), one obtains $\hspace{6cm}$ (86)

$$a_2 = \frac{K}{\rho h r^2}\left(n^2 + 1\right)\left(1 + n^2 \frac{D}{Kr^2}\right) + 2\left(n^2 + 2\right)\Omega^2$$

$$a_1 = 4\Omega n\left[\frac{K}{\rho h r^2}\left(1 + n^2 \frac{D}{Kr^2}\right) + 2\Omega^2\right] \tag{87}$$

$$a_0 = \left(\frac{K}{\rho h r^2}\right)^2 n^2\left(n^2 - 1\right)^2 \frac{D}{Kr^2} + \frac{K}{\rho h r^2}n^2\left(n^2 - 3\right)\left(1 + n^2 \frac{D}{Kr^2}\right)\Omega^2 + n^2\left(n^2 - 4\right)\Omega^4.$$

Eq. (85) can be solved analytically in a rather complicate way, as shown in Appendix H. However, an approximate solution of Eq. (85) with ignored small terms of higher order is at disposal, [27]. The first solution is related to extensional natural frequency of rotating ring in case that $n$ and $\Omega$ are relatively small quantities

$$\widetilde{\omega}_e = \frac{2n}{n^2 + 1}\Omega \pm \sqrt{\left(\omega_e^0\right)^2 + 2\left(n^2 + 2\right)\Omega^2} \ , \tag{88}$$

where

$$\omega_e^0 = \sqrt{\left(n^2 + 1\right)\left(1 + n^2 \frac{D}{Kr^2}\right)} \sqrt{\frac{K}{\rho h r^2}} \tag{89}$$

is an extensional natural frequency of the non-rotating ring.

The second root of Eq. (85) is related to bending natural frequencies

$$\widetilde{\omega}_b = \frac{2n}{n^2 + 1}\Omega \pm \sqrt{\left(\omega_b^0\right)^2 + \frac{n^2\left(n^2 - 1\right)^2}{\left(n^2 + 1\right)^2}\Omega^2} \ , \tag{90}$$

where

$$\omega_b^0 = \frac{n(n^2 - 1)}{\sqrt{\left(n^2 + 1\right)\left(1 + n^2 \frac{D}{Kr^2}\right)}} \sqrt{\frac{D}{\rho h r^4}} \tag{91}$$

is a flexural natural frequency of the non-rotating ring.

Since the ring tension stiffness is much higher than the flexural stiffness, values of $\widetilde{\omega}_e$ are much higher than those of $\widetilde{\omega}_b$. Therefore, $\widetilde{\omega}_b$ is of primary interest.

## 6.2 Out-of-plane vibration

This type of vibrations is analysed by considering the toroidal shell segment in the vicinity of angle $\vartheta = \pi$, with two degrees of freedom, i.e. deflection $W$ and twist angle $\Psi$, Fig. 9. Since extensional displacements $U$ and $V$ are zero, the strain energy according to Eq. (11) is reduced to [27]

$$E_S = \frac{1}{2}q_1\left(W''\right)^2 + \frac{1}{2}q_2\left(W'\right)^2 + \frac{1}{2}q_3 W^2 + q_4 W'' W' + q_5 W'' W + q_6 W' W , \qquad (92)$$

where referring to Appendix A, and setting $K=0$

$$
\begin{aligned}
q_1 &= \pi \frac{D}{a^2}\frac{r}{a} \\[4pt]
q_2 &= \pi \frac{D}{ar}\left[1 + 2\left(1-v\right)n^2\right] \\[4pt]
q_3 &= \pi \frac{a}{r}\frac{D}{r^2}n^2\left[n^2 + 2\left(1-v\right)\right] \\[4pt]
q_4 &= \pi v \frac{D}{a^2} \\[4pt]
q_5 &= -\pi v \frac{D}{ar}n^2 \\[4pt]
q_6 &= -\pi\left[1 + 2\left(1-v\right)\right]\frac{D}{r^2}n^2.
\end{aligned}
\qquad (93)
$$

Stiffness $K$ and stiffness $D$ are defined with Eq. (82). Poisson's coefficient $v$ is not ignored in (93) (as in the case of in-plane vibrations), since it is introduced through the shear modulus $G = E/\left(2(1+v)\right)$ at the very beginning of the development of toroidal shell vibration theory.

The deflection derivative is actually the twist angle, Fig. 9, and a new variable is introduced for simplicity:

$$W' = \frac{\mathrm{d}W}{\mathrm{d}\vartheta} = a\Psi = \frac{a}{r}X . \qquad (94)$$

In a similar way, one can write for the curvature

$$W'' = \frac{\mathrm{d}^2 W}{\mathrm{d}\vartheta^2} = a^2 \theta = \left(\frac{a}{r}\right)^2 Y \ . \tag{95}$$

Substituting expressions (94)) and (95) into (92) yields

$$
\begin{aligned}
E_S = {} & \frac{1}{2} q_1 \left(\frac{a}{r}\right)^4 Y^2 + \frac{1}{2} q_2 \left(\frac{a}{r}\right)^2 X^2 + \frac{1}{2} q_3 W^2 \\
& + q_4 \left(\frac{a}{r}\right)^3 XY + q_5 \left(\frac{a}{r}\right)^2 YW + q_6 \left(\frac{a}{r}\right) XW \ .
\end{aligned}
\tag{96}
$$

Furthermore,

$$
\begin{aligned}
\frac{\partial E_S}{\partial W} &= q_3 W + q_5 \left(\frac{a}{r}\right)^2 Y + q_6 \left(\frac{a}{r}\right) X \\
\frac{\partial E_S}{\partial X} &= q_2 \left(\frac{a}{r}\right)^2 X + q_4 \left(\frac{a}{r}\right)^3 Y + q_6 \left(\frac{a}{r}\right) W \\
\frac{\partial E_S}{\partial Y} &= q_1 \left(\frac{a}{r}\right)^4 Y + q_4 \left(\frac{a}{r}\right)^3 X + q_5 \left(\frac{a}{r}\right)^2 W = 0.
\end{aligned}
\tag{97}
$$

Since the displacement $Y$ is neither accompanied by the inertia term nor present in the geometric strain energy, the right-hand side of the last equation of (97) is set to zero. Hence, one obtains

$$Y = - \frac{q_4 \left(\dfrac{a}{r}\right)^3}{q_1 \left(\dfrac{a}{r}\right)^4} X - \frac{q_5 \left(\dfrac{a}{r}\right)^2}{q_1 \left(\dfrac{a}{r}\right)^4} W \ . \tag{98}$$

Substituting (98) into the first two equations of (97), the system of equations is reduced to

$$\frac{\partial E_S}{\partial W} = a_{11}^* W + a_{12}^* X$$

$$\frac{\partial E_S}{\partial X} = a_{21}^* W + a_{22}^* X \,, \tag{99}$$

where coefficients $a_{ij}$, taking into account Eq. (93), are given by:

$$a_{11}^* = \pi \frac{a}{r} \frac{D}{r^2} \left(1 - v^2\right) n^2 \left(n^2 + \frac{2}{1+v}\right)$$

$$a_{22}^* = \pi \frac{a}{r} \frac{D}{r^2} \left(1 - v^2\right) \left(1 + \frac{2}{1+v} n^2\right) \tag{100}$$

$$a_{12}^* = a_{21}^* = -\pi \frac{a}{r} \frac{D}{r^2} \left(1 - v^2\right) n^2 \left(1 + \frac{2}{1+v}\right).$$

The geometric strain energy, Eq. (12), has only one term, i.e.

$$E_G = \frac{1}{2} c_7 W^2 \,, \tag{101}$$

where, according to Appendix A and after applying the membrane force due to the centrifugal load $N_\varphi = \rho h r^2 \Omega^2$, it yields

$$c_7 = \pi \frac{a}{r} n^2 N_\varphi = \pi \rho h a r \Omega^2 n^2 \,. \tag{102}$$

The kinetic energy, Eq. (13), has also got only one term, $\rho h \omega^2 W$, which is related to the inertia force. Since a rotation of the ring cross-section $\Psi$ is introduced, the rotary inertia must be taken into account, too. Based on the analogy between inertia force and the moment of rotary inertia, as well as taking into account the substitution $\Psi = \frac{1}{r} X$, Eq. (94), one can write

$$hW^2 : h\frac{h^2}{12}\Psi^2 = \frac{i_p}{r^2}X^2, \quad i_p = \frac{h^3}{12}. \tag{103}$$

In this way, the kinetic energy can be written as

$$E_K = \frac{1}{2}\pi\rho\,har\,\omega^2 W^2 + \frac{1}{2}\pi\rho\frac{a}{r}i_p\omega^2 X^2. \tag{104}$$

Now, Eq. (99) is extended to the total energy $E = E_S + E_G - E_K$, and one can write

$$\frac{\partial E}{\partial W} = a_{11}^* W + a_{12}^* X + \alpha\,\Omega^2 n^2 W - \alpha\,\omega^2 W = 0$$

$$\frac{\partial E}{\partial X} = a_{21}^* W + a_{22}^* X - \beta\,\omega^2 X^2 = 0, \tag{105}$$

where $\alpha = \pi\rho\,har$ and $\beta = \pi\rho(a/r)i_p$. If the first and the second equation in (105) are divided by $\alpha$ and $\beta$, respectively, one obtains an asymmetric matrix equation

$$\begin{bmatrix} a_{11} - \omega^2 & a_{12} \\ a_{21} & a_{22} - \omega^2 \end{bmatrix}\begin{Bmatrix} W \\ X \end{Bmatrix} = \{0\}, \tag{106}$$

where

$$a_{11} = \frac{D}{\rho\,hr^4}\left(1-v^2\right)n^2\left(n^2 + \frac{2}{1+v}\right) + n^2\Omega^2$$

$$a_{22} = \frac{D}{\rho\,i_p r^2}\left(1-v^2\right)\left(1 + \frac{2}{1+v}n^2\right)$$

$$a_{12} = -\frac{D}{\rho\,hr^4}\left(1-v^2\right)n^2\left(1 + \frac{2}{1+v}\right)$$

$$a_{21} = -\frac{D}{\rho\,i_p r^2}\left(1-v^2\right)n^2\left(1 + \frac{2}{1+v}\right). \tag{107}$$

The determinant of the matrix in equation (106) must vanish, i.e.

$$\omega^4 - a_2\omega^2 + a_0 = 0, \tag{108}$$

where

$$\begin{aligned} a_2 &= a_{11} + a_{22} \\ a_0 &= a_{11}a_{22} - a_{12}a_{21}. \end{aligned} \tag{109}$$

Inserting (107) into (109) yields

$$a_2 = (1-v^2)\left[\frac{D}{\rho h r^4}n^4\left(n^2 + \frac{2}{1+v}\right) + \frac{D}{\rho i_p r^2}\left(1 + \frac{2}{1+v}n^2\right)\right] + n^2\Omega^2$$

$$a_0 = \left[\frac{D}{\rho r^2}(1-v^2)\right]^2\frac{1}{h i_p r^2}n^2\left[\left(n^2 + \frac{2}{1+v}\right)\left(1 + \frac{2}{1+v}n^2\right) - \left(1 + \frac{2}{1+v}\right)^2 n^2\right]$$

$$+ \frac{D}{\rho i_p r^2}(1-v^2)n^2\left(1 + \frac{2}{1+v}n^2\right)\Omega^2. \tag{110}$$

Now, it is necessary to substitute all the shell parameters specified per unit length with the ring parameters of breadth $b$, Fig. 9

$$\frac{D(1-v^2)}{i_p} = \frac{E}{I_p}, \quad \frac{D(1-v^2)}{h} = \frac{E}{A}, \quad \frac{i_p}{h} = \frac{I_p}{A}. \tag{111}$$

The moment of inertia of the shell cross-section $i_p = h^3/12$, related to the rotary inertia, is substituted by the equivalent ring polar moment of inertia $I_p = (h^2 + b^2)bh/12$.

Furthermore, formulae (110) are derived for a shell segment, and the strain energy includes the energy of both twist moments at the meridional and circumferential shell cross-sections, $M_{12} = M_{21}$. Their energy is represented in the formula for the total

strain energy in Eq. (5) by the term $(1-\nu)\kappa_{\vartheta\varphi}^2 / 2$, where $\kappa_{\vartheta\varphi}$ is the twist strain. This is shown in Eqs. (110) by the coefficient $2/(1+\nu)$. Therefore, only one half of this coefficient must be taken into account in Eqs. (110). In this way, formulae (110) derived for the toroidal shell are modified in such a way to be valid for a ring

$$a_2 = \frac{E}{\rho r^2}\left[\frac{I}{Ar^2}n^2\left(n^2 + \frac{1}{1+\nu}\right) + \frac{I}{I_p}\left(1 + \frac{1}{1+\nu}n^2\right)\right] + n^2\Omega^2$$

$$a_0 = \left(\frac{E}{\rho r^2}\right)^2 \frac{I}{Ar^2}\frac{I}{I_p}\frac{1}{1+\nu}n^2(n^2-1)^2 + \frac{E}{\rho r^2}\frac{I}{I_p}n^2\left(1 + \frac{1}{1+\nu}n^2\right)\Omega^2 . \tag{112}$$

The solutions of the bi-quadratic equation (108) can be presented in the form

$$\omega_{t,b} = \sqrt{\frac{a_2}{2}\left[1 \pm \sqrt{1 - \frac{4a_0}{a_2^2}}\right]} . \tag{113}$$

The first solution represents natural frequencies of predominantly torsional vibrations, while the second one represents natural frequencies of predominantly flexural vibrations. This can easily be seen in the case of a non-rotating ring. By setting $\Omega = 0$ in Eqs. (110), it becomes obvious that the second term under the inner square root of Eq. (113) is very small. By using the approximation $\sqrt{1-\varepsilon} \approx 1 - \varepsilon/2$, one obtains the following expressions for natural frequencies of torsional and flexural vibrations of a stationary ring:

$$\omega_t^0 = \sqrt{\left(1 + \frac{n^2}{1+\nu}\right) + \frac{I_p}{Ar^2}n^2\left(n^2 + \frac{1}{1+\nu}\right)}\sqrt{\frac{E}{\rho r^2}\frac{I}{I_p}} \tag{114}$$

$$\omega_b^0 = \frac{n(n^2-1)}{\sqrt{n^2 + 1 + \nu + \frac{I_p}{Ar^2}n^2\left[(1+\nu)n^2+1\right]}}\sqrt{\frac{E}{\rho r^2}\frac{I}{Ar^2}} . \tag{115}$$

For a toroidal ring $I/I_p = 1/2$ and $I_p/(AR^2) = (a/R)^2$.

It is observed that both the centrifugal load and the Coriolis load induced by the ring rotation are involved in the ring in-plane vibrations (the terms with $\Omega^2$ and $\Omega$ in Eqs. (87), respectively). With the out-of-plane vibrations, only the centrifugal load participates (the terms with $\Omega^2$ in Eqs. (110)). Hence, there is no bifurcation of natural frequencies in the latter case.

### 6.3 Rigorous solution of the characteristic equation

Solving quartic equation has been a challenging subject of investigation since the 16th century. There are several well-known names among scientists: Lodovico Ferrari, Gerolamo Cardano, Descartes, Euler, [31], [32]. The problem is still relevant nowadays [33], [34].

The non-linear characteristic equation for the rotating ring in-plane vibrations, Eq. (85), is actually a depressed quartic equation, i.e. quartic equation without the cubic term. It can be solved by following the mathematical procedure described in [35]. One of the possibilities to solve Eq. (85) is to assume that it is reducible by factorization. Hence, the four roots of Eq. (85) coincide with two pairs of roots of two quadratic equations

$$\omega^2 + \frac{1}{2}A\omega + \left(y - \frac{a_1}{A}\right) = 0, \tag{116}$$

where

$$A = \pm\sqrt{8y + 4a_2} \tag{117}$$

and $y$ is a real root of the cubic resolvent of Eq. (85)

$$8y^3 + 4a_2 y^2 - 8a_0 y - (4a_2 a_0 + a_1^2) = 0. \tag{118}$$

Eq. (118) can be condensed into a simpler form by shifting $y$. Substituting $y = x - a_2/6$ into (118) yields

$$x^3 + 3px + 2q = 0, \tag{119}$$

where

$$p = -\frac{1}{36}(12\,a_0 + a_2^2)$$

(120)

$$q = \frac{1}{432}\left(2a_2^3 - 72\,a_2 a_0 - 27\,a_1^2\right).$$

(121)

The three real roots of Eq. (119) are assumed in the form

$$x_1 = u + v, \quad x_2 = \varepsilon_1 u + \varepsilon_2 v, \quad x_3 = \varepsilon_2 u + \varepsilon_1 v\,,$$

(122)

where $\varepsilon_1$ and $\varepsilon_2$ are the roots of equation $\varepsilon^2 + \varepsilon + 1 = 0$, i.e.

$$\varepsilon_{1,2} = -\frac{1}{2} \pm i\,\frac{\sqrt{3}}{2}\,.$$

(123)

The first root $x_1$ in (122) is determined by Cardano's formula

$$u = \sqrt[3]{z_1}\,, \quad v = \sqrt[3]{z_2}\,,$$

(124)

where

$$z_{1,2} = -q \pm \sqrt{q^2 + p^3}$$

(125)

are roots of the equation $z^2 + 2qz - p = 0$. If the discriminant $D = q^2 + p^3 < 0$, one can write

$$z_{1,2} = -q + i\,w, \quad w = \sqrt{\left|q^2 + p^3\right|}\,.$$

(126)

The complex quantity $z_{1,2}$ can be presented in the exponential form (De Moire's formula), i.e.

$$z_{1,2} = \rho\,\mathrm{e}^{\pm i\varphi}, \quad \rho = \sqrt{q^2 + w^2}, \quad \varphi = \mathrm{arctg}\!\left(\frac{w}{-q}\right),$$

(127)

where $-\pi \le \varphi \le \pi$ . Substituting (127) into (124) yields

$$u,v = \sqrt[3]{z_{1,2}} = \sqrt[3]{\rho}\mathrm{e}^{\pm i\varphi/3} = \sqrt[3]{\rho}\left[\cos(\varphi/3) \pm i\sin(\varphi/3)\right]. \qquad (128)$$

Finally, one obtains for the first root of Eq. (119), according to Eqs. (122)

$$x_1 = 2\sqrt[3]{\rho}\cos(\varphi/3) . \qquad (129)$$

The values of $x_1$ are real, since the imaginary parts of $u$ and $v$ cancel each other. Furthermore, the solutions of Eq. (130) read

$$\omega_{1,2} = -\frac{A}{4} \pm \sqrt{\left(\frac{A}{4}\right)^2 - \left(y - \frac{a_1}{A}\right)}. \qquad (130)$$

Substituting (A3) and $y = x_1 - a_2/6$ into (116), one obtains

$$\omega_{1,2,3,4} = \frac{1}{2\sqrt{3}}\left[-s\sqrt{2a_2 + 6x_1} \pm \sqrt{4a_2 - 6x_1 + \frac{6\sqrt{3}a_1}{s\sqrt{2a_2 + 6x_1}}}\right], \qquad (131)$$

where $s = \mathrm{sign}(A)$, Eq. (117).

The following example can be used as a benchmark for the application of the above procedure:

Data: $a_0 = 1, \quad a_1 = \frac{32}{3}, \quad a_2 = \frac{38}{3}$ .

Eq. (131): $\frac{1}{2\sqrt{3}}\left(-s \cdot 6.9282 \pm \sqrt{28 + s \cdot 16}\right)$.

Solution: $\omega_1 = -3.91485, \quad \omega_2 = -0.085146, \quad \omega_3 = 1.0, \quad \omega_4 = 3.0$ .

# 7. NUMERICAL EXAMPLES

## 7.1 Closed toroidal shell

### 7.1.1    Vibration analysis

The application of developed numerical procedures is illustrated by a case of a closed toroidal shell with the following geometric and physical properties, Fig. 5: $R$=1 m, $a$=0.4 m, $h$=0.01 m, $E$=2.1·$10^{11}$ N/m², $\upsilon$=0.3 and $\rho$=7850 kg/m³.

The first 11 natural frequencies for stationary shell, $\Omega$=0, determined by RRM and FSM, are listed in Table 1 and compared with the FEM Abaqus results determined by finite element S8R5 [36]. The convergence analysis shows that stable results are obtained by 15 sine and cosine terms in RRM, 200 finite strips of higher order in FSM, and the finite element mesh 200x500 in the meridional and circumferential directions in FEM. All values shown in Table 1 mutually agree very well.

The distribution of displacements $U$, $V$ and $W$ over shell cross-section for the first six natural modes, determined by RRM and FSM, are identical and shown in Fig. 10. Some mode profiles are symmetric, and some asymmetric, with respect to the vertical symmetry plane. Natural modes determined by FEM are shown in Figs. 10 and 11 in the isometric view and orthogonal planes, respectively. The shell cross-section mode profiles obtained by RRM and FSM are almost the same, while the FEM profiles are similar, Figs. 10 and 12.

**Table 1.** Natural frequencies of closed toroidal shell, $\omega$ [Hz], R=1 m, $a$= 0.4 m, $h$=0.01 m
***Tablica 1.*** Prirodne frekvencije zatvorene torusne ljuske, $\omega$ [Hz], R=1 m, $a$=0.4 m, $h$=0.01 m

| Mode no. | Mode type | $n$ | RRM 2·15 terms | FSM 200 FS | FEM 200x500 |
|---|---|---|---|---|---|
| 1 | Asym. | 0 | 80.73 | 81.26 | 80.67 |
| 2 | Asym. | 2 | 111.11 | 111.29 | 110.22 |
| 3 | Sym. | 2 | 123.05 | 123.19 | 122.08 |
| 4 | Asym. | 3 | 207.40 | 207.52 | 205.30 |
| 5 | Sym. | 3 | 207.85 | 207.98 | 205.75 |
| 6 | Sym. | 4 | 309.74 | 309.84 | 306.67 |
| 7 | Asym. | 4 | 309.89 | 309.99 | 306.82 |
| 8 | Asym. | 1 | 351.06 | 351.16 | 350.98 |
| 9 | Asym. | 2 | 398.61 | 398.68 | 398.44 |
| 10 | Sym. | 2 | 401.28 | 401.33 | 401.15 |
| 11 | Sym. | 1 | 415.22 | 415.27 | 415.17 |
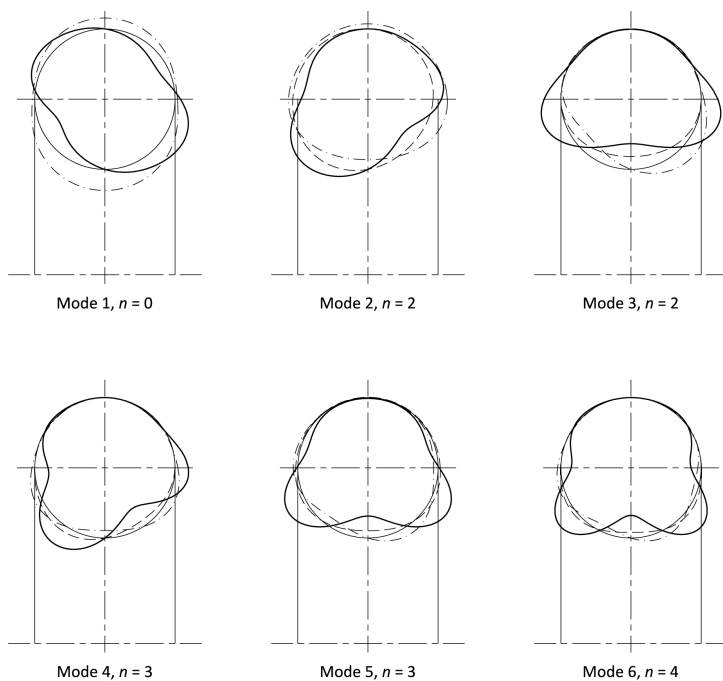
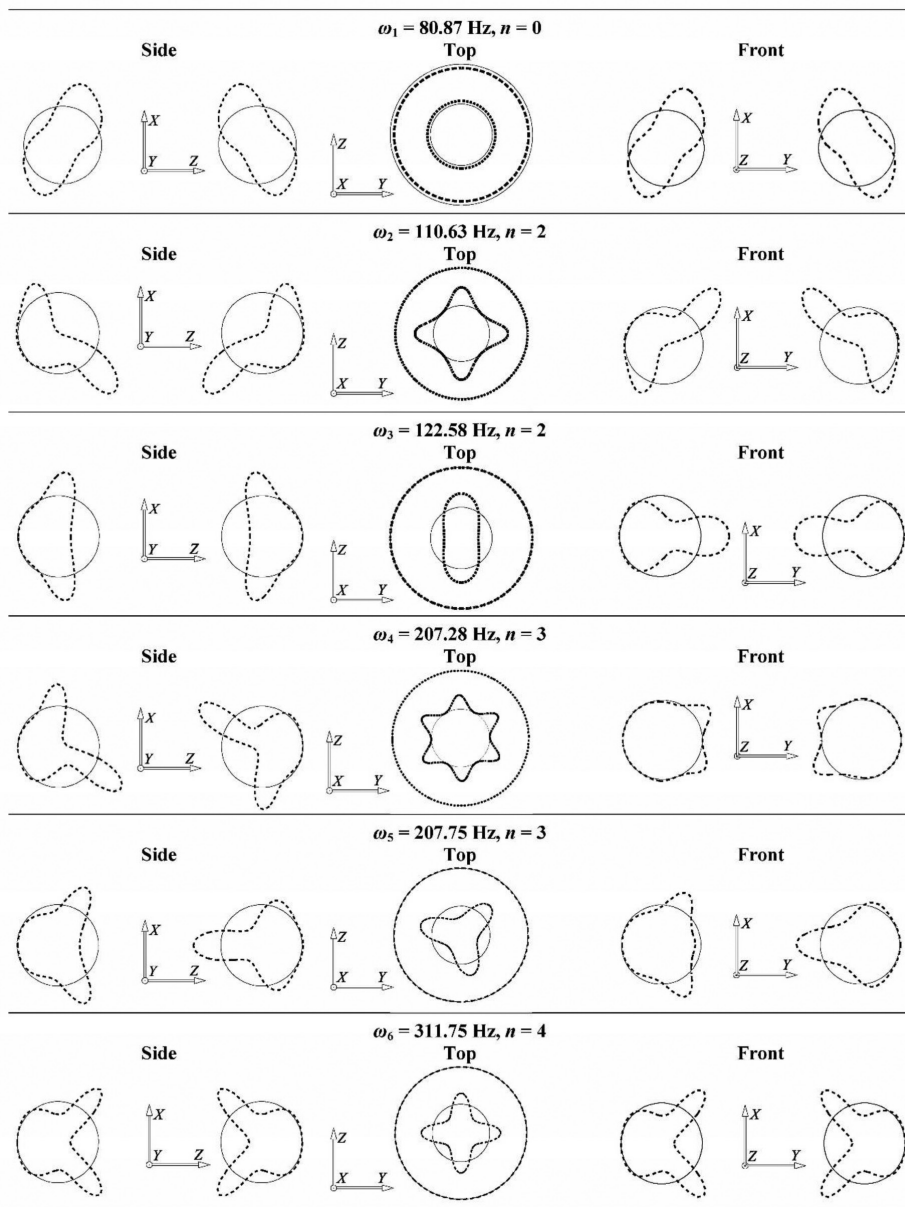**Fig. 10.** Modal displacements of closed toroidal shell, – · – U, - - - V, ––– W
*Sl. 10.* Pomaci prirodnih oblika vibracija na poprečnom presjeku zatvorene torusne ljuske: – · – U, - - - V, ––– W
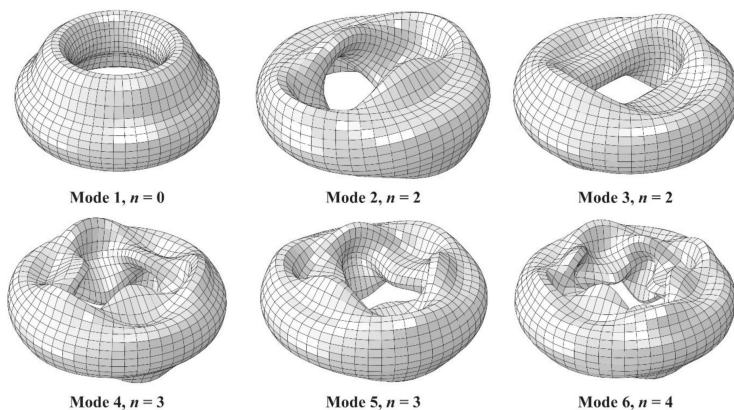


**Fig. 11.** The first six natural modes of closed toroidal shell (ABAQUS)
*Sl. 11.* Prvih šest prirodnih oblika vibriranja zatvorene torusne ljuske (ABAQUS)

**Fig. 12.** Natural modes of FEM model in the coordinate planes (ABAQUS)
***Sl. 12.*** Prirodni oblici vibriranja modela konačnih elemenata u koordinatnim ravninama (ABAQUS)

In the convergence analysis, the converged RRM results from Table 1 are used as referent values. The convergence of FSM is considered taking $N$=50, 100, 150 and 200 finite strips into account. The error is defined as $\varepsilon(\%) = \dfrac{\omega_{FSM} - \omega_{RRM}}{\omega_{RRM}} \cdot 100$. As shown in Fig. 13, the results converge from upside, and convergence is faster for higher mode number $n$.
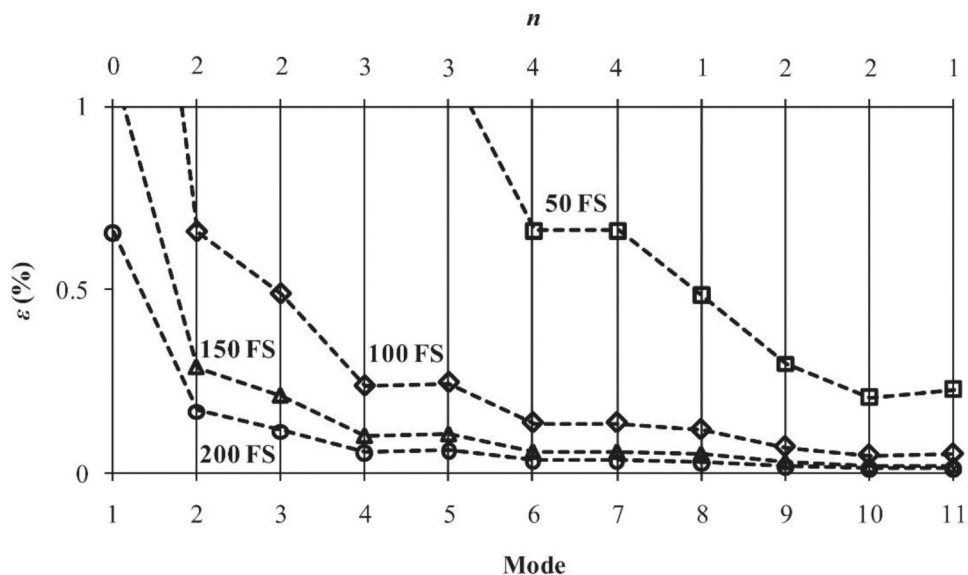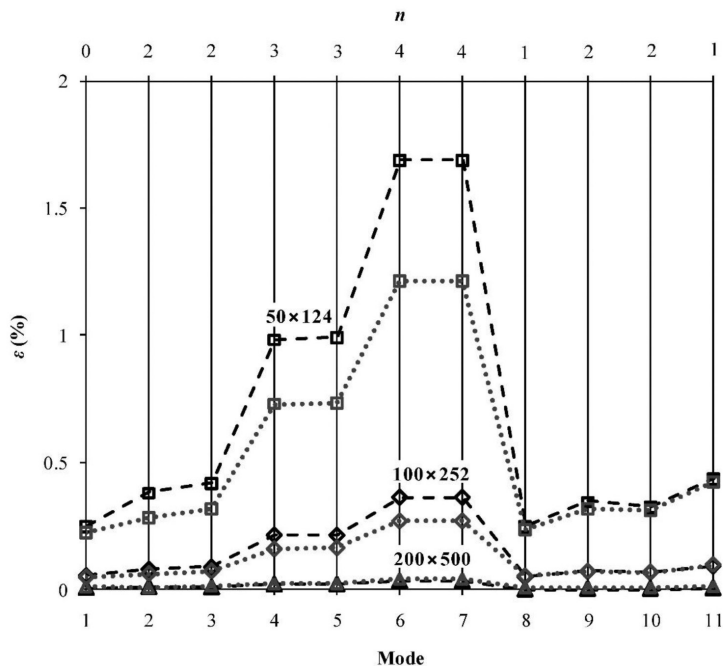


**Fig. 13.** Convergence of natural frequencies, FSM

*Sl. 13.* Konvergencija prirodnih frekvencija, metoda vrpčastih elemenata

The convergence of FEM results is also analysed by taking into account different finite element mesh density: 50x124, 100x252 and 200x500. The NASTRAN results obtained by finite element CQUAD4, [37], for 300x600 mesh density are used as the referent ones, Fig. 14. It is observed that the values of natural frequencies $\omega_4$, $\omega_5$, $\omega_6$ and $\omega_7$ converge slower to the referent values than the others.

The converged natural frequencies determined by FEM differ from those determined by RRM analysis for ca 1%, Fig. 15. This is due to both the applied shell theory and the type of used finite elements.

**Fig. 14.** Convergence of natural frequencies, FEM- - - ABAQUS, · · · NASTRAN

***Sl. 14.*** Konvergencija prirodnih frekvencija, metoda konačnih elemenata:
- - - ABAQUS, · · · NASTRAN
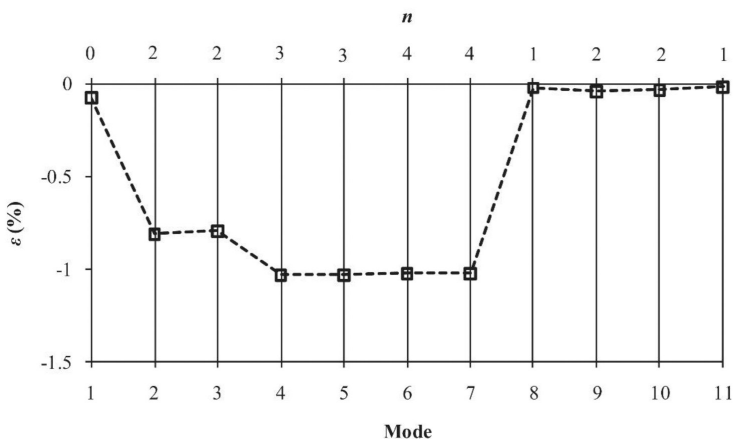


**Fig. 15.** Relative difference of FEM and RRM natural frequencies

***Sl. 15.*** Relativna razlika prirodnih frekvencija određenih metodom konačnih elemenata i Rayleigh-Ritzovom metodom

Furthermore, the bifurcation phenomenon of natural frequencies caused by the shell rotation is considered. The tension forces due to centrifugal load are determined by RRM and FSM, as described in Section 5.2 and 5.3. The shell cross-section deformation obtained by RRM and FSM, as well as FEM for $\Omega=60$ rad/s, is shown in Fig. 16. The results are almost the same. The diagrams of tension forces are shown in Fig. 17. All three methods used give the same results.
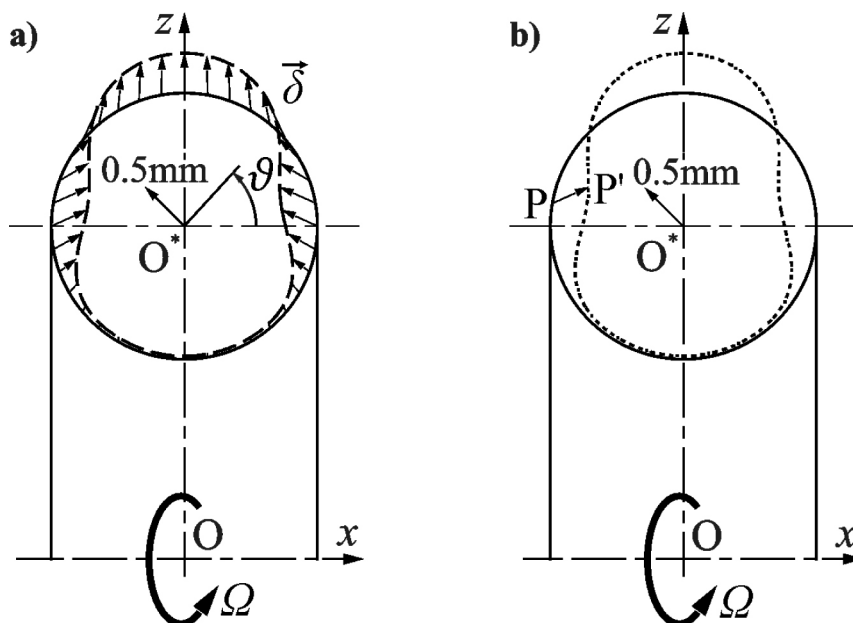


**Fig. 16.** Shell cross-section deformation due to rotation, $\Omega=60$ rad/s, a) RRM, FSM; b) FEM
*Sl. 16.* Deformacija poprečnog presjeka ljuske uslijed vrtnje, $\Omega=60$ rad/s, a) RRM, FSM; b) FEM
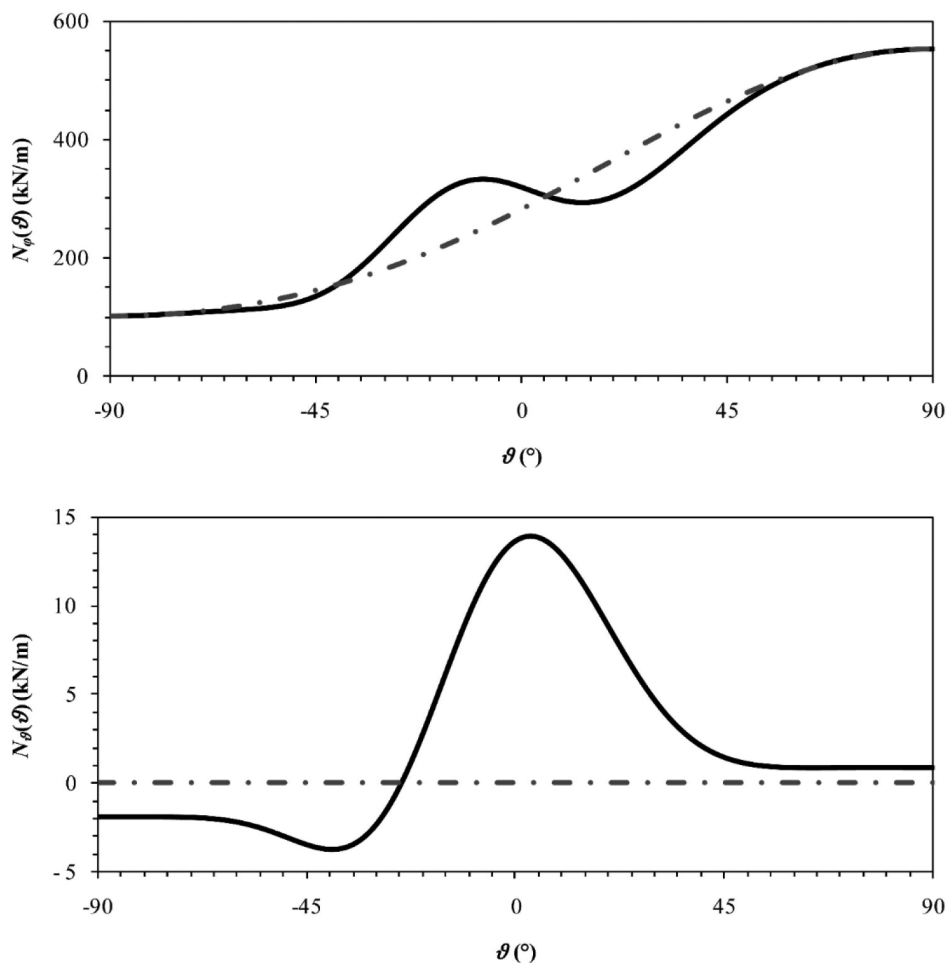
**Fig. 17.** In-plane forces of rotating toroidal shell, Ω=60 rad/s
*Sl. 17.* Ravninske sile u ljusci uslijed vrtnje, Ω=60 rad/s

The same values of natural frequencies determined by RRM and FSM are obtained. They are shown separately for asymmetric and symmetric modes in Figs. 18 and 19, with their comparisons to FEM results. Some differences between the diagrams can be noticed as a result of different numerical methods. If the Coriolis force is omitted ($\omega \Omega = 0$, Eq. (29)), there is no bifurcation of natural frequencies, as can be seen in Figs. 18 and 19.
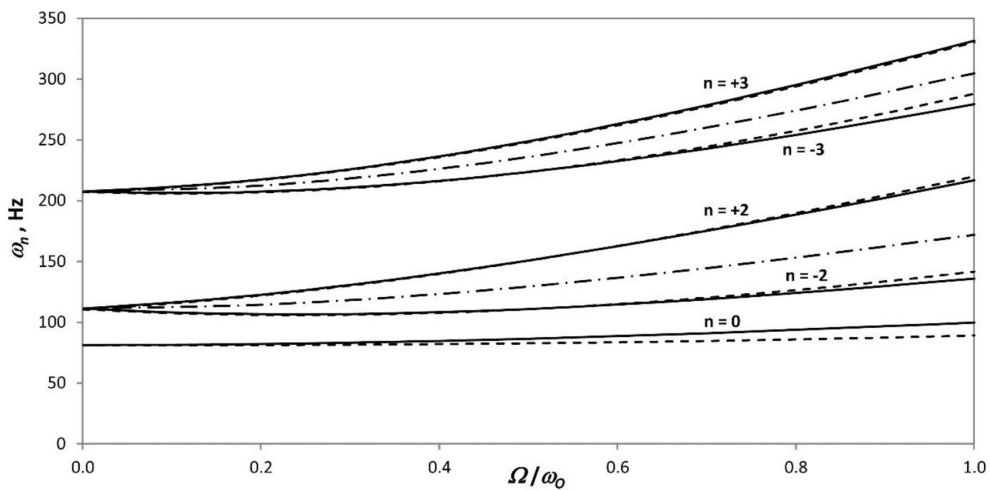
**Fig. 18.** Natural frequencies of the rotating closed toroidal shell, asymmetric modes, $\omega_0 = 80.73$ Hz, ––– RRM, FSM; – – – FEM; – · – · – RRM, FSM, Fcor. = 0

***Sl. 18.*** Prirodne frekvencije rotirajuće zatvorene toroidne ljuske, asimetrični modovi, $\omega_0 = 80.73$ Hz, ––– RRM, FSM; – – – FEM; – · – · – RRM, FSM, Fcor. = 0
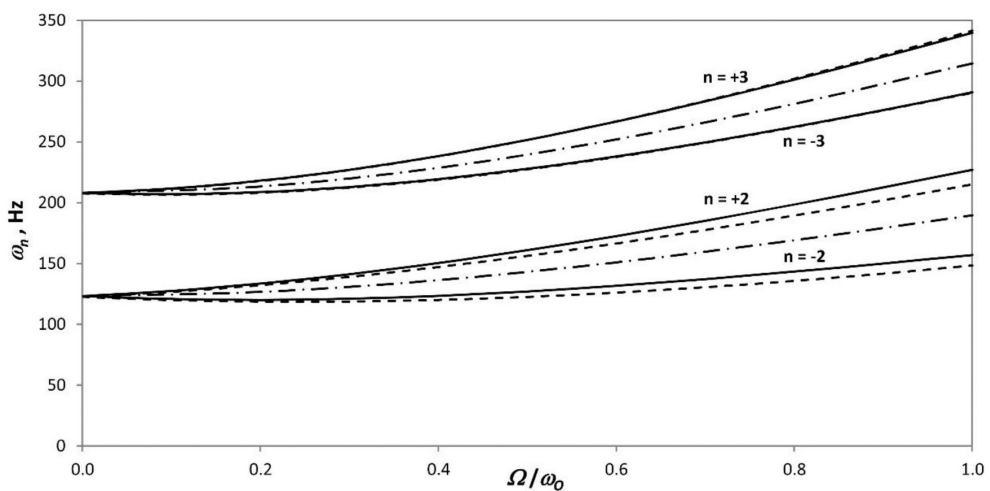


**Fig. 19.** Natural frequencies of the rotating closed toroidal shell, symmetric modes, $\omega_0 = 80.73$ Hz, ––– RRM, FSM; – – – FEM; – · – · – RRM, FSM, Fcor. = 0

***Sl. 19.*** Prirodne frekvencije rotirajuće zatvorene toroidne ljuske, simetrični modovi, $\omega_0 = 80.73$ Hz, ––– RRM, FSM; – – – FEM; – · – · – RRM, FSM, Fcor. = 0

### 7.1.2 Buckling analysis

The stability of the closed toroidal shell specified in Section 7.1.1 exposed to action of the uniform external pressure is considered. Tension forces due to uniform pressure $p=1$MPa are determined analytically by the simple membrane formulae (61). The rigorous forces based on the shell theory are obtained according to the procedure presented in Section 5.2. Diagrams of both membrane and total tension forces are shown in Fig. 20. The same total forces are obtained by FSM, Section 5.3, and FEM.
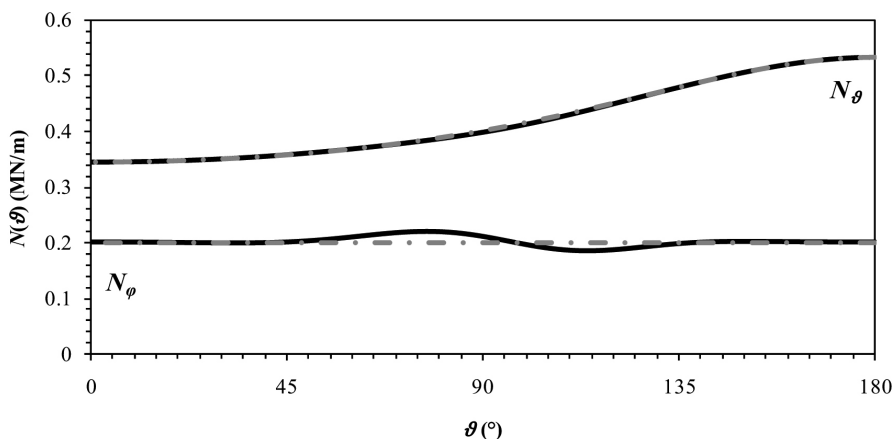


**Fig. 20.** In-plane forces of closed toroidal shell due to uniform external pressure p=1MPa:
––– RRM, – · – · – membrane theory

***Sl. 20.*** Ravninske sile zatvorene torusne ljuske uslijed jednolikog vanjskog tlaka p=1MPa:
––– RRM, – · – · – membranska teorija

The values of buckling parameters determined by RRM, FSM and FEM are listed in Table 2. The RRM and FSM results agree very well, since both methods are based on the same toroidal shell theory. Among the FEM results, there are some differences. The best agreement between RRM and FEM results is achieved in the case of *Catia* (finite element QD8) [38], and *SolidWorks* (finite element SHELL6) [39] application.

Concerning the buckling modes, it is observed that they are identical to the natural modes for closed toroidal shell, Figs. 10, 11 and 12, as in the case of simply supported beam.

Critical pressure is minimal pressure value causing shell buckling, $p_1 = \lambda_1 p = 3.874$ MPa. Shell stability can be increased by built-in $N=2n$ cross-sectional rings. According to Table 2, by the shell reinforcement with four very stiff rings, the critical pressure is increased to $p_2 = \lambda_2 p = 4.568$ MPa, and by six rings to $p_4 = \lambda_4 p = 5.936$ MPa.

**Table 2.** Buckling parameter $\lambda$ of closed toroidal shell; $R = 1$ m, $a = 0.4$ m, $h = 0.01$ m, $p = 1$ MPa
**Tablica 2.** Parametar izvijanja $\lambda$ zatvorene torusne ljuske; $R = 1$ m, $a = 0.4$ m, $h = 0.01$ m, $p = 1$ MPa

| Mode No. | Mode type | n | RRM, 2 × 15 terms | | FSM, 200 FS | | FEM | | | |
|---|---|---|---|---|---|---|---|---|---|---|
| | | | $N_\vartheta, N_\varphi$ membrane | $N_\vartheta, N_\varphi$ shell | $N_\vartheta, N_\varphi$ membrane | $N_\vartheta, N_\varphi$ shell | Nastran CQUAD4 50 × 124 | Abaqus S8R5 50 × 124 | Catia QD8 50 × 124 | SolidWorks SHELL6 100 × 248 |
| 1 | Asym. | 0 | 3.850 | 3.874 | 3.887 | 3.912 | 4.116 | 4.083 | 3.869 | 3.873 |
| 2 | Asym. | 2 | 4.545 | 4.568 | 4.561 | 4.585 | 4.416 | 4.384 | 4.570 | 4.574 |
| 3 | Sym. | 2 | 4.687 | 4.711 | 4.700 | 4.725 | 4.418 | 4.386 | 4.756 | 4.760 |
| 4 | Asym. | 3 | 5.915 | 5.936 | 5.926 | 5.947 | 5.607 | 5.565 | 5.842 | 5.848 |
| 5 | Sym. | 3 | 5.921 | 5.959 | 5.932 | 5.971 | 5.625 | 5.582 | 5.863 | 5.870 |
| 6 | Asym. | 4 | 7.712 | 7.748 | 7.725 | 7.760 | 7.437 | 7.371 | 7.597 | 7.610 |
| 7 | Asym. | 4 | 7.713 | 7.749 | 7.725 | 7.762 | 7.438 | 7.373 | 7.598 | 7.612 |

## 7.2 Open toroidal shell

### 7.2.1    Vibration analysis

The vibration analysis of an open, simply supported toroidal shell, shown in Fig. 6, is carried out. The shell geometric and physical properties are the same as in the previous example. The shell central angle in the cross-section plane is $\vartheta_0 = \pm 3\pi/4$. Values of the first six natural frequencies are listed in Table 3 and compared with those determined by the finite strip method (FSM), and the finite element method (FEM) by employing two commercial software packages with different shell finite elements. If the rigorous Rayleigh-Ritz results are used as the referent ones, discrepancies of the FSM and FEM results are within 1%.

Displacement components of the shell cross-sections determined by RRM for the first six natural modes are shown in Fig. 21. Displacements $U$ and $W$ are symmetric, and $V$ is antisymmetric, with respect to the *y-z* plane, for modes 3, 5 and 6, resulting with symmetric modes. In case of modes 1, 2 and 4, displacements $U$ and $W$ are antisymmetric, and $V$ is symmetric, so that the modes are asymmetric. This is indicated in Table 3.

**Table 3.** Natural frequencies of simply supported toroidal shell, $\omega$ [Hz], $R$=1 m, $a$=0.4 m, $h$=0.01 m, $\vartheta_0 = 3\pi/4$

***Tablica 3.*** Prirodne frekvencije slobodno oslonjene torusne ljuske, $\omega$ [Hz], $R$=1 m, $a$=0.4 m, $h$=0.01 m, $\vartheta_0 = 3\pi/4$

| Mode | $n$ | Mode type | RRM | FSM (3*q*, 3*f*) 150 FS | FEM CATIA QD8 38×176 FE | FEM ABAQUS S4R 38×124 FE |
|---|---|---|---|---|---|---|
| 1 | 0 | Asym. | 47.64 | 47.98 | 47.62 | 47.70 |
| 2 | 1 | Asym. | 173.84 | 173.94 | 173.80 | 173.91 |
| 3 | 1 | Sym. | 383.35 | 383.30 | 383.19 | 384.81 |
| 4 | 2 | Asym. | 416.75 | 416.63 | 416.44 | 417.71 |
| 5 | 0 | Sym. | 429.79 | 429.67 | 429.49 | 431.24 |
| 6 | 2 | Sym. | 447.58 | 447.38 | 447.09 | 450.68 |
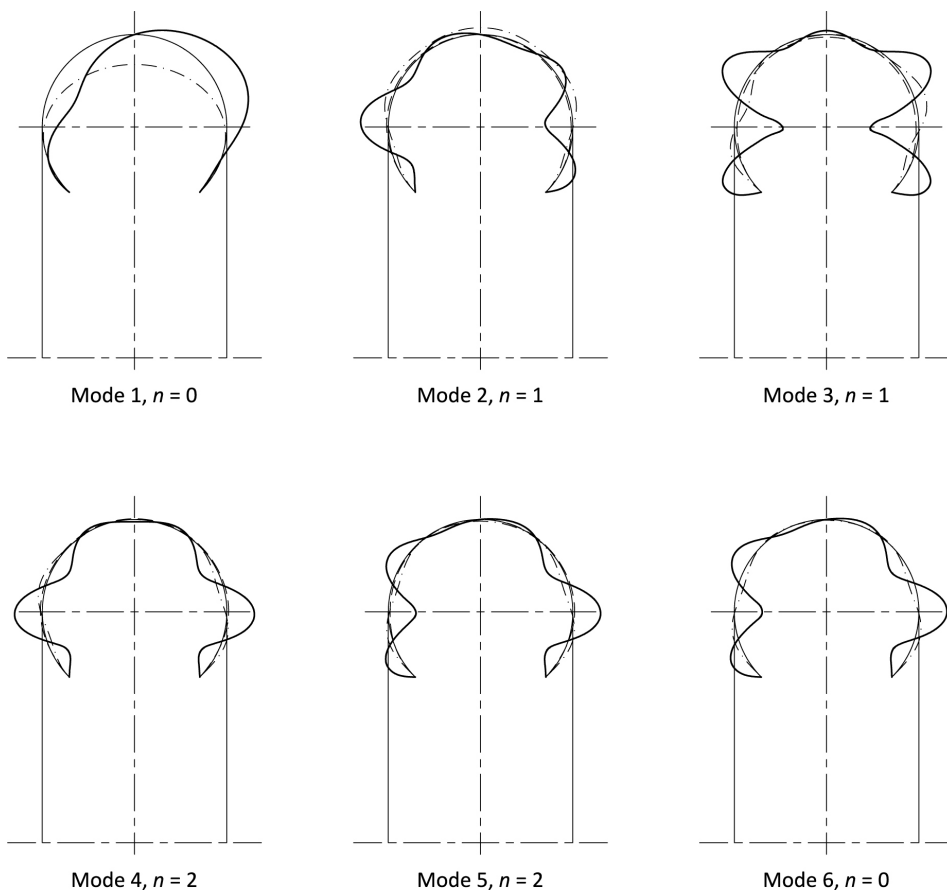
**Fig. 21.** Cross-section displacements of simply supported toroidal shell,
$- \cdot -$ U, $- - -$ V, $---$ W

**Sl. 21.** Pomaci poprečnog presjeka slobodno oslonjene torusne ljuske,
$- \cdot -$ U, $- - -$ V, $---$ W

The first six natural modes generated by ABAQUS are shown in Figs. 22 and 23 in isometric view and coordinate planes, respectively. The RRM mode profiles, Fig. 21, agree very well with FEM mode profiles, Fig. 23.
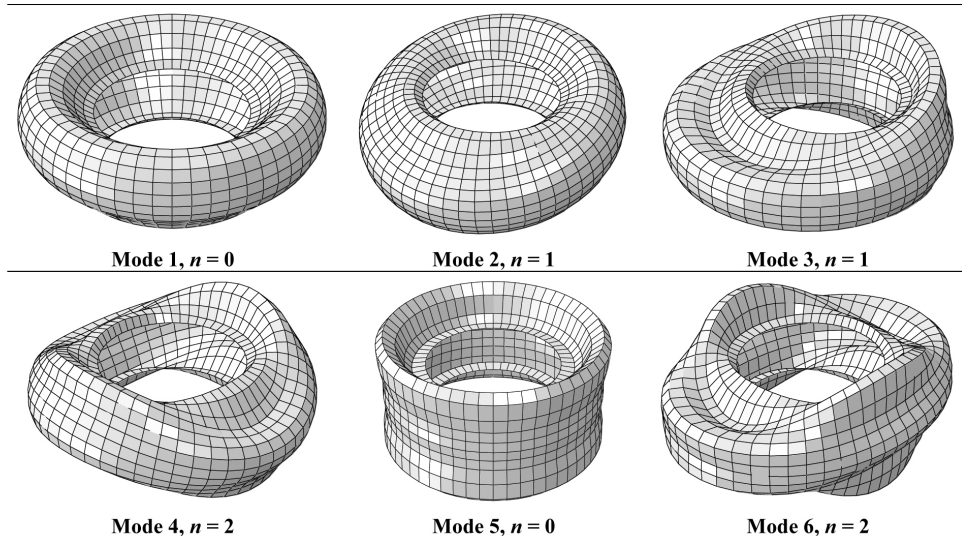
**Fig. 22.** Natural modes of simply supported toroidal shell (ABAQUS)
*Sl. 22.* Prirodni oblici vibriranja slobodno oslonjene torusne ljuske (ABAQUS)

$\omega_1 = 47.708$ Hz, $n = 0$

Side Top Front

$\omega_2 = 173.881$ Hz, $n = 1$

Side Top Front

$\omega_3 = 384.798$ Hz, $n = 1$

Side Top Front

$\omega_4 = 417.633$ Hz, $n = 2$

Side Top Front

$\omega_5 = 431.240$ Hz, $n = 0$

Side Top Front

$\omega_6 = 450.619$ Hz, $n = 2$

Side Top Front
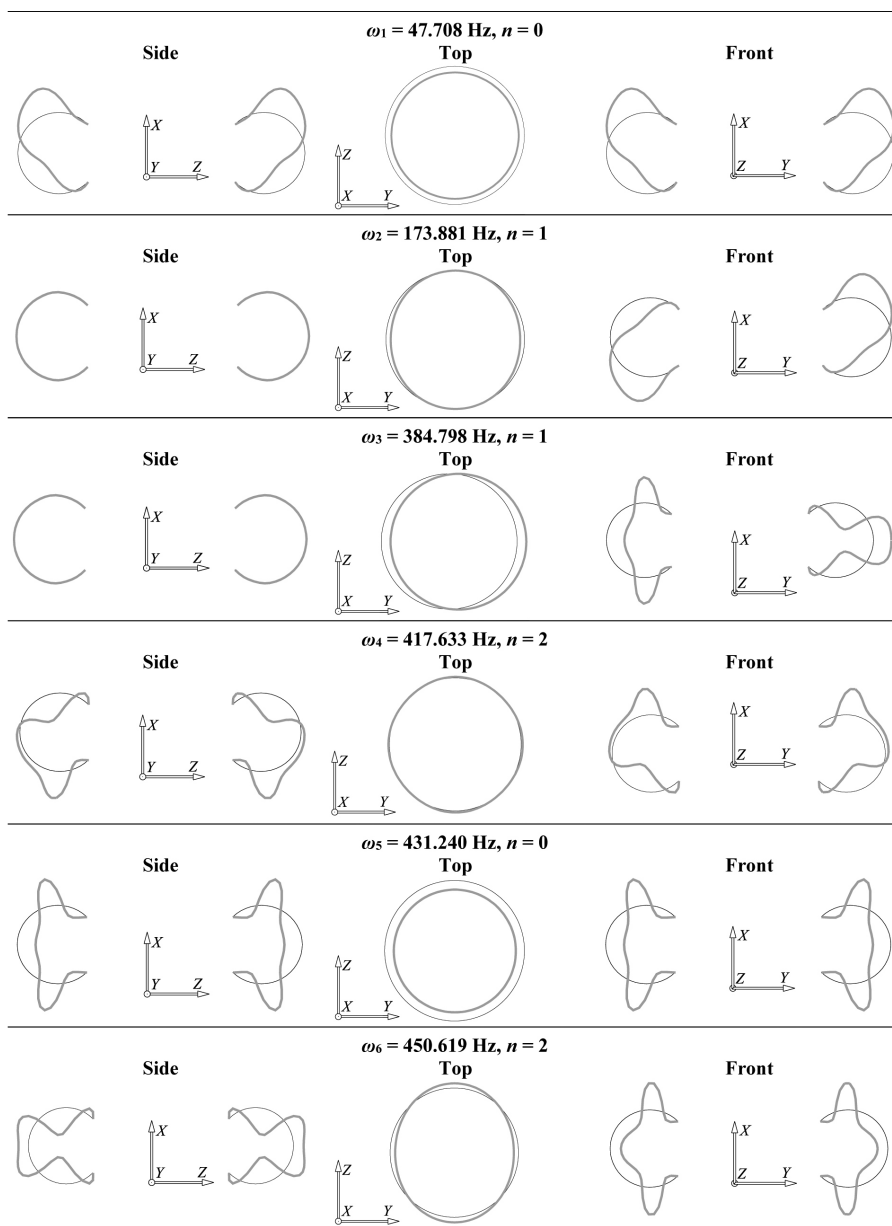
**Fig. 23.** Natural modes of simply supported toroidal shell in the coordinate planes (ABAQUS)
***Sl. 23.*** Prirodni oblici vibriranja slobodno oslonjene torusne ljuske u koordinatnim ravninama (ABAQUS)

Cross-section deformation due to centrifugal load, determined by the procedure presented in Section 5.2 for rotation speed of 50 rad/s, is shown in Fig. 24. The corresponding tension forces are shown in Fig. 25. The circumferential force, $N_\varphi$, is much higher than the meridional force, $N_\vartheta$. The values calculated by FSM, Section 5.3, and FEM are very close to RRM results shown in Fig. 25. Diagrams of natural frequencies for the circumferential wave number $n=0,\ \pm 1,\ \pm 2$, where the sign designates the forward and backward travelling modes, are shown in Figs. 26, 27 and 28, respectively, as functions of dimensionless rotation speed. The problem is also solved by FSM and FEM. In the former case, values of natural frequencies are very close to those of RRM, while FEM results show some discrepancies.
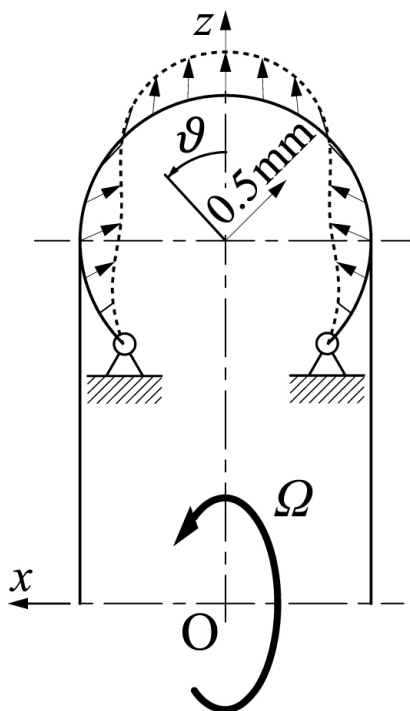


**Fig. 24.** Cross-section deformation of rotating toroidal shell, $\Omega$ =50 rad/s
*Sl. 24.* Deformacija poprečnog presjeka rotirajuće torusne ljuske, $\Omega$ =50 rad/s
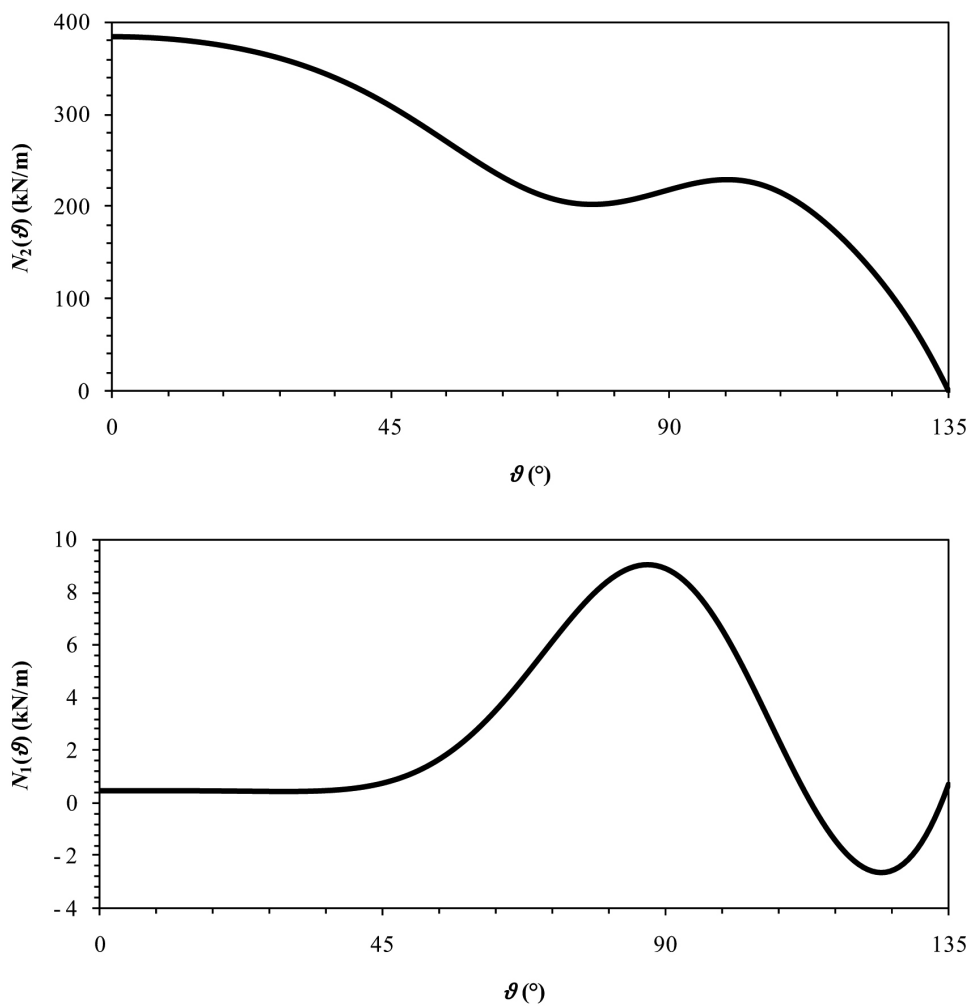
**Fig. 25.** Tension forces of rotating toroidal shell, $\Omega$ =50 rad/s
*Sl. 25.* Rastezne sile rotirajuće torusne ljuske, $\Omega$ =50 rad/s
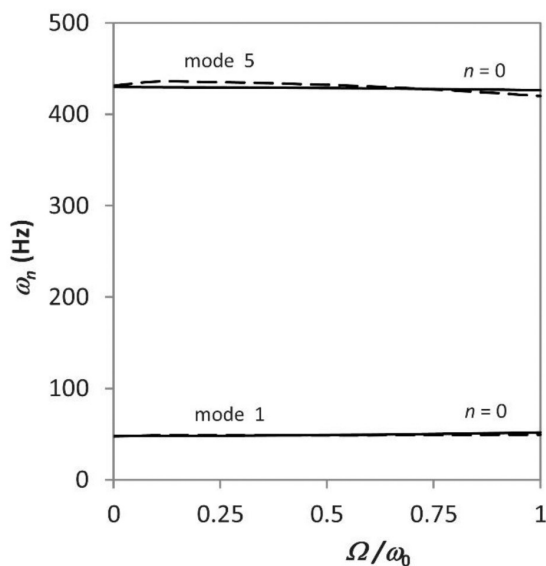
**Fig. 26.** Natural frequencies of rotating open toroidal shell, n = 0: ––– RRM, FSM; - - - FEM
*Sl. 26.* Prirodne frekvencije rotirajuće otvorene torusne ljuske, n = 0: ––– RRM, FSM; - - - FEM
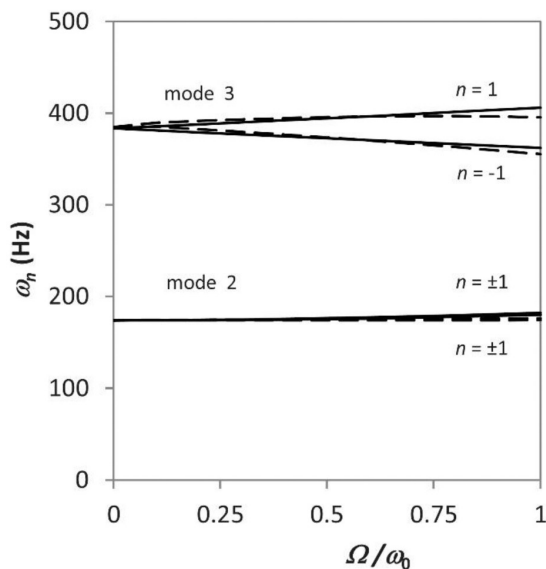


**Fig. 27.** Natural frequencies of rotating open toroidal shell, n = ±1: ––– RRM, FSM; - - - FEM
*Sl. 27.* Prirodne frekvencije rotirajuće otvorene torusne ljuske, n = ±1: ––– RRM, FSM; - - - FEM
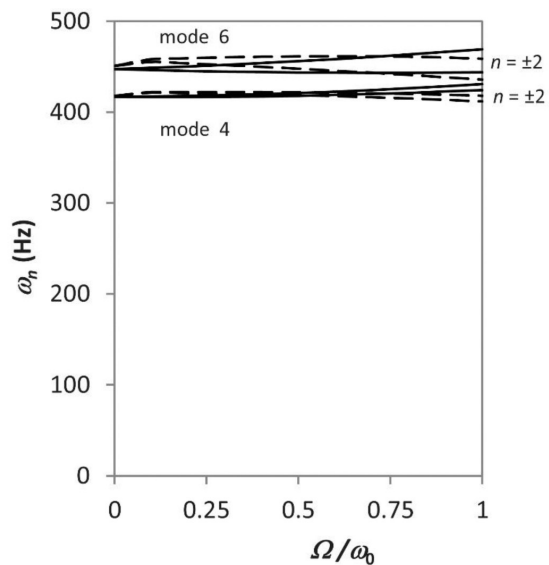
**Fig. 28.** Natural frequencies of rotating open toroidal shell, n = ±2: −−− RRM, FSM; - - - FEM
*Sl. 28.* Prirodne frekvencije rotirajuće otvorene torusne ljuske, n = ±2: −−− RRM, FSM; - - - FEM

### 7.2.2 Buckling analysis

The buckling analysis is performed for the same simply supported open toroidal shell as specified in the previous section. The shell cross-section deformation due to internal pressure of 10 MPa is shown in Fig. 29, and the tension forces due to $p$=1MPa in Fig. 30. It is observed that the meridional membrane force of the closed shell is very good approximation of the total meridional force for open shell, $N_\vartheta$. This is not the case for the circumferential tension force, $N_\varphi$, Fig. 30.
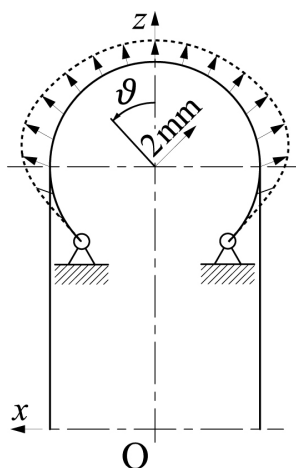


**Fig. 29.** Deformation of shell cross-section due to internal pressure $p$=10MPa

**Sl. 29.** Deformacija poprečnog presjeka ljuske uslijed unutarnjeg tlaka $p$=10MPa
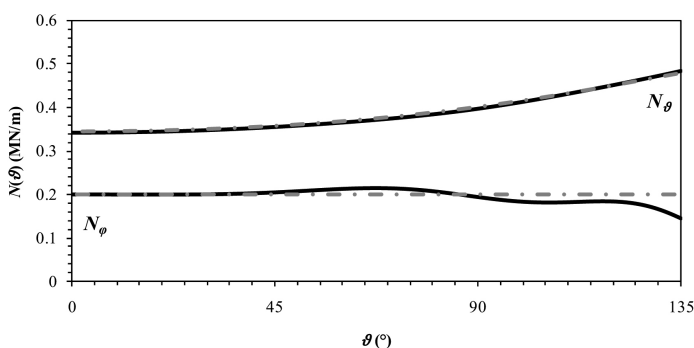


**Fig. 30.** Tension forces of simply supported open toroidal shell due to internal pressure $p$=1MPa, ––– RRM, FSM; – · – membrane theory

**Sl. 30.** Rastezne sile slobodno oslonjene torusne ljuske uslijed tlaka $p$=1MPa, ––– RRM, FSM; – · – membranska teorija

Buckling parameters determined by RRM, FSM and FEM, by employing four commercial software with different types of finite elements, are shown in Table 4. From the engineering point of view, all values agree quite well.

Buckling modes determined by RRM and FSM, as well as FEM, are shown in Fig. 31, and Figs. 32 and 33, respectively. The mode profiles of shell cross-section obtained by RRM and FSM agree very well with those of FEM.

Values of critical pressure $p_1 = \lambda_1 p = 3.853$ MPa can be considerably increased to $p_2 = \lambda_2 p = 16.283$ MPa, Table 4, by shell reinforcement with two stiff rings.

**Table 4.** Buckling parameter $\lambda$ of open simply supported toroidal shell, $R = 1$ m, $a = 0.4$ m, $h = 0.01$ m, $\vartheta_0 = \pm 3\pi/4$, $p = 1$ MPa

***Tablica 4.*** Parametar izvijanja $\lambda$ slobodno oslonjene torusne ljuske, $R = 1$ m, $a = 0.4$ m, $h = 0.01$ m, $\vartheta_0 = \pm 3\pi/4$, $p = 1$ MPa

| Mode No. | Mode type | n | RRM, 2 × 15 terms | | FSM, 150 FS | | FEM | | | |
|---|---|---|---|---|---|---|---|---|---|---|
| | | | $N_\vartheta, N_\varphi$ membrane | $N_\vartheta, N_\varphi$ shell | $N_\vartheta, N_\varphi$ membrane | $N_\vartheta, N_\varphi$ shell | Nastran CQUAD4 38 × 124 | Abaqus S8R5 38 × 124 | Catia QD8 38 × 124 | SolidWorks SHELL6 76 × 248 |
| 1 | Asym. | 0 | 3.852 | 3.853 | 3.905 | 3.934 | 4.109 | 4.077 | 3.869 | 3.872 |
| 2 | Asym. | 1 | 16.208 | 16.283 | 16.180 | 16.249 | 15.965 | 15.634 | 16.150 | 16.148 |
| 3 | Sym. | 1 | 16.271 | 16.329 | 16.238 | 16.307 | 16.055 | 15.668 | 16.200 | 16.198 |
| 4 | Sym. | 2 | 16.338 | 16.540 | 16.293 | 16.365 | 16.167 | 15.751 | 16.260 | 16.248 |
| 5 | Sym. | 2 | 16.363 | 16.570 | 16.312 | 16.383 | 16.170 | 15.772 | 16.325 | 16.269 |
| 6 | Asym. | 0 | 16.532 | 16.541 | 16.499 | 16.569 | 16.290 | 15.923 | 16.482 | 16.463 |

Mode 1, $n = 0$     Mode 2, $n = 1$     Mode 3, $n = 1$

Mode 4, $n = 2$     Mode 5, $n = 2$     Mode 6, $n = 0$
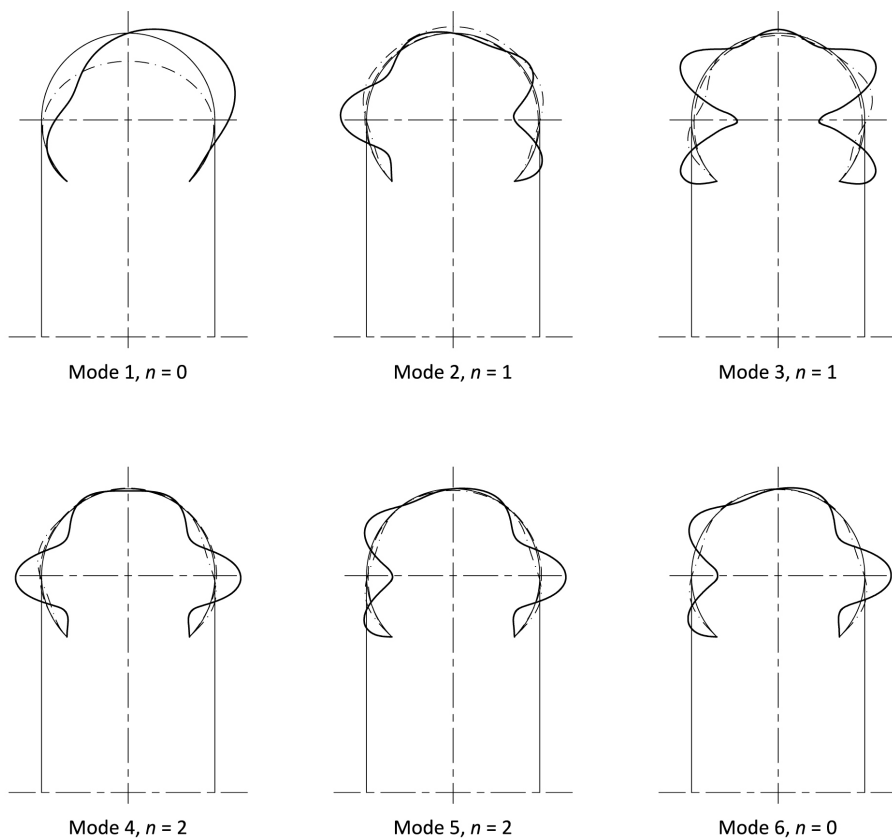
**Fig. 31.** Displacement components of buckling modes, simply supported toroidal shell, RRM, FSM: $- \cdot - U$, $- - - V$, $--- W$

***Sl. 31.*** Pomaci izvijanja slobodno oslonjene torusne ljuske, RRM, FSM: $- \cdot - U$, $- - - V$, $--- W$
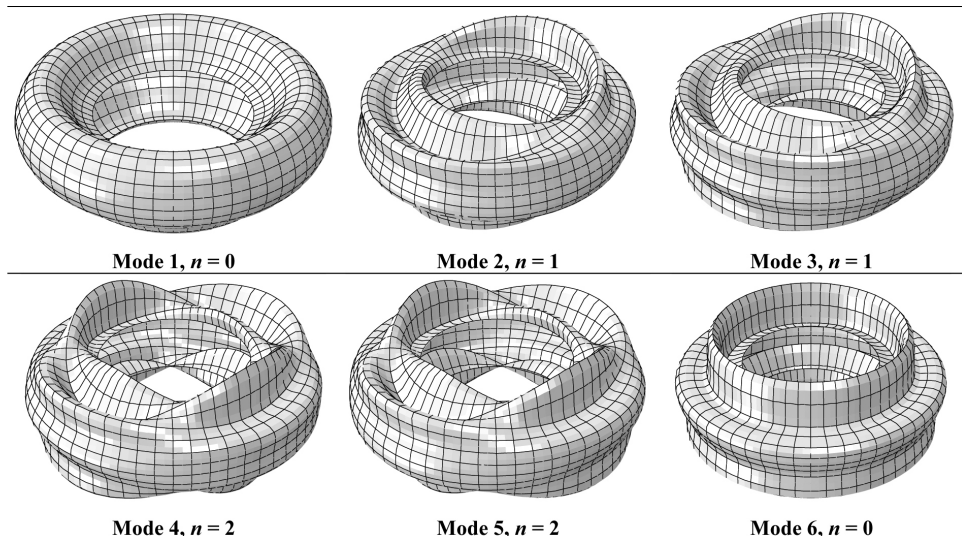
**Fig. 32.** Buckling modes of simply supported open toroidal shell under external pressure (ABAQUS)

**Sl. 32.** Oblici izvijanja slobodno oslonjene otvorene torusne ljuske izložene vanjskom tlaku (ABAQUS)
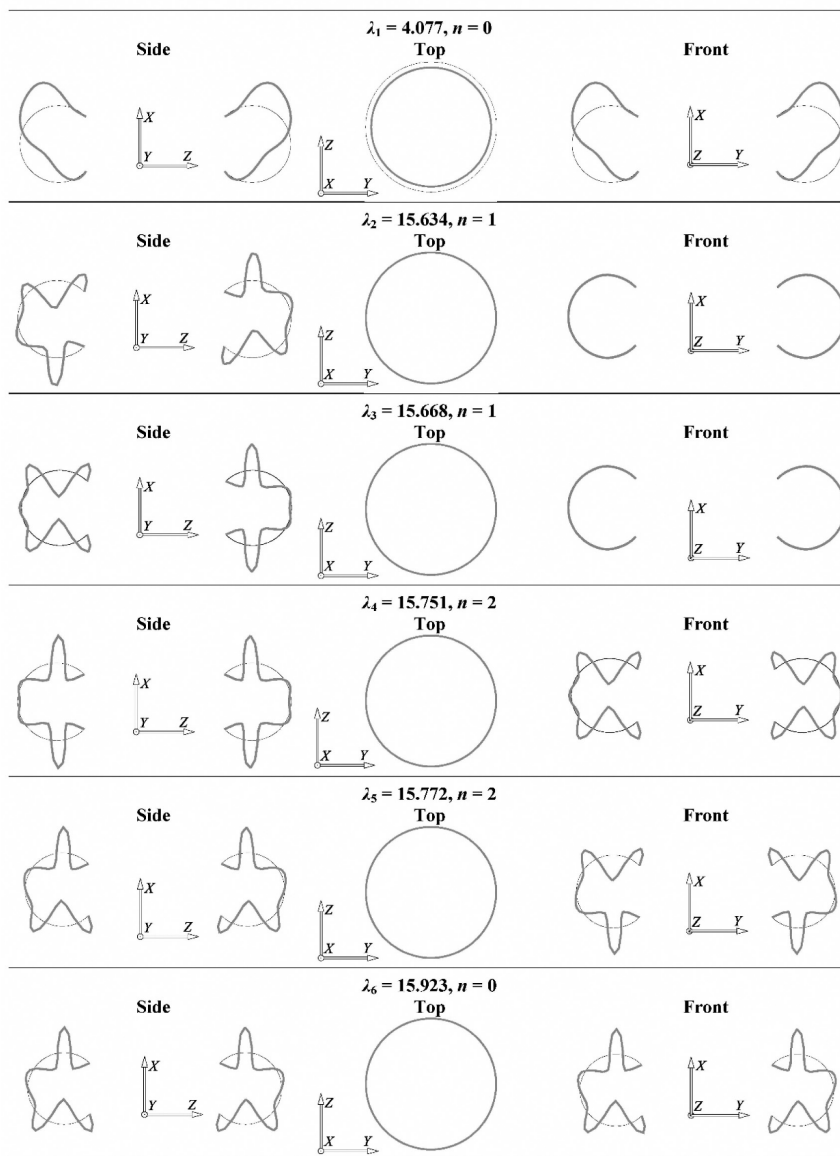
**Fig. 33.** Buckling modes of simply supported open toroidal shell in the coordinate planes (ABAQUS)

**Sl. 33.** Oblici izvijanja slobodno oslonjene otvorene torusne ljuske u koordinatnim ravninama (ABAQUS)

## 7.3 Ring vibration

As explained in [27] a toroidal shell of small radius ratio $a/R$ behaves as a ring. Vibration analysis is performed for a thin-walled toroidal ring of the following geometric and physical properties: $R$=1 m, $a$=0.05 m, $h$=0.01 m, $E$=2.1·10$^{11}$ N/m², $\nu$=0.3, $\rho$=7850 kg/m³. Natural frequencies for the first four flexural modes of non-rotating ring are determined by corresponding formulae (91) and (115) and are listed in Table 5. Natural frequencies of in-plane flexural vibrations are slightly higher than those for out-of-plane vibrations.

The same problem is also solved considering ring as a thin toroidal shell. Software ABAQUS with 54R shell element is used. 3D FEM model with mesh density in circular and meridional directions 20x416 includes 8320 finite elements. The first four natural modes are shown in Fig. 34. Natural frequencies determined by FEM model agree very well with those of ring determined by simple formulae, Table 5. Table 5 further includes values of natural frequencies determined by the finite strip method (FSM). Toroidal shell cross-section is modelled with 200 three nodes higher order strips. Values of ring natural frequencies are bounded by the FEM and FSM values.

**Table 5.** Flexural natural frequencies of stationary thin-walled toroidal ring, $\omega$ (Hz), $R$=1 m, $a$=0.05 m, $h$=0.01 m, $\Omega$=0

***Tablica 5.*** Fleksijske prirodne frekvencije stacionarnog tankostijenog torusnog prstena, $\omega$ (Hz), $R$=1 m, $a$=0.05 m, $h$=0.01 m, $\Omega$=0

| Mode no. | Mode type | Eq. | n | Ring | Shell, FEM 20 × 416 | FSM (3,3) 200 FS |
|---|---|---|---|---|---|---|
| 1 | In-plane | (91) | 2 | 77.32 | 75.02 | 84.85 |
| 2 | Out-of-plane | (115) | 2 | 75.41 | 72.98 | 80.94 |
| 3 | In-plane | (91) | 3 | 216.07 | 209.10 | 218.04 |
| 4 | Out-of-plane | (115) | 3 | 214.68 | 205.61 | 216.85 |

$\omega_1 = 72.984$ Hz, $n = 2$

$\omega_2 = 75.024$ Hz, $n = 2$

$\omega_3 = 205.61$ Hz, $n = 3$

$\omega_4 = 209.10$ Hz, $n = 3$
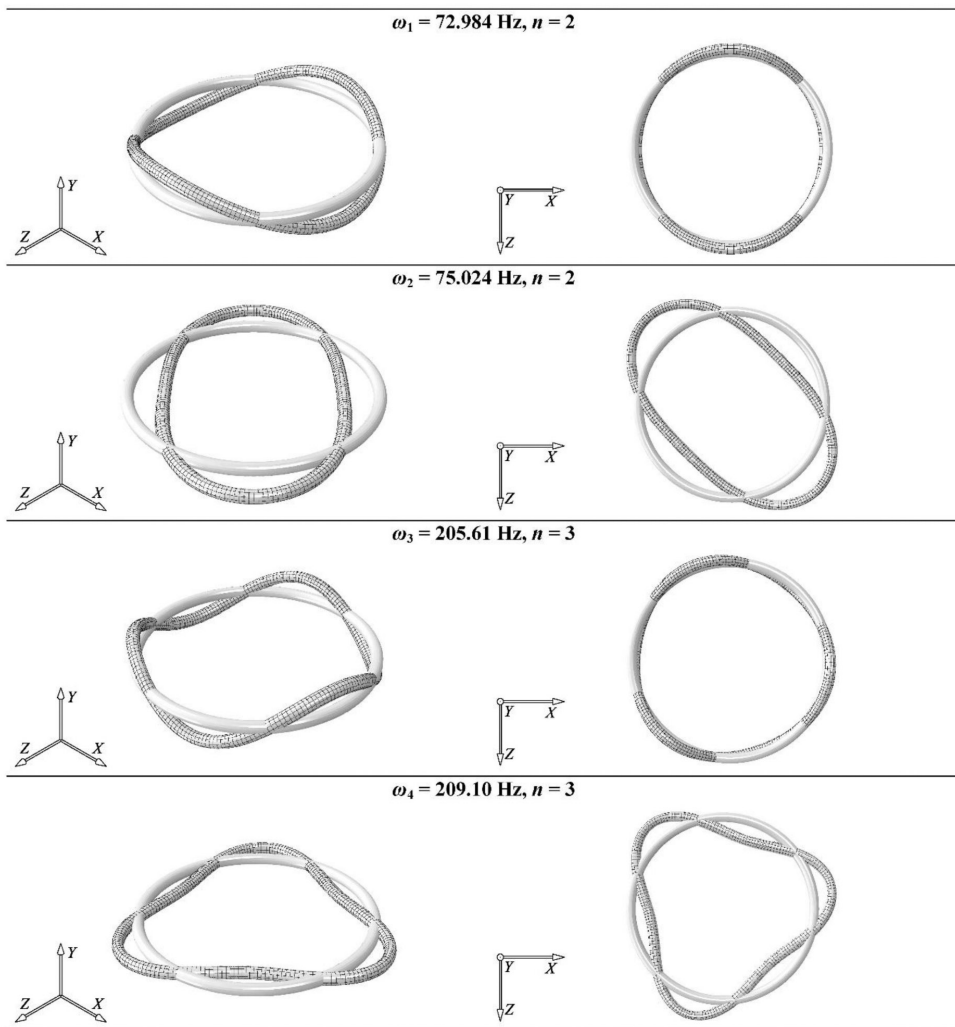
**Fig. 34.** Natural vibration modes of thin-walled toroidal ring (ABAQUS)
*Sl. 34.* Prirodni oblici vibriranja tankostijenog torusnog prstena (ABAQUS)

Natural frequencies of the in-plane vibrations of the rotating ring, i.e. flexural and extensional, are determined analytically by employing exact procedure, Eq. (131), approximated formulae, and formulae for estimation, Eqs. (90) and (88), Table 6. Three values of rotation speed $\Omega$ are selected, and $n=2$ is taken into account for illustration. Approximated formulae give values of natural frequencies very close to the exact ones. The accuracy of formulae for the estimation of natural frequencies is acceptable only for relatively small values of rotational speed.

Natural frequencies of the rotating ring out-of-plane vibrations, i.e. flexural and torsional determined by Eq. (113), are shown in Table 7. In this case, there is no bifurcation, and values of natural frequencies of both spectra are increased by increasing rotation speed.

**Table 6.** Natural frequencies of rotating thin-walled toroidal ring in-plane vibrations, $\widetilde{\omega}$ (Hz), $R=1$ m, $a=0.05$ m, $h=0.01$ m, $n=2$, $\omega_0 =75.41$ Hz

***Tablica 6.*** Prirodne frekvencije rastezanja rotirajućeg tankostijenog torusnog prstena, $\widetilde{\omega}$ (Hz), $R=1$ m, $a=0.05$ m, $h=0.01$ m, $n=2$, $\omega_0 =75.41$ Hz

| $\Omega / \omega_0$ | Method | Flexural, $\widetilde{\omega}_b$ | | Extensional, $\widetilde{\omega}_e$ | |
|---|---|---|---|---|---|
| | | Forward | Backward | Forward | Backward |
| 0 | All | 77.97 | 77.97 | 1843.6 | 1843.6 |
| 1 | Rigorous, Eq. (131) | 58.54 | 184.09 | 1796.0 | 1921.6 |
| | Approximated, Eqs. (90), (88) | 59.36 | 184.00 | 1802.6 | 1927.2 |
| 2 | Rigorous, Eq. (131) | 73.51 | 327.23 | 1776.8 | 2030.5 |
| | Approximated, Eqs. (90), (88) | 77.90 | 327.18 | 1797.9 | 2047.2 |

**Table 7.** Natural frequencies of rotating thin-walled toroidal ring out-of-plane vibrations, $\widetilde{\omega}$ (Hz), $R$=1 m, $a$=0.05 m, $h$=0.01 m, $\omega_0$ =75.41 Hz

***Tablica 7.*** Prirodne frekvencije uvijanja rotirajućeg tankostijenog torusnog prstena, $\widetilde{\omega}$ (Hz), $R$=1 m, $a$=0.05 m, $h$=0.01 m, $\omega_0$ =75.41 Hz

| $n$ | $\Omega / \omega_0$ | Flexural, $\widetilde{\omega}_b$ , Eq. (113) | Torsional, $\widetilde{\omega}_t$ , Eq. (113) |
|---|---|---|---|
| 2 | 0 | 75.57 | 1179.73 |
|   | 1 | 168.18 | 1179.80 |
|   | 2 | 309.79 | 1180.04 |
| 3 | 0 | 216.53 | 1646.82 |
|   | 1 | 312.30 | 1646.99 |
|   | 2 | 499.32 | 1647.52 |
| 4 | 0 | 417.39 | 2135.85 |
|   | 1 | 513.89 | 2136.12 |
|   | 2 | 730.33 | 2136.98 |
| 5 | 0 | 676.69 | 2634.81 |
|   | 1 | 773.38 | 2635.18 |
|   | 2 | 1009.05 | 2636.41 |

Natural frequencies of rotating ring as a thin toroidal shell, are determined by FEM in the fixed coordinate system for $n$=2 and 3. Dimensionless rotational speed $\Omega/\omega_0$ is varied between 0 and 1. The obtained results for the forward and backward mode waves are given in [27]. They are transformed into rotating coordinate system by the expressions

$$\tilde{\omega}_F = \omega_F + n\Omega, \qquad \tilde{\omega}_B = \omega_B - n\Omega \tag{132}$$

and presented in [37]. In case of out-of-plane vibrations, there is no bifurcation of natural frequencies. The analytically determined natural frequencies for the rotating toroidal ring are compared with FEM values for thick-walled toroidal shell, Figs. 35 and 36.
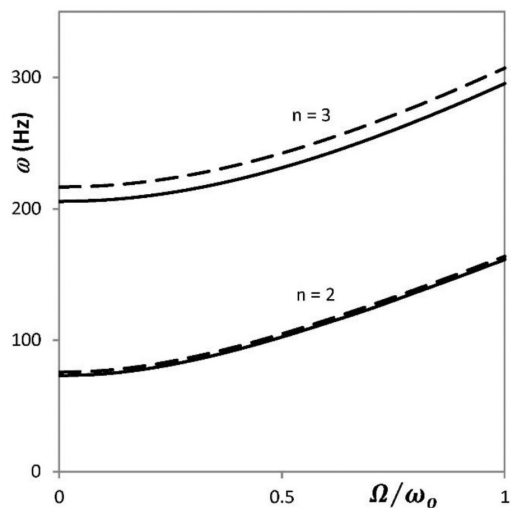
**Fig. 35.** Natural frequencies of rotating toroidal ring, out-of-plane vibrations,
––– FEM, - - - analytical

***Sl. 35.*** Prirodne frekvencije uvijanja rotirajućeg torusnog prstena, ––– FEM,
- - - analitičko rješenje
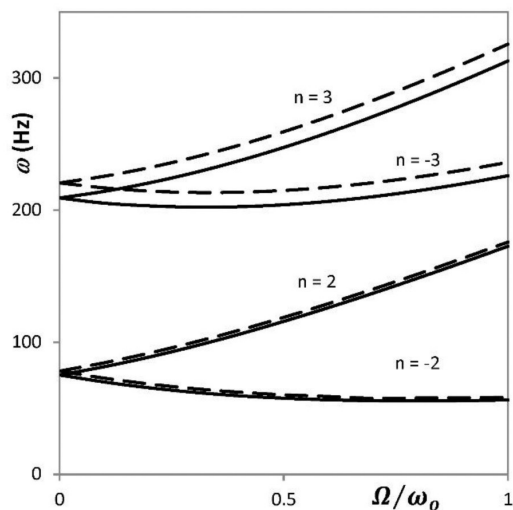


**Fig. 36.** Natural frequencies of rotating toroidal ring, in-plane vibrations,
––– FEM, - - - analytical

***Sl. 36.*** Prirodne frekvencije savijanja rotirajućeg torusnog prstena, ––– FEM,
- - - analitičko rješenje

## 8. CONCLUSION

In this self-contained paper, vibrations of pressurised rotating toroidal shells with open and closed cross-section are analysed by the Rayleigh-Ritz method. The Fourier series are used to describe the displacement components as a function of the meridional coordinate, whereas their dependence on the circumferential coordinate is described exactly using convenient trigonometric sine and cosine functions. Linear strain-displacement relationships, the ordinary strain energy, and the kinetic energy are derived from general expressions for thin shells of revolution. For the strain energy due to pre-stressing, the Green-Lagrange non-linear strain-displacement relation is employed. Pre-stressing tension forces due to the internal pressure and centrifugal load are derived by employing the membrane and the shell theory. Numerical examples show that tension forces determined according to the membrane assumption are very close to those determined by the shell theory (membrane + bending), in case of internal pressure. However, with centrifugal load, there are some differences between the tension forces calculated according to the membrane theory and the total tension forces calculated according to the shell theory.

The developed procedure for vibration analysis of toroidal shells by employing the Rayleigh-Ritz method and the Fourier series is rather complicated. Ordinary stiffness matrix, geometric stiffness matrix and mass matrices, related to the pressurisation and the centrifugal loads, the Coriolis force and the inertia load, depend on a large number of variable coefficients and submatrices. Nevertheless, the procedure is presented in a consistent and physically transparent way, which is also easy for computer coding. The quadratic eigenvalue problem, $\mathrm{Det}\left[K\left(\omega^0, \omega^1, \omega^2\right)\right]_{dyn} = 0$, is solved by a commercial package as a polynomial eigenvalue problem [40]. Forward and backward modes rotating in the circumferential direction and the corresponding natural frequencies are obtained.

Vibrations of three characteristic toroidal shells are analysed, *i.e.* closed shell of an ordinary ratio of geometric parameters, open shell of the same parameters, and the third one, which can be seen as a thin-walled toroidal ring. In all examples, two distinctive spectra of natural frequencies are obtained. In the first two examples, they are related to symmetric and asymmetric natural modes, respectively. In the third example, typical in-plane and out-of-plane natural modes of the ring are recognized. The convergence of results is very fast. Only 15 sine and cosine terms of the three sets of the Fourier series for displacements is sufficient to achieve accurate results. These three numerical examples can be used as a benchmark for evaluation of numerical methods.

The presented finite strip method for vibration analysis of rotating pre-stressed toroidal shells is developed in a detailed systematic and physically transparent way.

A two node finite strip is developed by interpolating within the strip the in-surface displacements with bar shape functions, and the normal bending deflections with beam shape functions. The finite strip properties, i.e. its stiffness matrix, geometric stiffness matrix and mass matrices, are derived by applying the minimum total energy principle. Each matrix consists of a set of variable coefficients and submatrices with recognized physical meaning.

In order to improve the convergence of the results, a three-node finite strip is developed as an effective solution. It is shown that the free vibration problem of a closed toroidal shell can be solved directly in the polar (local) coordinate system, which is an advantage. Furthermore, an arbitrary axisymmetric shell can be modelled by the toroidal finite strip, since any shell geometry can be approximated by a set of toroidal segments.

The application of the developed finite strip is illustrated in cases of a closed toroidal shell. Natural vibrations of stationary and rotating shells, with influence of pre-stressing, are analysed. The convergence analysis of the closed toroidal shell shows that the shell cross-section has to be modelled by at least 200 finite strips. This task is also solved by FEM, and the same meridional subdivision is required. It is interesting to point out that FSM and FEM results do not converge to the same values for a few lowest-order natural frequencies in the beginning of the frequency spectrum. As a reference, the rigorous results of vibration analysis performed by the Rayleigh-Ritz method are used. An advantage of the finite strip method is a considerably reduced number of degrees of freedom.

Rotating ring in-plane and out-of-plane vibrations are carried out, based on the toroidal shell theory. The strain and the kinetic energies are formulated indirectly by deducing from the corresponding energies of a toroidal shell. In the relevant literature, this problem is ordinary analysed by solving differential equations of motion derived from the balance of strain and kinetic energy via Hamilton's principle.

The in-plane vibration modes consist of combined flexural and extensional deformations, whereas the out-of-plane modes comprise combined flexural and torsional deformations. The problem is solved in an exact sophisticated way and in an approximate way that yields relatively simple formulae for practical use. The formulae for the natural frequencies of the in-plane and the out-of-plane flexural vibrations are very similar and give almost the same results assuming the same circumferential wave number. The simplified expression for the in-plane natural frequencies is identical to the well-known formula in the relevant literature.

The application of the developed ring vibration theory is illustrated by a number of numerical examples. The obtained results agree very well with those determined by the FEM analysis and the FSM analysis of a slender toroidal shell. The structure of the derived formulae for the in-plane vibrations indicates how centrifugal forces, induced

by the ring rotation, increase the mean value of natural frequencies, and the Coriolis forces cause their bifurcation.

The presented theory for the in-plane and out-of-plane free vibration of a rotating ring, based on the application of the toroidal shell theory, seems to be rather complicated. On the other hand, it is very educative, since it points out the universality of the toroidal shell theory and sheds more light on this still challenging problem.

*Acknowledgement*

# References

[1] Love, A.E.H.: Treatise on the Mathematic Theory of Elasticity, Dover Publications (4th edition), 1927.

[2] Vlasov, V.Z.: The General Theory of Shells and its Industrial Applications, Gostekhizdat, Moscow, 1949 (in Russian).

[3] Goldenveizer, A.L.: Theory of Thin Shells, Pergamon Press, Elmsford, NY, 1961.

[4] Novozhilov, V.V.: Thin Shell Theory, P. Noordhoff, Groningen, The Netherlands, 1964.

[5] Soedel, W.: Vibrations of Shells and Plates (3rd edition), New York, Marcel Dekker, Inc. 2004.

[6] Alujević, N., Campillo-Davo, N., Kindt, P., Desmet, W., Pluymers, B., Vercammen, S. Analytical solution for free vibrations of rotating cylindrical shells having free boundary conditions (2017), Engineering Structures, 132, pp. 152-171.

[7] Sun S, Chu S, Cao D. Vibration characteristics of thin rotating cylindrical shells with various boundary conditions, J Sound Vib (2012);331:4170–86.

[8] Sun S, Cao D, Han Q. Vibration studies of rotating cylindrical shells with arbitrary edges using characteristic orthogonal polynomials in the Rayleigh-Ritz method. Int J Mech Sci. (2013);68:180–9.

[9] Kim Y-J, Bolton JS. Effects of rotation on the dynamics of a circular cylindrical shell with application to tire vibration. J Sound Vib 2004;275:605–21.

[10] Lecomte, C, Graham, W.R. Dale, M. A shell model for tyre belt vibrations, J. Sound Vib 329(10), (2010), 1717–1742.

[11] Senjanović, I.: Theory of Shells of Revolution, Brodarski Institut, Zagreb, 1972.

[12] Burcher, R., Rydill, L.: Concepts in Submarine Design, Cambridge University Press, Cambridge, 1998.

[13] Ross, C.T.F.: Pressure Vessels, External Pressure Technology, Woodhead Publishing, Oxford, 2011.

[14] Senjanović, I., Rudan, S., Tomić, M., Vladimir, N.: Some structural aspects of LPG cargo tank design and construction. Proceeding of International Conference on Design and Operation of LPG Ships, RINA, London, 2008.

[15] Harte, R., Eckstein, U.: Derivation of geometrically nonlinear finite shell elements via tensor notation, Int. J. Num. Mech. Eng. 23(1986)367-384.

[16] Eckstein, U.: Nichtlineare Stabilitätsberechnung elastischer Schalentragwerke, TWM 83, Ruhr-Universität Bochum, Bochum, 1983.

[17] Bathe, K.J.: Finite Element Procedures, Prentice-Hall, Englewood Cliffs, 1996.

[18] Gavrić, L.: Finite element computation of dispersion properties of thin-walled waveguides, Journal of Sound and Vibration 173(1994) 113-124.

[19] Finnveden, S., Fraggstedt, M.: Waveguide finite elements for curved structures, Journal of Sound and Vibration 312(2008) 644-671.

[20] Waki, Y., Mace, B.R., Brennan, M.J.: Free and forced vibrations of a tyre using a wave/finite element approach, Journal of Sound and Vibration 323(2009) 737-756.

[21] Sabiniarz, P., Kropp, W.: A waveguide finite element aided analysis of the wave field on a stationary tyre, not is contact with the ground, Journal of Sound and Vibration 329(2010) 3041-3064.

[22] Hoever, C., Tsotras, A., Saemann, E.U., Kropp, W.: A comparison between finite element and waveguide finite element methods for the simulation of tyre/road interaction. Proceedings of the Inter Noise Conference, Innsbruck, Austria, 2013.

[23] Szilard, R.: Theories and Applications of Plate Analysis, Classical, Numerical and Engineering Methods, John Wiley & Sons, Inc., Hoboken, New Jersey, 2004.

[24] Senjanović, I., Alujević, N., Ćatipović, I, Čakmak, D., Vladimir, N.: Vibration analysis of rotating toroidal shell by the Rayleigh-Ritz method and Fourier series, Engineering Structures, 173(2008) 870-891.

[25] Senjanović, I., Alujević, N., Ćatipović, I., Čakmak, D., Vladimir, N., Cho, D.S.: Buckling analysis of toroidal shell by the Rayleigh-Ritz method, Journal of Pressure Vessel Technology, DOI 10.1115/1.4043594.

[26] Senjanović, I., Ćatipović, I., Alujević, N., Čakmak, D., Vladimir, N.: A finite strip for the vibration analysis of rotating toroidal shell under internal pressure, Journal of Vibration and Acoustics, April 2019, Vol. 141/021013-1.

[27] Senjanović, I., Ćatipović, I., Alujević, N., Čakmak, D., Vladimir, N.: Free in-plane and out-of-plane vibrations of rotating thin ring based on the toroidal shell theory, Archives of Mechanics, 70, 5, pp. 429-455, Warszawa 2018.

[28] Crifield, M.A.: Non-linear finite element analysis of solids and structures, Volume 1: essentials. Chichester, West Sussex, England: John Wiley & Sons, 1991.

[29] Sorić, J.: Finite Element Method, Golden marketing – Tehnička knjiga, Zagreb, 2004 (in Croatian).

[30] Young, W.C., Budynas, R.G., Sadegh, A.M.: Roark's Formulas for Stress and Strain, Eight Edition, McGraw Hill, New York, 2012.

[31] University of Kentucky, College of Arts & Sciences, MA330 *History of Mathematics*, Lecture Notes (http://www.ms.uky.edu/~sohum/ma330/files/eqns_4.pdf).

[32] UCD School of Mathematics and Statistics, MST3022 *History of Mathematics*, Lecture Notes (http://mathsa.ucd.ie/courses/mst3022/history4.pdf).

[33] Yacoub, M.D., Fraidenraich, G.: A new simple solution of the general quartic equation, The Math. Gaz., 2011.

[34] Shmakov, S.L.: A universal method of solving quartic equation, International Journal of Pure and Applied Mathematics, 71, 251-253, 2011.

[35] Bronstein, I.N., Semendjajew, K.A., Musiol, G., Mühlig, H.: Taschenbuch der Mathematik, Thun und Frankfurt am Main, Verlag Harri Deutsch, 2001.

[36] Dassault Systèmes, ABAQUS 6.9 User's guide and theoretical manual, Hibbitt, Karlsson & Sorensen, Inc., 2009.

[37] MSC.MD NASTRAN 2010 Dynamic Analysis User's Guide, MSC Software, 2010.

[38] Dassault Systèmes, Catia V5R19 Documentation: Finite Element Reference Guide, 2007.

[39] Dassault Systèmes, SolidWorks 2012 SP5.0 Documentation, 2012.

[40] Dedieu, J.P., Tisseur, F.: Perturbation theory for homogeneous polynomial eigenvalue problems, Linear Algebra and its Applications 358, 2003, 71-94.

# Appendix A
## Variable coefficients of the strain energy

$$p_1 = \pi \left( K + \frac{D}{a^2} \right) \frac{r}{a}$$

$$p_2 = \pi \left( K + \frac{D}{a^2} \right) \frac{a}{r} \left[ \cos^2 \vartheta + \frac{1}{2}(1-\nu)n^2 \right]$$

$$p_3 = \pi \left( K + \frac{D}{a^2} \right) \nu \cos \vartheta$$

$$p_4 = \frac{1}{2}\pi(1-\nu)\left( K + \frac{D}{r^2}\sin^2 \vartheta \right)\frac{r}{a}$$

$$p_5 = \pi \frac{a}{r}\left\{ K\left[ n^2 + \frac{1}{2}(1-\nu)\cos^2 \vartheta \right] + \frac{D}{r^2}\left[ n^2 \sin^2 \vartheta + \frac{1}{2}(1-\nu)\left(\frac{r}{a}\right)^2 \cos^2 \vartheta \left( 1 - 2\frac{a}{r}\sin \vartheta \right)^2 \right] \right\}$$

$$p_6 = \frac{1}{2}\pi(1-\nu)\cos \vartheta \left[ -K + \frac{D}{ar}\sin \vartheta \left( 1 - 2\frac{a}{r}\sin \vartheta \right) \right]$$

$$p_7 = \pi \nu\, n\left( K + \frac{D}{ar}\sin \vartheta \right)$$

$$p_8 = -\frac{1}{2}\pi(1-\nu)n\left( K + \frac{D}{ar}\sin \vartheta \right)$$

$$p_9 = \frac{1}{2}\pi\, n\cos \vartheta \left\{ K(3-\nu)\frac{a}{r} + \frac{D}{r^2}\left[ 2\sin \vartheta - (1-\nu)\frac{r}{a}\left( 1 - 2\frac{a}{r}\sin \vartheta \right) \right] \right\}. \tag{A1}$$

$$q_1 = \pi \frac{D}{a^2} \frac{r}{a}$$

$$q_2 = \pi \frac{D}{ar} \left[ \cos^2 \vartheta + 2(1-\nu)n^2 \right]$$

$$q_3 = \pi \left\{ K \left( \frac{r}{a} + \frac{a}{r} \sin^2 \vartheta + 2\nu \sin \vartheta \right) + \frac{D}{r^2} \frac{a}{r} n^2 \left[ n^2 + 2(1-\nu) \cos^2 \vartheta \right] \right\}$$

$$q_4 = \pi \nu \frac{D}{a^2} \cos \vartheta$$

$$q_5 = -\pi \nu \frac{D}{a \, r} n^2$$

$$q_6 = -\pi (3 - 2\nu) \frac{D}{r^2} n^2 \cos \vartheta$$

$$q_7 = -\pi \frac{D}{a^2} \frac{r}{a}$$

$$q_8 = -\pi \nu \frac{D}{a^2} \cos \vartheta$$

$$q_9 = -\pi \frac{D}{ar} \left[ \cos^2 \vartheta + (1-\nu)n^2 \right]$$

$$q_{10} = \pi \left[ K \frac{r}{a} \left( 1 + \nu \frac{a}{r} \sin \vartheta \right) + \nu \frac{D}{ar} n^2 \right]$$

$$q_{11} = \pi \left[ K \left( \frac{a}{r} \sin \vartheta + \nu \right) \cos \vartheta + (2-\nu) \frac{D}{r^2} n^2 \cos \vartheta \right]$$

$$q_{12} = -\pi \nu \frac{D}{a \, r} n \sin \vartheta$$

$$q_{13} = \pi (1-\nu) \frac{D}{a \, r} n \sin \vartheta$$

$$q_{14} = \pi \frac{D}{r^2} n \cos \vartheta \left[ (1-\nu) \frac{r}{a} \left( 1 - 2 \frac{a}{r} \sin \vartheta \right) - \sin \vartheta \right]$$

$$q_{15} = -\pi (1-\nu) \frac{D}{r^2} n \sin \vartheta \cos \vartheta$$

$$q_{16} = \pi n \left\{ K \left( \frac{a}{r} \sin \vartheta + \nu \right) + \frac{D}{r^2} \left[ \frac{a}{r} n^2 \sin \vartheta - (1-\nu) \cos^2 \vartheta \left( 1 - 2 \frac{a}{r} \sin \vartheta \right) \right] \right\} \qquad \text{(A2)}$$

# Appendix B
## Variable coefficients of the strain energy due to pre-stressing

$$c_1 = c_3 = c_6 = c_9 = \pi \frac{r}{a} N_\vartheta$$

$$c_2 = \pi \left[ \frac{r}{a} N_\vartheta + \frac{a}{r} (n^2 + \cos^2 \vartheta) N_\varphi \right]$$

$$c_4 = \pi \frac{a}{r} \left[ \cos^2 \vartheta\, N_\vartheta + (n^2 + \sin^2 \vartheta) N_\varphi \right]$$

$$c_5 = -\pi \cos \vartheta\, N_\vartheta$$

$$c_7 = \pi \left[ \frac{r}{a} N_\vartheta + \frac{a}{r} (n^2 + \sin^2 \vartheta) N_\varphi \right]$$

$$c_8 = \pi \frac{a}{r} n \cos \vartheta\, N_\varphi$$

$$c_{10} = \pi \frac{a}{r} \sin \vartheta \cos \vartheta\, N_\varphi$$

$$c_{11} = 2\pi \frac{a}{r} n \sin \vartheta\, N_\varphi. \tag{B1}$$

$N_\vartheta$ and $N_\varphi$ are in-plane forces due to pressure and centrifugal load.

**Appendix C**
**Submatrices of the stiffness matrices**

$$[k]_1 = \begin{bmatrix} \begin{bmatrix} f_k' f_m' \end{bmatrix} & \begin{bmatrix} f_k' g_m' \end{bmatrix} \\ \begin{bmatrix} g_k' f_m' \end{bmatrix} & \begin{bmatrix} g_k' g_m' \end{bmatrix} \end{bmatrix}$$

$$[k]_2 = \begin{bmatrix} \begin{bmatrix} f_k f_m \end{bmatrix} & \begin{bmatrix} f_k g_m \end{bmatrix} \\ \begin{bmatrix} g_k f_m \end{bmatrix} & \begin{bmatrix} g_k g_m \end{bmatrix} \end{bmatrix}$$

$$[k]_4^0 = \begin{bmatrix} \begin{bmatrix} f_k' f_m \end{bmatrix} & \begin{bmatrix} f_k' g_m \end{bmatrix} \\ \begin{bmatrix} g_k' f_m \end{bmatrix} & \begin{bmatrix} g_k' g_m \end{bmatrix} \end{bmatrix}$$

$$[k]_4^* = \begin{bmatrix} \begin{bmatrix} f_k f_m' \end{bmatrix} & \begin{bmatrix} f_k g_m' \end{bmatrix} \\ \begin{bmatrix} g_k f_m' \end{bmatrix} & \begin{bmatrix} g_k g_m' \end{bmatrix} \end{bmatrix}$$

$$[k]_5^0 = \begin{bmatrix} \begin{bmatrix} f_k' f_m'' \end{bmatrix} & \begin{bmatrix} f_k' g_m'' \end{bmatrix} \\ \begin{bmatrix} g_k' f_m'' \end{bmatrix} & \begin{bmatrix} g_k' g_m'' \end{bmatrix} \end{bmatrix}$$

$$[k]_5^* = \begin{bmatrix} \begin{bmatrix} f_k'' f_m' \end{bmatrix} & \begin{bmatrix} g_k'' f_m' \end{bmatrix} \\ \begin{bmatrix} f_k'' g_m' \end{bmatrix} & \begin{bmatrix} g_k'' g_m' \end{bmatrix} \end{bmatrix}$$

$$[k]_6^0 = \begin{bmatrix} \begin{bmatrix} f_k f_m'' \end{bmatrix} & \begin{bmatrix} f_k g_m'' \end{bmatrix} \\ \begin{bmatrix} g_k f_m'' \end{bmatrix} & \begin{bmatrix} g_k g_m'' \end{bmatrix} \end{bmatrix}$$

$$[k]_6^* = \begin{bmatrix} \begin{bmatrix} f_k'' f_m \end{bmatrix} & \begin{bmatrix} g_k'' f_m \end{bmatrix} \\ \begin{bmatrix} f_k'' g_m \end{bmatrix} & \begin{bmatrix} g_k'' g_m \end{bmatrix} \end{bmatrix}$$

$$[k]_7 = \begin{bmatrix} \begin{bmatrix} f_k'' f_m'' \end{bmatrix} & \begin{bmatrix} f_k'' g_m'' \end{bmatrix} \\ \begin{bmatrix} g_k'' f_m'' \end{bmatrix} & \begin{bmatrix} g_k'' g_m'' \end{bmatrix} \end{bmatrix}$$

$$[k]_3 = [k]_4^0 + [k]_4^*$$

$$[k]_8 = [k]_5^0 + [k]_5^*$$

$$[k]_9 = [k]_6^0 + [k]_6^* \tag{C1}$$

# Appendix D
## Submatrices of the mass matrices

$$[B]_{11} = \alpha \int_0^{2\pi} r \cos^2 \vartheta [k]_2 \, d\vartheta$$

$$[B]_{22} = \alpha \int_0^{2\pi} r [k]_2 \, d\vartheta$$

$$[B]_{33} = \alpha \int_0^{2\pi} r \sin^2 \vartheta [k]_2 \, d\vartheta \tag{D1}$$

$$[B]_{13} = \alpha \int_0^{2\pi} r \sin \vartheta \cos \vartheta [k]_2 \, d\vartheta$$

$$[B]_{31} = [B]_{13}^T$$

$$[C]_{12} = 2\alpha \int_0^{2\pi} r \cos \vartheta [k]_2 \, d\vartheta$$

$$[C]_{23} = 2\alpha \int_0^{2\pi} r \sin \vartheta [k]_2 \, d\vartheta \tag{D2}$$

$$[C]_{21} = [C]_{12}^T, \quad [C]_{32} = [C]_{23}^T$$

$$[M]_{11} = [M]_{22} = [M]_{33} = \alpha \int_0^{2\pi} r [k]_2 \, d\vartheta \tag{D3}$$

$$\alpha = \pi \rho h a \tag{D4}$$

# Appendix E
## Submatrices of the finite strip stiffness matrix

$$[K]_1 = \int_{\vartheta_1}^{\vartheta_2} p_1 \left[ g_i^{'} g_j^{'} \right] \mathrm{d}\vartheta$$

$$[K]_2 = \int_{\vartheta_1}^{\vartheta_2} p_2 \left[ g_i g_j \right] \mathrm{d}\vartheta$$

$$[K]_3 = \int_{\vartheta_1}^{\vartheta_2} p_3 \left[ g_i^{'} g_j + g_i g_j^{'} \right] \mathrm{d}\vartheta$$

$$[K]_4 = \int_{\vartheta_1}^{\vartheta_2} p_4 \left[ g_i^{'} g_j^{'} \right] \mathrm{d}\vartheta$$

$$[K]_5 = \int_{\vartheta_1}^{\vartheta_2} p_5 \left[ g_i g_j \right] \mathrm{d}\vartheta$$

$$[K]_6 = \int_{\vartheta_1}^{\vartheta_2} p_6 \left[ g_i^{'} g_j + g_i g_j^{'} \right] \mathrm{d}\vartheta$$

$$[K]_7 = \int_{\vartheta_1}^{\vartheta_2} q_1 \left[ f_i^{''} f_j^{''} \right] \mathrm{d}\vartheta$$

$$[K]_8 = \int_{\vartheta_1}^{\vartheta_2} q_2 \left[ f_i^{'} f_j^{'} \right] \mathrm{d}\vartheta$$

$$[K]_9 = \int_{\vartheta_1}^{\vartheta_2} q_3 \left[ f_i f_j \right] \mathrm{d}\vartheta$$

$$[K]_{10} = \int_{\vartheta_1}^{\vartheta_2} q_4 \left[ f_i^{''} f_j^{'} + f_i^{'} f_j^{''} \right] \mathrm{d}\vartheta$$

$$[K]_{11} = \int_{\vartheta_1}^{\vartheta_2} q_5 \left[ f_i^{''} f_j + f_i f_j^{''} \right] \mathrm{d}\vartheta$$

$$[K]_{12} = \int_{\vartheta_1}^{\vartheta_2} q_6 \left[ f_i^{'} f_j + f_i f_j^{'} \right] \mathrm{d}\vartheta$$

93

$$[K]_{13} = \int_{\vartheta_1}^{\vartheta_2} p_7 \left[ g_i' g_j \right] \mathrm{d}\vartheta$$

$$[K]_{14} = \int_{\vartheta_1}^{\vartheta_2} p_8 \left[ g_i g_j' \right] \mathrm{d}\vartheta$$

$$[K]_{15} = \int_{\vartheta_1}^{\vartheta_2} p_9 \left[ g_i g_j \right] \mathrm{d}\vartheta$$

$$[K]_{16} = \int_{\vartheta_1}^{\vartheta_2} q_7 \left[ g_i' f_j'' \right] \mathrm{d}\vartheta$$

$$[K]_{17} = \int_{\vartheta_1}^{\vartheta_2} q_8 \left[ g_i f_j'' + g_i' f_j' \right] \mathrm{d}\vartheta$$

$$[K]_{18} = \int_{\vartheta_1}^{\vartheta_2} q_9 \left[ g_i f_j' \right] \mathrm{d}\vartheta$$

$$[K]_{19} = \int_{\vartheta_1}^{\vartheta_2} q_{10} \left[ g_i' f_j \right] \mathrm{d}\vartheta$$

$$[K]_{20} = \int_{\vartheta_1}^{\vartheta_2} q_{11} \left[ g_i f_j \right] \mathrm{d}\vartheta$$

$$[K]_{21} = \int_{\vartheta_1}^{\vartheta_2} q_{12} \left[ g_i f_j'' \right] \mathrm{d}\vartheta$$

$$[K]_{22} = \int_{\vartheta_1}^{\vartheta_2} q_{13} \left[ g_i' f_j' \right] \mathrm{d}\vartheta$$

$$[K]_{23} = \int_{\vartheta_1}^{\vartheta_2} q_{14} \left[ g_i f_j' \right] \mathrm{d}\vartheta$$

$$[K]_{24} = \int_{\vartheta_1}^{\vartheta_2} q_{15} \left[ g_i' f_j \right] \mathrm{d}\vartheta$$

$$[K]_{25} = \int_{\vartheta_1}^{\vartheta_2} q_{16} \left[ g_i f_j \right] \mathrm{d}\vartheta. \tag{E1}$$

**Appendix F**
**Submatrices of the finite strip geometric stiffness matrix**

$$[G]_1 = \int_{\vartheta_1}^{\vartheta_2} c_1 \left[ g_i' g_j' \right] \mathrm{d}\vartheta$$

$$[G]_2 = \int_{\vartheta_1}^{\vartheta_2} c_2 \left[ g_i g_j \right] \mathrm{d}\vartheta$$

$$[G]_3 = \int_{\vartheta_1}^{\vartheta_2} c_3 \left[ g_i' g_j' \right] \mathrm{d}\vartheta$$

$$[G]_4 = \int_{\vartheta_1}^{\vartheta_2} c_4 \left[ g_i g_j \right] \mathrm{d}\vartheta$$

$$[G]_5 = \int_{\vartheta_1}^{\vartheta_2} c_5 \left[ g_i' g_j + g_i g_j' \right] \mathrm{d}\vartheta$$

$$[G]_6 = \int_{\vartheta_1}^{\vartheta_2} c_6 \left[ f_i' f_j' \right] \mathrm{d}\vartheta$$

$$[G]_7 = \int_{\vartheta_1}^{\vartheta_2} c_7 \left[ f_i f_j \right] \mathrm{d}\vartheta$$

$$[G]_8 = \int_{\vartheta_1}^{\vartheta_2} c_8 \left[ g_i g_j \right] \mathrm{d}\vartheta$$

$$[G]_9 = \int_{\vartheta_1}^{\vartheta_2} c_9 \left[ g_i' f_j - g_i f_j' \right] \mathrm{d}\vartheta$$

$$[G]_{10} = \int_{\vartheta_1}^{\vartheta_2} c_{10} \left[ g_i f_j \right] \mathrm{d}\vartheta$$

$$[G]_{11} = \int_{\vartheta_1}^{\vartheta_2} c_{11} \left[ g_i f_j \right] \mathrm{d}\vartheta .$$

$$(F1)$$

# Appendix G
## Submatrices of the finite strip mass matrices

$$[M]_1 = \int_{\vartheta_1}^{\vartheta_2} d_1 \left[ g_i g_j \right] \mathrm{d}\vartheta$$

$$[M]_2 = \int_{\vartheta_1}^{\vartheta_2} d_1 \left[ f_i f_j \right] \mathrm{d}\vartheta$$

$$[M]_3 = \int_{\vartheta_1}^{\vartheta_2} d_2 \left[ g_i g_j \right] \mathrm{d}\vartheta$$

$$[M]_4 = \int_{\vartheta_1}^{\vartheta_2} d_3 \left[ f_i f_j \right] \mathrm{d}\vartheta$$

$$[M]_5 = \int_{\vartheta_1}^{\vartheta_2} d_6 \left[ g_i f_j \right] \mathrm{d}\vartheta$$

$$[M]_6 = 2 \int_{\vartheta_1}^{\vartheta_2} d_4 \left[ g_i g_j \right] \mathrm{d}\vartheta$$

$$[M]_7 = 2 \int_{\vartheta_1}^{\vartheta_2} d_5 \left[ g_i f_j \right] \mathrm{d}\vartheta. \tag{G1}$$

# POLU-ANALITIČKE METODE ZA ANALIZU VIBRACIJA I STABILNOSTI TLAČNIH I ROTIRAJUĆIH TORUSNIH LJUSKI ENERGETSKIM PRISTUPOM

## Sažetak

Prikazane su polu-analitičke metode za analizu vibracija torusnih ljuski izloženih tlaku, koje rotiraju oko svoje osi simetrije. Ovisnost deformacija rastezanja i savijanja o pomacima ljuske izvedena je iz općih izraza za rotacijske ljuske. Izrazi za deformacijsku (potencijalnu) i kinetičku energiju izvedeni su za rotirajući polarni koordinatni sustav. Potencijalna energija je najprije formulirana za slučaj velikih deformacija, a zatim je rastavljena na linearni i nelinearni dio, koji je zatim lineariziran. Korištena je nelinearna Green-Lagrangeova formulacija. Kinetička energija osim vibracijske komponente uključuje centrifugalni i Coriolisov dio. Za promjenu pomaka $u$, $v$ i $w$ u cirkularnom smjeru postavljeni su točni harmonijski izrazi. Pomaci u meridijalnom smjeru su pretpostavljeni u obliku Fourierovih redova. Korištena je Rayleigh-Ritzova metoda za minimiziranje ukupne energije. To je rezultiralo općom matricom krutosti, geometrijskom matricom krutosti uslijed prednaprezanja, te trima matricama masa vezanim za kvadrat prirodne frekvencije, umnožak prirodne frekvencije i brzine vrtnje, te kvadrat brzine vrtnje. Primjena razvijenog postupka ilustrirana je na primjeru zatvorene i otvorene torusne ljuske i tankostijenog torusnog prstena. Dobiveni rezultati (prirodne frekvencije i oblici vibriranja) uspoređeni su s rezultatima dobivenim metodom konačnih elemenata i uočeno je dobro podudaranje. Prednost prikazanog postupka je u znatno skraćenom vremenu obrade problema na računalu.

U nastavku je razvijena metoda vrpčastih elemenata za analizu istih problema. Za deformacijsku i kinetičku energiju korišteni su ranije postavljeni izrazi u okviru Rayleigh-Ritzove metode. Ljuska je u meridijalnom smjeru modelirana nizom dvočvornih vrpčastih elemenata. Promjena pomaka $u$, $v$ i $w$ u meridijalnom smjeru unutar svakog elementa aproksimirana je štapnim i grednim funkcijama oblika. Minimiziranjem ukupne energije vrpčastog elementa formirane su matrice krutosti i matrice masa. U svrhu ubrzanja konvergencije rješenja razvijen je vrpčasti element višeg reda s tri čvora. Prikazanom metodom riješen je problem zatvorene torusne ljuske. Dobiveni rezultati uspoređeni su s rezultatima Rayleigh-Ritzove metode i metode konačnih elemenata.

Nadalje, razmatrane su fleksijske i torzijske vibracije rotirajućeg prstena. Fleksijske vibracije se sprežu sa rasteznim vibracijama, a torzijske sa savojnim vibracijama. Odgovarajuće jednadžbe gibanja izvedene su iz teorije vibracija torusne ljuske. U prvom slučaju prsten je promatran kao vršni segment torusne ljuske, a u drugom slučaju kao bočni segment. Po-

kazano je da rotacija prstena dovodi do bifurkacije fleksijskih prirodnih frekvencija, a ne i torzijskih frekvencija. Teorija vibracija prstena ocjenjena je usporedbom rezultata analize vibracija jednog prstena s rezultatima metode konačnih elemenata i metode vrpčastih elemenata, te izmjerenim vrijednostima dostupnim u literaturi.

**Ključne riječi:** torusna ljuska; vibracije; izvijanje; tlak; rotacija; Rayleigh-Ritzova metoda; metoda vrpčastih elemenata.

**Ivo Senjanović**

University of Zagreb
Faculty of Mechanical Engineering
and Naval Architecture
Ivana Lučića 5, 10000 Zagreb
Croatia
e-mail: ivo.senjanovic@fsb.hr

**Neven Alujević**

University of Zagreb
Faculty of Mechanical Engineering
and Naval Architecture
Ivana Lučića 5, 10000 Zagreb
Croatia
e-mail: neven.alujevic@fsb.hr

**Ivan Ćatipović**

University of Zagreb
Faculty of Mechanical Engineering
and Naval Architecture
Ivana Lučića 5, 10000 Zagreb
Croatia
e-mail: ivan.catipovic@fsb.hr

**Damjan Čakmak**

University of Zagreb
Faculty of Mechanical Engineering
and Naval Architecture
Ivana Lučića 5, 10000 Zagreb
Croatia
e-mail: damjan.cakmak@fsb.hr

**Nikola Vladimir**

University of Zagreb
Faculty of Mechanical Engineering
and Naval Architecture
Ivana Lučića 5, 10000 Zagreb
Croatia
e-mail: nikola.vladimir@fsb.hr